Mathematics Dissertations   Department of Mathematics and Statistics

5-10-2017

A Mathematical Model of the Combined β1- and β2-Adrenergic Signaling System in the Mouse Ventricular Myocyte

Kelvin Rozier

A MATHEMATICAL MODEL OF THE COMBINED β_1- AND β_2-ADRENERGIC SIGNALING SYSTEM IN THE MOUSE VENTRICULAR MYOCYTE

by

KELVIN E. ROZIER

Under the Direction of Vladimir E. Bondarenko, PhD, FAHA

ABSTRACT

The β_1- and β_2-adrenergic signaling systems play different roles in the functioning of cardiac cells. Experimental data shows that the activation of the β_1-adrenergic signaling system produces significant inotropic, lusitropic, and chronotropic effects in the heart, while the effects of the β_2-adrenergic signaling system is less apparent. In this dissertation, a comprehensive experimentally-based mathematical model of the combined β_1- and β_2-adrenergic signaling systems in mouse ventricular myocytes is developed to simulate the experimental findings and make testable predictions of the behavior of the cardiac cells under different physiological conditions. Simulations describe the dynamics of major signaling molecules in different subcellular

compartments; kinetics and magnitudes of phosphorylation of ion channels, transporters, and Ca^{2+} handling proteins; modifications of action potential shape and duration; and $[Ca^{2+}]_i$ and $[Na^+]_i$ dynamics upon stimulation of β_1- and β_2-adrenergic receptors (β_1- and β_2-ARs). The model reveals physiological conditions when β_2-ARs do not produce significant physiological effects and when their effects can be measured experimentally. Simulations demonstrated that stimulation of β_2-ARs with isoproterenol caused a marked increase in the magnitude of the L-type Ca^{2+} current, $[Ca^{2+}]_i$ transient, and phosphorylation of phospholamban only upon additional application of pertussis toxin (PTX) or inhibition of phosphodiesterases of type 3 and 4. The model also made testable predictions of the changes in magnitudes of $[Ca^{2+}]_i$ and $[Na^+]_i$ fluxes, the rate of decay of $[Na^+]_i$ concentration upon both combined and separate stimulation of β_1- and β_2-ARs, and the contribution of phosphorylation of PKA targets to the changes in the action potential and $[Ca^{2+}]_i$ transient. A comprehensive mathematical model of the mouse ventricular myocyte overexpressing β_2-adrenergic receptors was also developed. It was found that most of the β_2-adrenergic receptors are active in control conditions in TG mice. Simulations describe the increased basal adenylyl cyclase activity; modifications of action potential; the effects on the L-type Ca^{2+} current and $[Ca^{2+}]_i$ transients upon stimulation of β_2-adrenergic receptors in control, after the application of PTX, upon stimulation with zinterol, and upon stimulation with zinterol in the presence of PTX. The model also describes the effects of inverse agonist ICI-118,551 on adenylyl cyclase activity, action potential, and $[Ca^{2+}]_i$ transients.

INDEX WORDS: Mathematical model, Adrenergic signaling system, Cardiac cell model

A MATHEMATICAL MODEL OF THE COMBINED β_1- AND β_2-ADRENERGIC

SIGNALING SYSTEM IN THE MOUSE VENTRICULAR MYOCYTE

by

KELVIN E. ROZIER

A Dissertation Submitted in Partial Fulfillment of the Requirements for the Degree of

Doctor of Philosophy

in the College of Arts and Sciences

Georgia State University

2017

A MATHEMATICAL MODEL OF THE COMBINED β₁- AND β₂-ADRENERGIC

SIGNALING SYSTEM IN THE MOUSE VENTRICULAR MYOCYTE

by

KELVIN E. ROZIER

Committee Chair: Vladimir Bondarenko

Committee: Igor Belykh

Yaroslav Molkov

Alexandra Smirnova

Electronic Version Approved:

Office of Graduate Studies

College of Arts and Sciences

Georgia State University

May 2017

DEDICATION

This dissertation is dedicated to my family and friends. Without their encouragement and support my quest for knowledge, and hence a better self, would be a much more difficult journey.

ACKNOWLEDGEMENTS

TABLE OF CONTENTS

LIST OF TABLES

LIST OF FIGURES

xiv

LIST OF ABBREVIATIONS

AC   Adenylyl cyclase

APD   action potential duration

AR   adrenergic receptor

ATP   adenosine triphosphate

AV   atrioventricular

Cav   caveolar

Cyt   cytosol

DAD   delayed afterdepolarization

Ecav   extracaveolar

FRET   fluorescence resonance energy transfer

GDP   guanosine diphosphate

GPCR   G protein coupled receptor

GRK2   G protein coupled receptor kinase of type 2

GTP   guanosine triphosphate

ISO   isoproterenol

JSR   junctional sarcoplasmic reticulum

NSR   Network sarcoplasmic reticulum

PDE   phosphodiesterase

PKA   protein kinase A

PKI   protein kinase inhibitor

PLB   phospholamban

PLM	phospholemman
PTX	pertussis toxin
RyR	ryanodine receptor
SA	sinoatrial
SR	sarcoplasmic reticulum
TG	transgenic
TnI	troponin I
WT	wild type

1   INTRODUCTION

Mathematical models are used with a great degree of reliance in many disciplines including engineering, physics, and economics. These models are used to design, study, and predict outcomes as it relates to those fields of study. Recently these mathematical models have become more integrated into the biological sciences. Biologically plausible mathematical models that advance our knowledge of the underlying processes will become increasingly valuable tools in the understanding of diseases and for drug development. Particularly, as it pertains here, are the models of cardiac cells that ultimately aid in the study of arrhythmias and other heart diseases including heart failure.

Since the mid 1900's, cardiac models have progressed from simple models that replicate the action potential to models which are detailed and describe the many interacting components that contribute to the action potential and ionic dynamics.   These advances have been commiserated with the advances in technology which have paved the way for the discovery of various ionic currents, pumps, transporters, exchangers, proteins and signaling pathways that all play a part in the complex dynamics of the cardiac myocyte.   The development of cardiac cell models has been an educational exchange between experiment and modelling where experiments have guided model development and models have made testable predictions for experiments.

In this chapter, we briefly describe the cardiac conduction system, major mathematical models that have made fundamental contributions to the progress in the field of cardiac modeling, and give an outline of the purpose of the study in this dissertation.

1.1   The Cardiac Conduction System

The cardiac conduction system is the system that controls the heartbeat. The electrical activity in the conduction system is in the form of the action potentials that propagate through the system. This pathway begins with the sinoatrial (SA) node where rhythmic activity is generated and spreads through the atria causing it to contract and send blood to the ventricles. The electric signal then reaches the atrioventricular (AV) node where it is briefly delayed before passing to the HIS bundle. The impulse subsequently passes through the left and right bundle branches and on to the Purkinje fibers where the electrical signal spreads through the ventricles thereby promoting ventricular contraction and sending blood through the lungs and the body.

While there are mathematical models that describes the whole heart behavior, they mostly rely on the relatively simple descriptions of the tissue and cellular processes[1,2]. Usually, they do not include the change in the heart geometry during contraction. Even at present there is no well-developed mathematical model that satisfactory describes physiological processes in the heart, which is built of the different cell types (sino-atrial nodal cells, atrial cells, ventricular cells, Purkinje cells, etc.). As the cardiac tissue properties are significantly dependent on the behavior of the cardiac cells (electrical activity, ionic dynamics, contraction), major attention is paid to the development of comprehensive mathematical models of isolated cardiac cells.
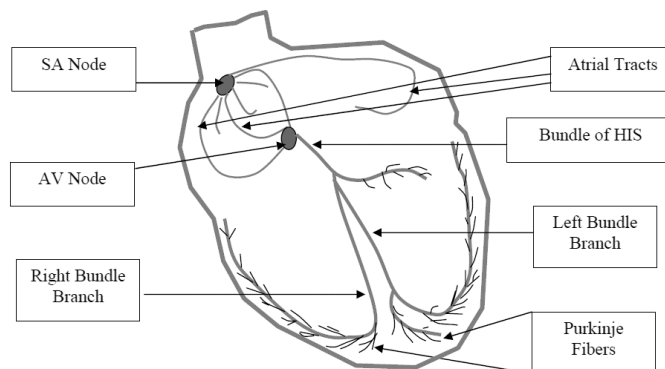
Figure 1.1 The Cardiac Conduction System

1.2   Cellular Cardiac Mathematical Models

Most cellular mathematical models have been developed for Purkinje fibers, ventricular cells, and atrial cells. Whereas some early models have been general models, there are many species specific models including those for the guinea pig, canine, rat, mouse, and human. Model development has increased in its scope over the past decades. Beginning with models that sought to describe the electrical activity with respect to the major ionic currents to models that include comprehensive descriptions of the Ca^{2+}, Na^+, and K^+ dynamics. Recent models have included protein signaling networks and the effects of signaling pathways on cellular functions. Whereas there have been numerous models developed for different purposes, we will limit the discussion here to a brief synopsis of a few models which have led to the model described in this dissertation.

The earliest cardiac model was Noble's[3] model of the Purkinje fiber cell which was based on the work of Hodgkin and Huxley's description of the properties of the squid axon nerve[4]. Noble's alterations of the Hodgkin & Huxley equations to replicate the action and pace-maker potentials of cardiac Purkinje fiber cells involved several alterations and observations. To coincide with experimental work at the time, Noble adopted the convention that positive currents are outwards such that the potential described is the inside potential with regard to the outside potential. Taking into account that decreases in membrane conductance coincide with depolarization[5], the Noble model implements the potassium current as passing through different channels with different conductance (g_{k1} and g_{k2}). Upon membrane depolarization, g_{k1} falls and is an instantaneous function of the membrane potential resulting in an inward current, whereas g_{k2} rises slowly upon depolarization and yields an outward current. The sodium conductance (g_{na}) is modeled closely to that of Hodgkin and Huxley where g_{na}, upon depolarization, has an

initial large increase that is a function of the prior membrane potential and subsequently falls, even with sustained depolarization. Capturing this activity required the use of two opposing membrane potential dependent variables whose time constants were independent of each other. The Noble Model also included a leak current, with conductance g_{An}, which was attributed to chloride ions. The four variable model is depicted schematically in Figure 1.2.
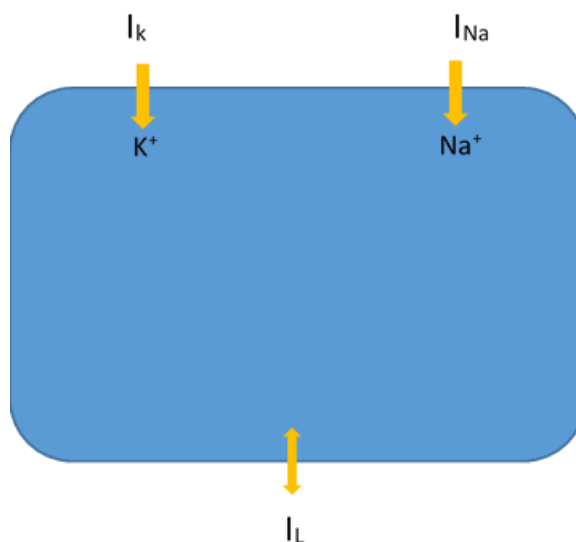
Figure 1.2 The Noble Model. A schematic representation of the Noble Model. The model includes two inward currents, representing K^+ and Na^+ currents along with an outward leak current.

The computations from Noble's equations yielded traces very close to that of the changes in the membrane potential of Purkinje fibers. A clear action potential with a distinctive spike that is trailed by a plateau with an interval of about 300ms which yields to a rapid repolarization and concludes with a slow depolarization until the next action potential is initiated. The acknowledged discrepancy with Noble's computations is that experimental action potentials had a much higher maximum rate of depolarization than the 100mV/sec obtained by Noble. Noble's work also included a description of the contributions of the various conductances to the action potential. It was noted that at the initiation of an action potential, g_k (the sum of the conductance

of g_{k1} and g_{k2}) decreases corresponding to the decrease in g_{k1}. The total conductance, g_k, then slowly rises due to the increase in g_{k2} during the plateau phase. Since g_{k1} increases upon repolarization, g_k continues to rise until depolarization where it begins to slowly fall. The spike in the action potential coincides with a large initial increase in g_{na} attributable to the fast rise in the membrane potential dependent m variable.   The subsequent fall is due to the opposing fall of the membrane potential dependent *h* variable. Following an undershoot, g_{na} reaches a plateau as the contrasting *m* and *h* variables keep the conductance relatively constant throughout the plateau of the action potential. Repolarization of the action potential coincides with a fall in g_{na} where it again remains relatively constant until the initiation of the next action potential. In addition to the change in conductances, Noble also computed the ionic currents and fluxes associated with the action potential. The model was also able to corroborate several experimental observations including all or nothing repolarization, impendence change, changes in ionic permeability, and decreased length of the action potential with an increased stimulation frequency[6].

The first ventricular cell model was presented by Beeler and Reuter[7] and was based primarily on voltage clamp experiments. The Beeler-Reuter model focused on the role of the inward current (I_s) carried by Ca^{2+} ions and its contributions to the action potential plateau. The model, as depicted in Figure 1.3, utilized 8 variables with 4 currents: an excitatory inward sodium current, I_{na}, a slow inward current, I_s, an outward potassium current, I_{k1}, and an inward rectifying current, I_{x1}, Where I_{na}, I_s, and I_{x1} are voltage- and time-dependent and I_{k1} being time independent.

The currents in the Beeler and Reuter model follow the Hodgkin and Huxley form for equations of ionic currents. Construction of the time activated and time independent currents, I_{x1} and I_{k1} respectively, were implemented from that of McAllister et al[8]. The inward sodium current, I_{na},

has its basis in the Hodgkin and Huxley equations with a modification taken from Haas et al[9]. in that a second inactivation parameter is implemented with the same membrane potential dependence and differing time constants. The Beeler-Reuter model successfully replicates the components of the standard action potential of the ventricular myocyte where the initial spike is followed by a characteristic "notch" which yields to the plateau of the action potential and then repolarization.
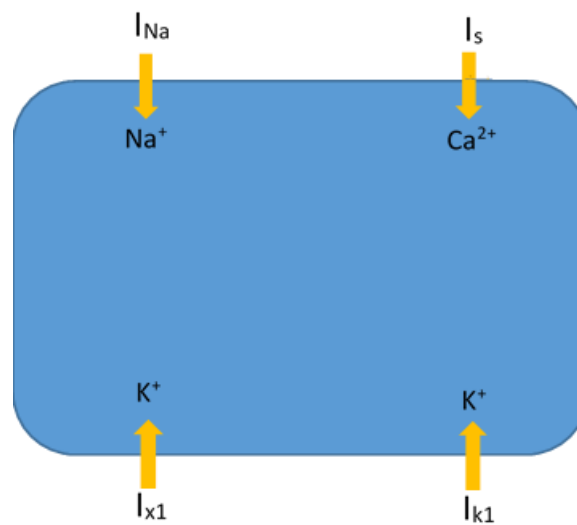
Figure 1.3 The Beeler-Reuter Model. A schematic representation of the eight variable and four current Beeler-Reuter model[7].

Beeler and Reuter observed that during the notch there is a slight delay between the fall of the inactivation parameter for I_s, f, and the rise of the activation parameter for I_{x1}, x1. The plateau, in this sense is maintained by the slightly steeper decline in the f parameter compared to the rise in x1. The Beeler –Reuter model was able to emulate several of the experimental observations such as all or nothing repolarization, the slow Na^+ recovery from inactivation as well as the dependence of action potential duration on frequency of stimulation.

Motivated by an increase in experimental data, particularly with regard to the sodium current, and a need to incorporate intracellular and extracellular ion concentration changes, DiFrancesco and Nobel published a new model of the Purkinje Fibers[10]. The sixteen variable DiFrancesco –Noble model (Fig 1.4) was the first to incorporate mechanisms by which ionic movement down the electrochemical gradient can be reversed in the form of the sodium-potassium pump and sodium-calcium exchanger.
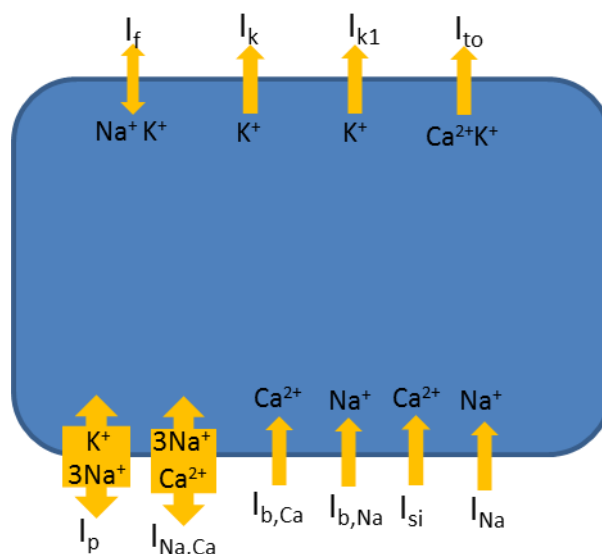
Figure 1.4 The DiFrancesco-Noble Model. A schematic representation of the DiFrancesco-Noble Model[10] which included the sodium-potassium pump and the sodium-calcium exchanger.

The model also implemented equations to represent calcium induced calcium release and calcium sequestration in the sarcoplasmic reticulum thereby incorporating intracellular events as well. A notable attribute of the model was its conjecture that the sodium calcium stoichiometry was actually 3:1 as opposed to the 2:1 neutral stoichiometry that had been widely accepted. This new stoichiometry was necessary if the resting calcium were to be maintained at proper levels. On the other hand, the model's representation of calcium handling was flawed in that the calcium transients were much higher than they were known to be.

Another ventricular cell model, The Luo-Rudy 2 model[11] (Fig 1.5), utilized the current experimental data at the time to study physiological events related to $[Ca^{2+}]_i$ and the excitation-contraction coupling process. The Luo-Rudy 2 (LR2) model was a species specific model and described the ventricular cell of the Guinea pig. The model used fifteen variables and included an intracellular space to house the network sarcoplasmic reticulum (NSR) and junctional sarcoplasmic reticulum (JSR) allowing the ability to investigate how intracellular calcium dynamics affect several properties of the ventricular myocyte. Luo and Rudy were able to replicate spontaneous Ca^{2+} release from the JSR and elucidate this spontaneous release's connection to early and delayed afterdepolarization as well as spontaneous rhythmic activity.
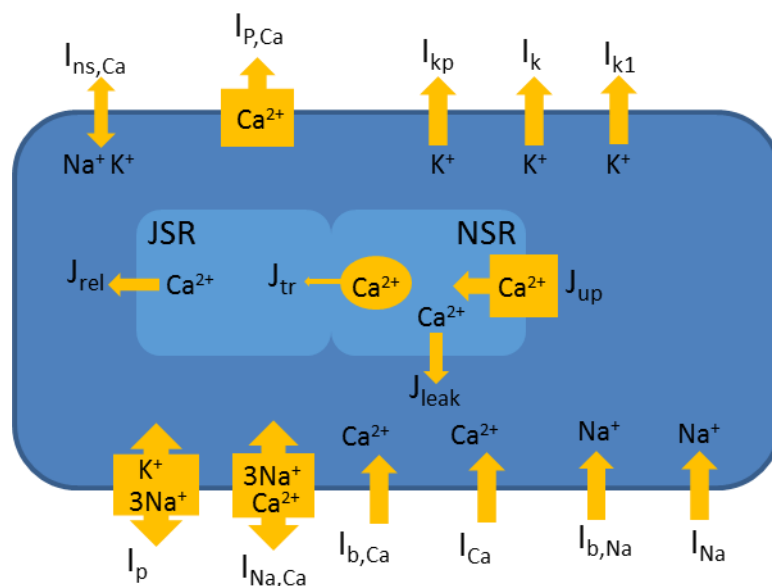
Figure 1.5 The Luo-Rudy Model. A schematic representation of the Luo-Rudy model[11] with subcellular compartments housing the junctional sarcoplasmic reticulum and the network sarcoplasmic reticulum.

Luo and Rudy also investigated conditions of maintained Ca^{2+} overload induced by a suppressed I_{NaK} coupled with an application of a β-adrenergic agonist. Under these conditions and pacing, the LR2 model renders triggered action potentials with decreasing coupling intervals that yield to a steady state dynamic. Luo and Rudy explained this triggered activity to be a result

of Ca^{2+} release from the sarcoplasmic reticulum. The LR2 model, as compared to some earlier models, is an example of how detailed mathematical models are necessary to uncover and explain some of the more complex interacting dynamics of cellular functions.

Jafri et al.[12] and Winslow et al.[13] developed the first models with local control of Ca^{2+}-induced Ca^{2+} release. The Jafri et al.[12] model was developed for guinea pig, while Winslow et al.[13] developed a canine ventricular cell model (Fig 1.6) with the goal of assessing the average functional change in the sodium-calcium exchanger and sarcoplasmic reticulum Ca^{2+}. Motivated by studies indicating strong similarities in the electrophysiology and the excitation coupling processes among failing human hearts and canine tachycardia-induced heart failure, Winslow et al. constructed their 33 variable model based on the work of the earlier guinea pig ventricular cell model developed by Jaffri et al[12]. The model successfully replicated normal and failing mid-myocardial action potentials as well as Ca^{2+} transients and showed that sarcoplasmic reticulum downregulation and sodium-calcium exchanger upregulation have the most prominent effects on action potential duration. Winslow et al. also noted that the prolonged plateau phase, hence prolonged action potential duration, in failing mid-myocardial myocytes is due to an increased inward current.

Based on their model results, Winslow et al. made the prediction that the mechanism for the prolonged action potential duration was a decrease in the Ca^{2+} induced L-type Ca^{2+} current inactivation resulting from a reduction of sarcoplasmic reticulum Ca^{2+} release. Predictions such as this, as well as those that arise from other models are examples of how mathematical models advance our understanding of complex dynamics and guide the need for future experiments. Along with the advances in technology, particularly disease research and drug development and the use of transgenic mouse experiments, Bondarenko et al.[14] developed the first mouse

ventricular myocyte model (Fig. 1.7). Bondarenko et al. used Markov models to represent the functional structure of the sodium, L-type calcium, and the rapid delayed rectifier potassium currents which allows the model to represent mutations that arise in the structure of these currents and thus yielding varying phenotypes.
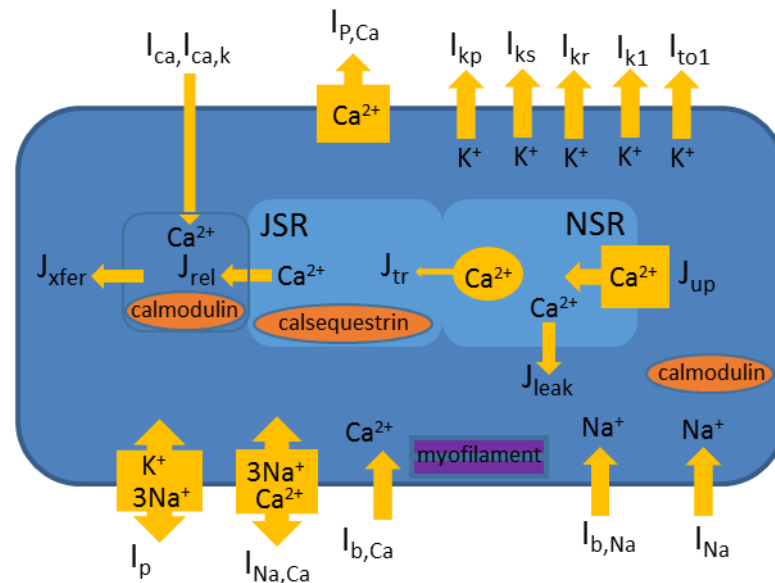
Figure 1.6 The Winslow-Rice Model. A schematic representation of the Winslow-Rice model[12] with components included to describe calcium-induced calcium release.

As action potential duration, shape, and ionic current contribution varies from species to species and in different regions of the heart, the 44 variable Bondarenko model replicates the characteristically short mouse action potential in the apical and septal regions, which differ in four of the seven potassium currents (the rapidly recovering transient outward K^+ current, the slowly recovering transient outward K^+ current, the ultra-rapidly activating delayed rectifier K^+ current, and the non-inactivating steady-state voltage-activated K^+ current), and their contributing currents. In comparison to other species the mouse Ca^{2+} handling system is relatively fast and the model accurately replicates experimentally observed Ca^{2+} fluxes. The

molecular basis of the model and detailed characterization of localized intracellular calcium dynamics renders the model the ability to replicate a multitude of "knock out" mouse experiments which were increasingly being used in genetic research.
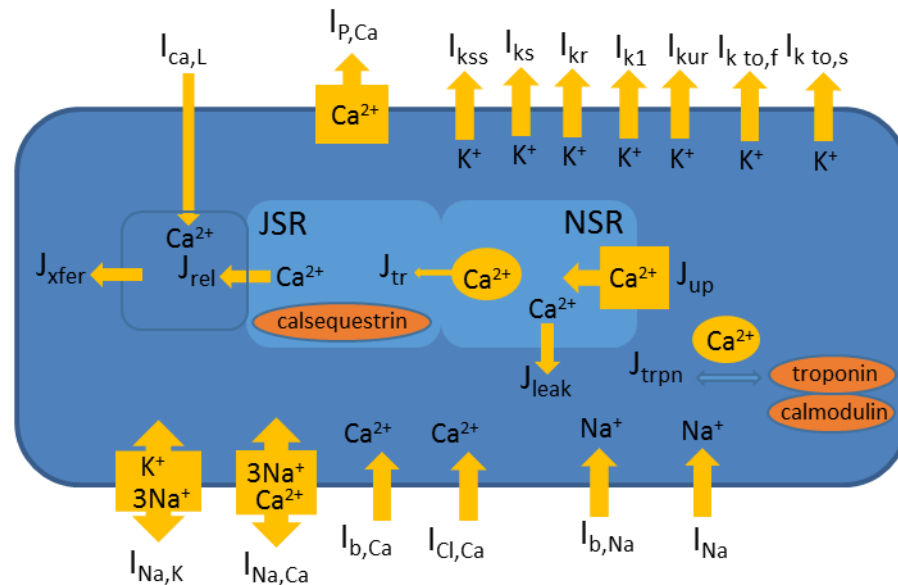
Figure 1.7 The Bondarenko et al. Model

1.3   Modelling Protein Signaling Pathways

All previous cardiac myocyte mathematical models were mostly devoted to the mechanisms of the action potential generation and propagation, Ca^{2+} dynamics, and gating properties of ionic currents. There were attempts to include the effects of the protein signaling systems into those models by modifications of model parameters to simulate activation of the system at the fixed stimulus strength[15]. However, these models were unable to provide comprehensive descriptions of the activation of the signaling systems in a wide range of the stimuli (agonist and antagonist concentrations). Therefore, most recent mathematical models of

ventricular myocytes, in addition to the description of the action potential and Ca^{2+} dynamics, incorporate protein signaling systems.

The ability of a myocyte to adapt to its environment and function accordingly relies on its ability to communicate with its surroundings. This function is achieved through various cellular signaling systems. Extracellular stimuli are detected by a multitude of receptors located on the cell membrane which initiate and regulate many of the cellular responses to the cell's environment. Among the physiological responses to cell signaling in cardiac myocytes are the regulation of heart rate and the excitation-contraction coupling process. Regulation of these and other events are almost invariably inclusive of phosphorylation and/or dephosphorylation of substrates via kinases and phosphatases respectively. Disruptions or modifications in one or several components of complex signaling pathways generally results in disease. As such, an understanding of the mechanisms that underlie these signaling paths has been an increasingly important tool in the elucidation of the causal nature of and the discovery of novel treatments for disease.

The most abundant cell receptors in cardiac myocytes are the G protein coupled receptors (GPCRs). GPCRs include AT_1 receptors, ET_{1B} receptors, α- and β-adrenergic receptors which are stimulated by angiotensin II, endothelin-1, epinephrine and norepinephrine, respectively. Adrenergic receptors α and β are comprised of subtypes α_1, α_2, β_1, β_2, and β_3, the most prevalent in cardiac myocytes being the β_1- and β_2-adrenergic receptors which are studied here. The activation process of GPCRs (Fig. 1.8) is initiated upon the binding of a Ligand to the receptor on the membrane of the cell. This promotes a conformational change in the G-protein which has alpha, beta, and gamma subunits attached. The alpha subunit which has a guanosine diphosphate (GDP) molecule attached gains a phosphate and GDP is replaced with guanosine triphosphate

(GTP). The active alpha subunit then detaches from the beta and gamma subunits. Inactivation occurs when GTP loses a phosphate and rejoins the beta and gamma subunits allowing for the process to be repeated.

The first models of the complete β_1-adrenergic system for the ventricular myocyte were developed by Saucerman et al.[16] for rat ventricular myocytes. The model included the electrophysiological and calcium handling components adapted from the Luo-Rudy 2 model[11] and rabbit ventricular myocyte[17] as well as the biochemical aspects of the signaling system. In this first model, Saucerman et al.[16] used only two protein kinase A (PKA) targets, the L-type Ca^{2+} channels and phospholamban. As the β_1-adrenergic system is a key effector in metabolism, gene mutations [18,19,20], and cardiac myocyte contraction, Saucerman et al.[16] used their model to conduct a comparative study of the overexpression of β_1-adrenergic receptors versus the overexpression of adenylyl cyclase as it relates to myocyte contraction[16].

Subsequently, the model was adapted to the rat ventricular myocyte[21] to investigate the gene mutation that results in the changes of β_1-adrenergic regulation of the calcium dynamics. In the second Saucerman et al. paper[22], the model was developed for the β_1-adrenergic signaling system in rabbit ventricular myocytes, which included PKA-mediated regulation of the L-type Ca^{2+} channels, phospholamban, troponin I, ryanodine receptors, and slow delayed rectifier K^+ current. The model was applied to study the effects of KCNQ1-G589D gene mutation on the action potential, Ca^{2+} dynamics, and arrhythmia development upon stimulation of the β_1-adrenergic signaling. Based on these two models[16,22], another mathematical model of the β_1-adrenergic signaling system were developed for guinea pig[23].

G protein activation/Inactivation
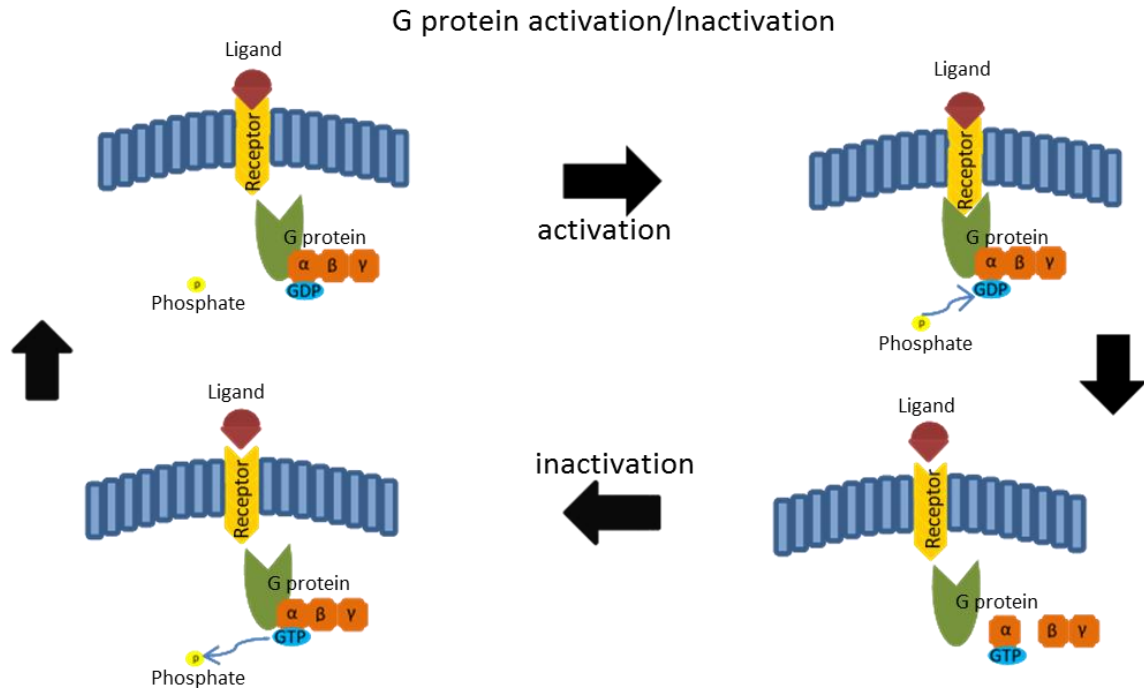
Figure 1.8 The activation/inactivation of G protein receptors. Activation of G protein receptors occurs when a ligand is bound to the receptor and the G protein couple with the receptor, undergoing a conformational change which allows the guanosine diphosphate that is attached to the alpha subunit of the G protein to gain a phosphate resulting in guanosine triphosphate. The alpha and beta-gamma subunits are active and able to bind to other effectors. Inactivation occurs when the alpha, beta and gamma subunits reattach to the G protein and a phosphate is loss from the guanosine triphosphate.

While the non-compartmentalized models contributed to our understanding of the role of the β_1-adrenergic system in cardiac myocytes on the whole cell level, more detailed models were needed to elucidate further the effects of β-adrenergic stimulation on specific targets i.e. phospholamban, troponin, ryanodine receptors, phospholemman, and several ion channels. These targets are localized in different sub-cellular domains which effectively restricts intracellular signaling.

Early compartmentalized models of the β_1-adrenergic signaling system were developed by Iancu et al.[24,25]. They included only the biochemical part of the β_1-adrenergic and M_2-muscarinic signaling systems and described the dynamics of cAMP and PKA in different

subcellular compartments (caveolar, extracaveolar, and cytosol). Further, Heijmann et al.[26] developed a compartmentalized model of the canine ventricular myocyte to elucidate the effects of this localization, particularly cAMP levels in sub-cellular compartments and their contributions to whole cell cAMP levels, action potential and calcium transients.

More recently, a compartmentalized model of the β_1-adrenergic signaling system was developed for the mouse ventricular myocyte by Bondarenko[27]. Like the earlier mathematical model, the Bondarenko model described the electrophysiological and biochemical aspects of the ventricular myocyte. In addition, the Bondarenko model incorporated new experimental data identifying localization of the two pools of the L-type Ca^{2+} channels, in the caveolar and extracaveolar compartments. The model describes the individual contributions of each subset of the L-type Ca^{2+} channel to the action potential and intracellular calcium transients, $[Ca^{2+}]_i$, along with the contribution of other major ionic currents to the action potential, subcellular cAMP dynamics, adenylyl cyclase and phosphodiesterase activation, and phosphorylation of protein kinase A targets.

The advances made by the Bondarenko model include an explanation of the mechanisms underlying prolonged action potential duration and increased intracellular calcium transients upon β_1-adrenergic stimulation in mouse ventricular myocyte. The model also predicts that stimulation of the β_1-adrenergic signaling system with isoproterenol at different frequencies affects the intracellular calcium amplitude and action potential duration. Like models prior to it, the Bondarenko model has its limitations. One of which is the absence of other myocyte signaling pathways that may be interdependent with the β_1-adrenergic signaling system, particularly the β_2-adrenergic and the CaMKII-mediated signaling systems. In this study we seek to address the inclusion of the β_2-adrenergic signaling system in the mouse ventricular myocyte.

Mathematical models which represent biological phenomena have been an invaluable tool in increasing our understanding of mechanisms that underlie many physiological outcomes. The models of cardiac cells are no different. These models have aided in our understanding of action potential generation and propagation, Ca^{2+} and Na^+ dynamics, and arrhythmias as well as the identification and investigation of potential therapeutic targets for treating diseases that arise from disruptions or mutations in the topology of the cellular system.

1.4 Purpose of the Study

In this work, a compartmentalized model of the combined β_1- and β_2-adrenergic signaling system is developed and an intuit of the effects of stimulation of β_1- and β_2-adrenergic receptors individually and concurrently are sought. The interest to this topic is motivated by several experimental findings that need to be explained by mathematical modeling. In addition, some new model predictions can be generated by simulations and they can be verified or disproved experimentally, leading to new more comprehensive mathematical ventricular myocyte models.

Experimental studies have shown remarkable differences in the physiological roles of the β_1- and β_2-adrenergic signaling systems in cardiac cells. First, they respond differently to stimulation by the same agonists and antagonists due to their different affinities. Secondly, extended stimulation of β_1-adrenergic receptors yields hypertrophic effects leading to heart failure[28], while modest increases in stimulation of β_2-adrenergic receptors has cardio-protective properties[29]. Thirdly, in some species, the effects of stimulation of β_2-adrenergic receptors are very small (rabbits, dogs, humans) or absent (mice), and cardiac myocytes need to be treated with pertussis toxin, G_i protein inhibitor, to reveal physiological effects of the receptors. Finally, mice overexpressing β_2-adrenergic receptors were generated and demonstrated increased cardiac

function at baseline conditions comparable to wild type littermates stimulated with maximal concentrations of agonist isoproterenol.

Therefore, we developed a comprehensive mathematical model of the combined β_1- and β_2-adrenergic signaling system to simulate their effects on the action potential, ionic currents, Ca^{2+} and Na^+ dynamics in mouse ventricular myocytes. This specie is chosen as it is extensively used in the experimental studies of the effects of overexpression and knock-out of the β_1- and/or β_2-adrenergic receptors themselves and the components of the β_1- and β_2-adrenergic signaling systems (G proteins, adenylyl cyclases, etc.). The model extensively verified by the experimental data obtained predominantly from mice. Using this model, we were able to simulate the effects of combined stimulation of both β_1- and β_2-adrenergic receptors, and their separate stimulation. Our simulations demonstrated lack of the effects of stimulation of β_2-adrenergic receptors under control conditions; the effects of β_2-adrenergic receptors were revealed upon inhibition of the inhibitory G protein, G_i. We also developed a mathematical model for mouse ventricular myocytes overexpressing β_2-adrenergic receptors, simulated experimental findings on adenylyl cyclase activity, protein kinase A activation, and the effects on action potential, ionic currents, and Ca^{2+} dynamics. Our mathematical models can be used by the experimental scientists in the field of cardiology to interpret their data, and for the development of mathematical models of the combined β_1- and β_2-adrenergic signaling systems in other species.

2   A MATHEMATICAL MODEL OF THE COMBINED β₁- AND β₂-ADRENERGIC SIGNALING SYSTEM IN MOUSE VENTRICULAR MYOCYTES

2.1   Model Development

A mathematical model for the combined β_1- and β_2-adrenergic signaling system in mouse ventricular myocytes (Fig. 2.1) is a natural extension of the previously published model for the β_1-adrenergic signaling system in mouse ventricular myocytes[27,30]. We incorporated a β_2-adrenergic signaling pathway in the Bondarenko model[27] and simulated biochemical reactions, electrical activity, Ca^{2+} and Na^+ dynamics (see Appendix). Our model cell consists of three compartments (caveolar (cav), extracaveolar (ecav), and cytosol (cyt); Fig. 2.1 and Appendix).

The localization of different signaling proteins and protein kinase A substrates in subcellular compartments can be found in Fig. 2.1 and the Appendix and will be described below in the corresponding chapters. In all compartments, the β_1- and β_2-adrenergic signaling systems are activated by agonist (isoproterenol) (Fig. 2.1). Stimulation of β_1-ARs activates G_s-mediated branch which includes the subsequent stimulation of $G_{s\alpha}$ and $G_{s\beta\gamma}$ subunits of G_s, adenylyl cyclases (AC4-7), which produce cyclic AMP. cAMP is hydrolyzed by phosphodiesterases (PDE2-4). cAMP further activates protein kinase A which phosphorylates target proteins, among them are PDE3 and PDE4. Stimulation of β_2-ARs activates both G_s- and G_i-mediated branches. Alpha subunits of
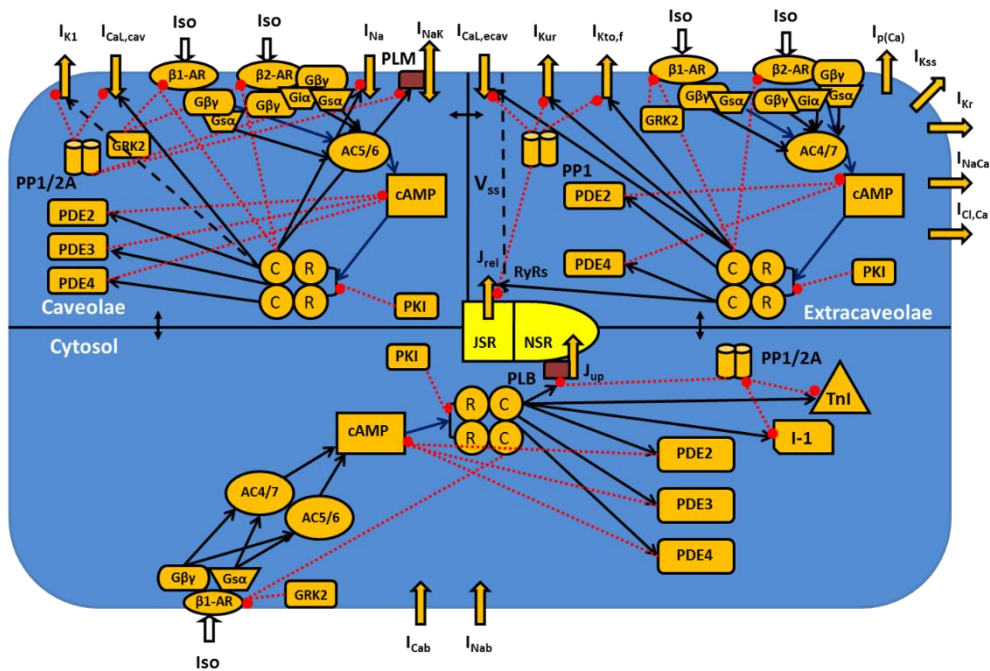
Figure 2.1 A schematic representation of the combined β₁- and β₂-adrenergic signaling system of the Mouse Ventricular Myocyte. A schematic representation of the combined β₁- and β₂-adrenergic signaling systems in mouse ventricular myocytes. The cell consists of three compartments (caveolar, extracaveolar, and cytosol) related to the combined β₁- and β₂-adrenergic signaling systems. The subspace volume (V_{ss}) is localized in the extracaveolar compartment. The biochemical portions of the combined β₁- and β₂-adrenergic signaling systems are the β₁-adrenergic receptors (β1-AR), the β₂-adrenergic receptors (β2-AR), the α-subunit of stimulatory G-protein ($G_{sα}$), the α-subunit of inhibitory G-protein ($G_{iα}$), the βγ-subunit of G_s and G_i ($G_{βγ}$), the adenylyl cyclases of type 5/6 or 4/7 (AC5/6 or AC4/7, respectively), the phosphodiesterases of type 2, 3, or 4 (PDE2, PDE3, or PDE4, respectively), the cyclic AMP (cAMP), regulatory (R) and catalytic (C) subunits of protein kinase A holoenzyme, the protein kinase A inhibitor (PKI), the G-protein-coupled receptor kinase of type 2 (GRK2), the protein phosphatases of type 1 and 2A (PP1 and PP2A, respectively), the inhibitor-1 (I-1). Targets of the combined β₁- and β₂-adrenergic signaling systems are in the caveolar (the fast Na^+ current (I_{Na}), the L-type Ca^{2+} current ($I_{CaL,cav}$), the Na^+/K^+ pump (I_{NaK}) which is regulated by phospholemman (PLM), phosphodiesterases PDE2-PDE4, and the time-independent K^+ current (I_{K1})), the extracaveolar (the L-type Ca^{2+} current ($I_{CaL,ecav}$), the rapidly recovering transient outward K^+ current ($I_{Kto,f}$), the ultrarapidly activating delayed rectifier K^+ current (I_{Kur}), ryanodine receptors (RyRs), and phosphodiesterases (PDE2, PDE4)), and cytosol (phospholamban (PLB) and troponin I (TnI)). Stimulatory links are shown by black arrows and inhibitory links are shown by red dashed lines with balls. Other transmembrane currents are the sarcolemmal Ca^{2+} pump ($I_{p(Ca)}$), the Na^+/Ca^{2+} exchanger (I_{NaCa}), the rapid delayed rectifier K^+ current (I_{Kr}), the noninactivating steady-state voltage activated K^+ current (I_{Kss}), the Ca^{2+} and Na^+ background currents (I_{Cab} and I_{Nab}), which are not affected by the combined β₁- and β₂-adrenergic signaling systems. The Ca^{2+} fluxes are uptake of Ca^{2+} from the cytosol to the network sarcoplasmic reticulum (NSR) (J_{up}) by the SERCA pump and Ca^{2+} release from the junctional sarcoplasmic reticulum (JSR) (J_{rel}) through the ryanodine receptors. $[Ca^{2+}]_i$, $[Na^+]_i$, and $[K^+]_i$ are the intracellular Ca^{2+}, Na^+, and K^+ concentrations in the caveolar, extracaveolar, and cytosol; $[Ca^{2+}]_o$, $[Na^+]_o$, and $[K^+]_o$ are the extracellular Ca^{2+}, Na^+, and K^+ concentrations.

G_s stimulate cAMP production by AC4-7 and $G_{i\alpha}$ subunits inhibit AC activity, thereby contributing to cAMP production by β_1-AR pathway. Both β_1-ARs and β_2-ARs are phosphorylated by PKA and G protein coupled receptor kinase of type 2 (GRK2). PKA is also regulated by heat-stable protein kinase inhibitor (PKI). Phosphorylation is removed by two types of phosphatases, protein phosphatase 1 and 2A. PKA target proteins are located in different compartments. The fast Na^+ current, I_{Na}, 20% of the L-type Ca^{2+} channels (the L-type Ca^{2+} current, I_{CaL}), the phospholemman, which regulates the Na^+-K^+ pump, I_{NaK}, and the time-independent K^+ current, I_{K1}, are localized in the caveolar compartment; the ultra-rapidly activating delayed rectifier K^+ current, I_{Kur}, the rapidly inactivating transient outward K^+ current, $I_{Kto,f}$, 80% of the L-type Ca^{2+} channels, and the ryanodine receptors, RyRs, are localized in the extracaveolar compartment; and phospholamban and troponin I are localized in the cytosolic compartment. The detailed description of the model development for the β_1-adrenergic signaling system can be found elsewhere[27,30]. In this chapter, we describe modifications of the model[27] that result in a mathematical model of the combined β_1- and β_2-adrenergic signaling system. We introduce a new "β_1- and β_2-adrenergic receptor module" with two types of adrenoceptors and activation of G_s and G_i proteins and also modified the "Adenylyl cyclase module" to account for the effects of G_i proteins on AC activity. The rest of the model is the same as in reference 27. The resulting model of the combined β_1- and β_2-adrenergic signaling system was verified by the experimental data (Figs. 3.1-3.6), and the model simulations are presented in Figs. 3.7-3.19.

To develop a mathematical model we used experimental data mostly from mice and from different laboratories to ensure that the model fits "average data". The model has a modular structure, starting from the "β_1- and β_2-adrenergic receptor module" and ending with the modules that describe phosphorylation of PKA target proteins (ion channels, transporters, and proteins

involved in Ca^{2+} dynamics). First, we adopted experimentally determined parameters for the model, such as concentrations of β_1- and β_2-adrenoceptors, their affinities to agonists, concentrations of G-proteins, etc. Then the simulation data of each module was fitted by the related experimental data that describes activities of the major proteins involved (adenylyl cyclases, phosphodiesterases, phosphatases, and others). Further, we simulated cAMP and PKA dynamics and compared them to the experimental data in different compartments and in the cell as a whole. The model parameters that were not measured experimentally or measured with low accuracy (the rates of G-protein activation and hydrolysis, background adenylyl cyclase activities) were adjusted to fit the output of the biochemical part of the model – cAMP and PKA dynamics. The electrophysiological part of the model was from the Bondarenko model[27].

2.2 β_1- and β_2-adrenergic receptor module

According to the experimental findings, the vast majority of β_2-adrenergic receptors and G_i proteins are located in caveolin-3-rich fractions, and most of the β_1-ARs are localized in the extracaveolar compartment[20,31]. The estimated total concentration of β_1-ARs and β_2-ARs in mouse ventricular myocytes are 0.0103 μM and 0.0053 μM, respectively[32]. The total concentration of G_i proteins was estimated based on the data of Rorabaugh et al.[33] and is equal to 10.086 μM while the total concentration of G_s protein is equal to 2.054 μM[27]. Therefore, in our model, we distribute the β_1-ARs almost evenly between the extracaveolar and cytosolic compartments, with only 1% located in the caveolar compartment[27]. In contrast, the β_2-ARs and G_i proteins almost completely are localized in the caveolar compartment (99%), and only 1% of β_2-ARs and G_i proteins are in the extracaveolar compartment, as some small cAMP production upon stimulation of β_2-ARs were observed in the extracaveolar[34]. Such distribution of β_2-ARs and G_i allowed us to obtain in the

model cAMP transients in the caveolar, extracaveolar compartments and in the cell, which are in line with the measurements of local cAMP concentrations in similar compartments in rat and mouse ventricular myocytes[34].

In the β_1- and β_2-adrenergic receptor module, the relatively fast ligand-receptor and G-protein-receptor interactions, with time scales of tens milliseconds[35], are described by algebraic equations in steady-state approximation. The slower processes of G-protein activation, PKA- and GRK2-mediated phosphorylation (hundreds of milliseconds; GRK2, G-protein-coupled receptor kinase of type 2), and cAMP accumulation (hundreds of seconds) are described by ordinary differential equations (see Appendix).

In order to derive algebraic equations which describe ligand-receptor and G-protein-receptor interactions in the caveolar compartment (see Appendix), we first consider the mass conservation laws for non-phosphorylated β_1- and β_2-adrenergic receptors and G_s-protein in that compartment:

$$[R_{\beta 1}]^{cav}_{np,tot} = [LR_{\beta 1}]^{cav}_{np} + [LR_{\beta 1}G_s]^{cav}_{np} + [R_{\beta 1}G_s]^{cav}_{np} + [R_{\beta 1}]^{cav}_{np,f},$$
(2.1)

$$[R_{\beta 2}]^{cav}_{np,tot} = [LR_{\beta 2}]^{cav}_{np} + [LR_{\beta 2}G_s]^{cav}_{np} + [R_{\beta 2}G_s]^{cav}_{np} + [R_{\beta 2}]^{cav}_{np,f},$$
(2.2)

$$[G_s]^{cav}_{\alpha\beta\gamma} = [LR_{\beta 1}G_s]^{cav}_{np} + [R_{\beta 1}G_s]^{cav}_{np} + [LR_{\beta 2}G_s]^{cav}_{np} + [R_{\beta 2}G_s]^{cav}_{np} + [G_s]^{cav}_f,$$
(2.3)

where $[R_{\beta 1}]^{cav}_{np,tot}$ is the total concentration of non-phosphorylated (*np*) β_1-ARs in the caveolar compartment, $[LR_{\beta 1}]^{cav}_{np}$ is the concentration of β_1-ARs with bound ligand *L* (concentration [*L*]), $[LR_{\beta 1}G_s]^{cav}_{np}$ is the concentration of β_1-ARs with bound ligand *L* and stimulatory G-protein G_s, $[R_{\beta 1}G_s]^{cav}_{np}$ is the concentration of β_1-ARs with bound G_s, $[R_{\beta 1}]^{cav}_{np,f}$ is the concentration of free β_1-ARs, $[R_{\beta 2}]^{cav}_{np,tot}$ is the total concentration of non-phosphorylated β_2-ARs in the caveolar compartment, $[LR_{\beta 2}]^{cav}_{np}$ is the concentration of β_2-ARs with bound ligand *L*, $[LR_{\beta 2}G_s]^{cav}_{np}$ is the

concentration of β2-ARs with bound ligand L and stimulatory G-protein G_s, $[R_{\beta2}G_s]_{np}^{cav}$ is the concentration of β2-ARs with bound G_s, $[R_{\beta2}]_{np,f}^{cav}$ is the concentration of free β2-ARs, $[G_s]_{\alpha\beta\gamma}^{cav}$ is the total concentration of the stimulatory G-protein G_s, and $[G_s]_f^{cav}$ is the concentration of free G_s.

Concentrations of complexes $[LR_{\beta1}]_{np}^{cav}$, $[LR_{\beta1}G_s]_{np}^{cav}$, $[R_{\beta1}G_s]_{np}^{cav}$, $[LR_{\beta2}]_{np}^{cav}$, $[LR_{\beta2}G_s]_{np}^{cav}$, and $[R_{\beta2}G_s]_{np}^{cav}$ can be obtained from the steady-state approximation for the corresponding biochemical reactions[27], provided that the related dissociation constants are known. They are given by the equations:

$$[LR_{\beta1}]_{np} = \frac{k_+[L][R_{\beta1}]}{k_-} = \frac{[L][R_{\beta1}]_{np,f}}{K_{\beta1,L}} \tag{2.4}$$

$$[LR_{\beta1}G_S]_{np} = \frac{[L][R_{\beta1}]_{np,f}[G_s]_f}{K_{\beta1,C}K_{\beta1,H}} \tag{2.5}$$

$$[R_{\beta1}G_S]_{np} = \frac{[R_{\beta1}]_{np,f}[G_s]_f}{K_{\beta1,C}} \tag{2.6}$$

$$[LR_{\beta2}]_{np} = \frac{k_+[L][R_{\beta2}]}{k_-} = \frac{[L][R_{\beta2}]_{np,f}}{K_{\beta2,L}} \tag{2.7}$$

$$[LR_{\beta2}G_S]_{np} = \frac{[L][R_{\beta2}]_{np,f}[G_s]_f}{K_{\beta2,C}K_{\beta2,H}} \tag{2.8}$$

$$[R_{\beta2}G_S]_{np} = \frac{[R_{\beta2}]_{np,f}[G_s]_f}{K_{\beta2,C}} \tag{2.9}$$

Substitution of the equations for $[LR_{\beta1}]_{np}^{cav}$, $[LR_{\beta1}G_s]_{np}^{cav}$, and $[R_{\beta1}G_s]_{np}^{cav}$ into equation (2.1) and for $[LR_{\beta2}]_{np}^{cav}$, $[LR_{\beta2}G_s]_{np}^{cav}$ and $[R_{\beta2}G_s]_{np}^{cav}$ into equation (2.2) gives:

$$\begin{aligned}
\left[R_{\beta1}\right]_{np,tot} &= \frac{[L]\left[R_{\beta1}\right]_{np,f}}{K_{\beta1,L}} + \frac{[L]\left[R_{\beta1}\right]_{np,f}[G_s]_f}{K_{\beta1,C}K_{\beta1,H}} + \frac{\left[R_{\beta1}\right]_{np,f}[G_s]_f}{K_{\beta1,C}} + \left[R_{\beta1}\right]_{np,f} \\
&= \left[R_{\beta1}\right]_{np,f}\left[\frac{[L]}{K_{\beta1,L}} + \frac{[L][G_s]_f}{K_{\beta1,C}K_{\beta1,H}} + \frac{[G_s]_f}{K_{\beta1,C}} + 1\right]
\end{aligned} \tag{2.10}$$

$$\left[R_{\beta 2}\right]_{np,tot} = \frac{[L]\left[R_{\beta 2}\right]_{np,f}}{K_{\beta 2,L}} + \frac{[L]\left[R_{\beta 2}\right]_{np,f}[G_s]_f}{K_{\beta 2,C}K_{\beta 2,H}} + \frac{\left[R_{\beta 2}\right]_{np,f}[G_s]_f}{K_{\beta 2,C}} + \left[R_{\beta 2}\right]_{np,f}$$

$$= \left[R_{\beta 2}\right]_{np,f}\left[\frac{[L]}{K_{\beta 2,L}} + \frac{[L][G_s]_f}{K_{\beta 2,C}K_{\beta 2,H}} + \frac{[G_s]_f}{K_{\beta 2,C}} + 1\right] \tag{2.11}$$

Solving for the concentration of free, non-phosphorylated β₁- and β₂-adrenergic receptors results in the following equations:

$$\left[R_{\beta 1}\right]_{np,f} = \frac{\left[R_{\beta 1}\right]_{np,tot}}{\left[1 + \dfrac{[L]}{K_{\beta 1,L}} + [G_s]_f\left(\dfrac{[L]}{K_{\beta 1,C}K_{\beta 1,H}} + \dfrac{1}{K_{\beta 1,C}}\right)\right]} \tag{2.12}$$

$$\left[R_{\beta 2}\right]_{np,f} = \frac{\left[R_{\beta 2}\right]_{np,tot}}{\left[1 + \dfrac{[L]}{K_{\beta 2,L}} + [G_s]_f\left(\dfrac{[L]}{K_{\beta 2,C}K_{\beta 2,H}} + \dfrac{1}{K_{\beta 2,C}}\right)\right]}. \tag{2.13}$$

Further substitution of the expressions for $[LR_{\beta 1}G_s]_{np}^{cav}$, $[R_{\beta 1}G_s]_{np}^{cav}$, $[LR_{\beta 2}G_s]_{np}^{cav}$, and $[R_{\beta 2}G_s]_{np}^{cav}$ into equation (2.3) results in:

$$[G_s]_{\alpha\beta\gamma} = [G_s]_f\left[\frac{[L]\left[R_{\beta 1}\right]_{np,f}}{K_{\beta 1,C}K_{\beta 1,H}} + \frac{\left[R_{\beta 1}\right]_{np,f}}{K_{\beta 1,C}} + \frac{[L]\left[R_{\beta 2}\right]_{np,f}}{K_{\beta 2,C}K_{\beta 2,H}} + \frac{\left[R_{\beta 2}\right]_{np,f}}{K_{\beta 2,C}} + 1\right]$$

$$= [G_s]_f\left[\left[R_{\beta 1}\right]_{np,f}\left(\frac{[L]}{K_{\beta 1,C}K_{\beta 1,H}} + \frac{1}{K_{\beta 1,C}}\right) + \left[R_{\beta 2}\right]_{np,f}\left(\frac{[L]}{K_{\beta 2,C}K_{\beta 2,H}} + \frac{1}{K_{\beta 2,C}}\right) + 1\right] \tag{2.14}$$

Substituting the expressions for free non-phosphorylated β₁- and β₂-adrenergic receptors gives:

$$[G_s]_{\alpha\beta\gamma} = [G_s]_f \left[\left(\left(\frac{[R_{\beta1}]_{np,\text{tot}}}{1 + \frac{[L]}{K_{\beta1,L}} + [G_s]_f \left(\frac{[L]}{K_{\beta1,C}K_{\beta1,H}} + \frac{1}{K_{\beta1,C}} \right)} \right) \left(\frac{[L]}{K_{\beta1,C}K_{\beta1,H}} + \frac{1}{K_{\beta1,C}} \right) + \left(\frac{[R_{\beta2}]_{np,\text{tot}}}{1 + \frac{[L]}{K_{\beta2,L}} + [G_s]_f \left(\frac{[L]}{K_{\beta2,C}K_{\beta2,H}} + \frac{1}{K_{\beta2,C}} \right)} \right) \left(\frac{[L]}{K_{\beta2,C}K_{\beta2,H}} + \frac{1}{K_{\beta2,C}} \right) + 1 \right]$$

$$[G_s]_{\alpha\beta\gamma} = [G_s]_f \left[\frac{[L][R_{\beta1}]_{np,\text{tot}}}{K_{\beta1,C}K_{\beta1,H} + \frac{[L]K_{\beta1,C}K_{\beta1,H}}{K_{\beta1,L}} + [G_s]_f([L]+K_{\beta1,H})} + \frac{[R_{\beta1}]_{np,\text{tot}}}{K_{\beta1,C} + \frac{[L]K_{\beta1,C}}{K_{\beta1,L}} + [G_s]_f\left(\frac{[L]}{K_{\beta1,H}}+1\right)} + \frac{[L][R_{\beta2}]_{np,\text{tot}}}{K_{\beta2,C}K_{\beta2,H} + \frac{[L]K_{\beta2,C}K_{\beta2,H}}{K_{\beta2,L}} + [G_s]_f([L]+K_{\beta2,H})} + \frac{[R_{\beta2}]_{np,\text{tot}}}{K_{\beta2,C} + \frac{[L]K_{\beta2,C}}{K_{\beta2,L}} + [G_s]_f\left(\frac{[L]}{K_{\beta2,H}}+1\right)} + 1 \right]$$

$$[G_s]_{\alpha\beta\gamma} = \frac{[G_s]_f[R_{\beta1}]_{np,\text{tot}}([L]+K_{\beta1,H})}{K_{\beta1,C}K_{\beta1,H} + \frac{[L]K_{\beta1,C}K_{\beta1,H}}{K_{\beta1,L}} + [G_s]_f([L]+K_{\beta1,H})} +$$

$$\frac{[G_s]_f[R_{\beta2}]_{np,\text{tot}}([L]+K_{\beta2,H})}{K_{\beta2,C}K_{\beta2,H} + \frac{[L]K_{\beta2,C}K_{\beta2,H}}{K_{\beta2,L}} + [G_s]_f([L]+K_{\beta2,H})} + [G_s]_f \qquad (2.15)$$

This equation needs to be solved for the concentration of free G_s protein, $[G_s]_f$:

$$[G_s]_{\alpha\beta\gamma} \left[K_{\beta1,C}K_{\beta1,H} + \frac{[L]K_{\beta1,C}K_{\beta1,H}}{K_{\beta1,L}} + [G_s]_f([L]+K_{\beta1,H}) \right] \left[K_{\beta2,C}K_{\beta2,H} + \frac{[L]K_{\beta2,C}K_{\beta2,H}}{K_{\beta2,L}} + [G_s]_f([L]+K_{\beta2,H}) \right] =$$

$$[G_s]_f[R_{\beta1}]_{np,\text{tot}}([L]+K_{\beta1,H}) \left[K_{\beta2,C}K_{\beta2,H} + \frac{[L]K_{\beta2,C}K_{\beta2,H}}{K_{\beta2,L}} + [G_s]_f([L]+K_{\beta2,H}) \right] +$$

$$[G_s]_f[R_{\beta2}]_{np,\text{tot}}([L]+K_{\beta2,H}) \left[K_{\beta1,C}K_{\beta1,H} + \frac{[L]K_{\beta1,C}K_{\beta1,H}}{K_{\beta1,L}} + [G_s]_f([L]+K_{\beta1,H}) \right] +$$

$$[G_s]_f \left[K_{\beta1,C}K_{\beta1,H} + \frac{[L]K_{\beta1,C}K_{\beta1,H}}{K_{\beta1,L}} + [G_s]_f([L]+K_{\beta1,H}) \right] \left[K_{\beta2,C}K_{\beta2,H} + \frac{[L]K_{\beta2,C}K_{\beta2,H}}{K_{\beta2,L}} + [G_s]_f([L]+K_{\beta2,H}) \right]$$

$$[G_s]_{\alpha\beta\gamma}\left(K_{\beta2,C}K_{\beta2,H}+\frac{[L]K_{\beta2,C}K_{\beta2,H}}{K_{\beta2,L}}\right)\left([L]+K_{\beta1,H}\right)[G_s]_f -$$

$$[G_s]_{\alpha\beta\gamma}\left([L]+K_{\beta1,H}\right)\left([L]+K_{\beta2,H}\right)[G_s]_f^{2}$$

$$-[G_s]_{\alpha\beta\gamma}\left(K_{\beta1,C}K_{\beta1,H}+\frac{[L]K_{\beta1,C}K_{\beta1,H}}{K_{\beta1,L}}\right)\left(K_{\beta2,C}K_{\beta2,H}+\frac{[L]K_{\beta2,C}K_{\beta2,H}}{K_{\beta2,L}}\right)-$$

$$[G_s]_{\alpha\beta\gamma}\left(K_{\beta1,C}K_{\beta1,H}+\frac{[L]K_{\beta1,C}K_{\beta1,H}}{K_{\beta1,L}}\right)\left([L]+K_{\beta2,H}\right)[G_s]_f -$$

$$+\left[R_{\beta1}\right]_{np,tot}\left([L]+K_{\beta1,H}\right)\left(K_{\beta2,C}K_{\beta2,H}+\frac{[L]K_{\beta2,C}K_{\beta2,H}}{K_{\beta2,L}}\right)[G_s]_f+\left[R_{\beta1}\right]_{np,tot}\left([L]+K_{\beta1,H}\right)\left([L]+K_{\beta2,H}\right)[G_s]_f^{2}+$$

$$\left[R_{\beta2}\right]_{np,tot}\left([L]+K_{\beta2,H}\right)\left(K_{\beta1,C}K_{\beta1,H}+\frac{[L]K_{\beta1,C}K_{\beta1,H}}{K_{\beta1,L}}\right)[G_s]_f+\left[R_{\beta2}\right]_{np,tot}\left([L]+K_{\beta2,H}\right)\left([L]+K_{\beta1,H}\right)[G_s]_f^{2}+$$

$$\left(K_{\beta1,C}K_{\beta1,H}+\frac{[L]K_{\beta1,C}K_{\beta1,H}}{K_{\beta1,L}}\right)\left(K_{\beta2,C}K_{\beta2,H}+\frac{[L]K_{\beta2,C}K_{\beta2,H}}{K_{\beta2,L}}\right)[G_s]_f+$$

$$\left(K_{\beta1,C}K_{\beta1,H}+\frac{[L]K_{\beta1,C}K_{\beta1,H}}{K_{\beta1,L}}\right)\left([L]+K_{\beta2,H}\right)[G_s]_f^{2}+\left(K_{\beta2,C}K_{\beta2,H}+\frac{[L]K_{\beta2,C}K_{\beta2,H}}{K_{\beta2,L}}\right)\left([L]+K_{\beta1,H}\right)[G_s]_f^{2}+$$

$$\left([L]+K_{\beta1,H}\right)\left([L]+K_{\beta2,H}\right)[G_s]_f^{3}=0$$

or

$$\left([L]+K_{\beta1,\text{H}}\right)\left([L]+K_{\beta2,\text{H}}\right)[G_s]_f^3 +$$

$$\begin{bmatrix} \left([L]+K_{\beta1,\text{H}}\right)\left([L]+K_{\beta2,\text{H}}\right)\left(\left[R_{\beta1}\right]_{np,tot}+\left[R_{\beta2}\right]_{np,tot}\right)+ \\ \left(K_{\beta1,\text{C}}K_{\beta1,\text{H}}+\dfrac{[L]K_{\beta1,\text{C}}K_{\beta1,\text{H}}}{K_{\beta1,\text{L}}}\right)\left([L]+K_{\beta2,\text{H}}\right)+\left(K_{\beta2,\text{C}}K_{\beta2,\text{H}}+\dfrac{[L]K_{\beta2,\text{C}}K_{\beta2,\text{H}}}{K_{\beta2,\text{L}}}\right)\left([L]+K_{\beta1,\text{H}}\right)+ \\ [G_s]_{\alpha\beta\gamma}\left([L]+K_{\beta1,\text{H}}\right)\left([L]+K_{\beta2,\text{H}}\right) \end{bmatrix}[G_s]_f^2 +$$

$$\begin{bmatrix} \left([L]+K_{\beta1,\text{H}}\right)\left(K_{\beta2,\text{C}}K_{\beta2,\text{H}}+\dfrac{[L]K_{\beta2,\text{C}}K_{\beta2,\text{H}}}{K_{\beta2,\text{L}}}\right)\left(\left[R_{\beta1}\right]_{np,tot}-[G_s]_{\alpha\beta\gamma}\right)+ \\ \left([L]+K_{\beta2,\text{H}}\right)\left(K_{\beta1,\text{C}}K_{\beta1,\text{H}}+\dfrac{[L]K_{\beta1,\text{C}}K_{\beta1,\text{H}}}{K_{\beta1,\text{L}}}\right)\left(\left[R_{\beta2}\right]_{np,tot}-[G_s]_{\alpha\beta\gamma}\right)+ \\ \left(K_{\beta1,\text{C}}K_{\beta1,\text{H}}+\dfrac{[L]K_{\beta1,\text{C}}K_{\beta1,\text{H}}}{K_{\beta1,\text{L}}}\right)\left(K_{\beta2,\text{C}}K_{\beta2,\text{H}}+\dfrac{[L]K_{\beta2,\text{C}}K_{\beta2,\text{H}}}{K_{\beta2,\text{L}}}\right) \end{bmatrix}[G_s]_f -$$

$$[G_s]_{\alpha\beta\gamma}\left(K_{\beta1,\text{C}}K_{\beta1,\text{H}}+\frac{[L]K_{\beta1,\text{C}}K_{\beta1,\text{H}}}{K_{\beta1,\text{L}}}\right)\left(K_{\beta2,\text{C}}K_{\beta2,\text{H}}+\frac{[L]K_{\beta2,\text{C}}K_{\beta2,\text{H}}}{K_{\beta2,\text{L}}}\right) = 0 \qquad (2.16)$$

As a result, we obtain a cubic equation in $[G_s]_f$ with coefficients:

$$a_{\beta2,\text{s}} = \left([L]+K_{\beta1,H}\right)\left([L]+K_{\beta2,H}\right)$$

$$b_{\beta2,\text{s}} = \left([L]+K_{\beta1,H}\right)\left([L]+K_{\beta2,H}\right)\left([R_{\beta1}]_{np,tot}+[R_{\beta2}]_{np,tot}\right)+$$
$$\left(K_{\beta1,C}K_{\beta1,H}+\frac{[L]K_{\beta1,C}K_{\beta1,H}}{K_{\beta1,L}}\right)\left([L]+K_{\beta2,H}\right)+\left(K_{\beta2,C}K_{\beta2,H}+\frac{[L]K_{\beta2,C}K_{\beta2,H}}{K_{\beta2,L}}\right)\left([L]+K_{\beta1,H}\right)-$$
$$[G_s]_{\alpha\beta\gamma}\left([L]+K_{\beta1,H}\right)\left([L]+K_{\beta2,H}\right)$$

$$c_{\beta2,\text{s}} = \left([L]+K_{\beta1,H}\right)\left(K_{\beta2,C}K_{\beta2,H}+\frac{[L]K_{\beta2,C}K_{\beta2,H}}{K_{\beta2,L}}\right)\left([R_{\beta1}]_{np,tot}-[G_s]_{\alpha\beta\gamma}\right)+$$
$$\left([L]+K_{\beta2,H}\right)\left(K_{\beta1,C}K_{\beta1,H}+\frac{[L]K_{\beta1,C}K_{\beta1,H}}{K_{\beta1,L}}\right)\left([R_{\beta2}]_{np,tot}-[G_s]_{\alpha\beta\gamma}\right)+$$
$$\left(K_{\beta1,C}K_{\beta1,H}+\frac{[L]K_{\beta1,C}K_{\beta1,H}}{K_{\beta1,L}}\right)\left(K_{\beta2,C}K_{\beta2,H}+\frac{[L]K_{\beta2,C}K_{\beta2,H}}{K_{\beta2,L}}\right)$$

$$d_{\beta2,\text{s}} = -[G_s]_{\alpha\beta\gamma}\left(K_{\beta1,C}K_{\beta1,H}+\frac{[L]K_{\beta1,C}K_{\beta1,H}}{K_{\beta1,L}}\right)\left(K_{\beta2,C}K_{\beta2,H}+\frac{[L]K_{\beta2,C}K_{\beta2,H}}{K_{\beta2,L}}\right)$$

$[G_s]_{\alpha\beta\gamma}$ is determined from the mass conservation law for a given compartment:

$$[G_s]_{\alpha\beta\gamma}^{cav} = f_{Gs}^{cav} \cdot [G_s]_{tot} \cdot \frac{V_{cell}}{V_{cav}} - [G_s]_{\alpha,GTP}^{cav} - [G_s]_{\alpha,GDP}^{cav} \qquad (2.17)$$

where $[G_s]_{\alpha,GTP}$ and $[G_s]_{\alpha,GDP}$ are described by the ordinary differential equations:

$$\frac{d[G_s]_{\alpha,GTP}}{dt} = k_{act2,Gs} \cdot ([R_{\beta1}G_s]_{np} + [R_{\beta2}G_s]_{np}) + k_{act1,Gs} \cdot ([LR_{\beta1}G_s]_{np} + [LR_{\beta2}G_s]_{np}) - k_{hyd,Gs} \cdot [G_s]_{\alpha,GTP}$$

$$(2.18)$$

$$\frac{d[G_s]_{\alpha,GDP}}{dt} = k_{hyd,Gs} \cdot [G_s]_{\alpha,GTP} - k_{reas,Gs} \cdot [G]_{\beta\gamma} \cdot [G_s]_{\alpha,GDP} \qquad (2.19)$$

$$\frac{d[G_i]_{\alpha,GTP}}{dt} = k_{act2,Gi} \cdot [R_{\beta2}G_i]_{PKA} + k_{act1,Gi} \cdot [LR_{\beta2}G_i]_{PKA} - k_{hyd,Gi} \cdot [G_i]_{\alpha,GTP} \qquad (2.20)$$

$$\frac{d[G_i]_{\alpha,GDP}}{dt} = k_{hyd,Gi} \cdot [G_i]_{\alpha,GTP} - k_{reas,Gi} \cdot [G]_{\beta\gamma} \cdot [G_i]_{\alpha,GDP} \qquad (2.21)$$

$$\frac{d[G]_{\beta\gamma}}{dt} = k_{act2,Gs} \cdot ([R_{\beta1}G_s]_{np} + [R_{\beta2}G_s]_{np}) + k_{act1,Gs} \cdot ([LR_{\beta1}G_s]_{np} + [LR_{\beta2}G_s]_{np}) + k_{act2,Gi} \cdot [R_{\beta2}G_i]_{PKA}$$

$$+ k_{act1,Gi} \cdot [LR_{\beta2}G_i]_{PKA} - k_{reas,Gs} \cdot [G]_{\beta\gamma} \cdot [G_s]_{\alpha,GDP} - k_{reas,Gi} \cdot [G]_{\beta\gamma} \cdot [G_i]_{\alpha,GDP} \qquad (2.22)$$

where $[G_s]_{\alpha,GTP}$ and $[G_s]_{\alpha,GDP}$ are the concentrations of stimulatory G proteins with guanosine

triphosphate and guanosine diphosphate respectively attached to their alpha subunits. $[G_i]_{\alpha,GTP}$

and $[G_i]_{\alpha,GDP}$ are the concentrations of inhibitory G proteins with guanosine triphosphate and

guanosine diphosphate attached to their alpha subunits. $[G]_{\beta\gamma}$ represents the concentration of

beta-gamma unit of G proteins. The constants k_{act1} and k_{act2} are the rates at which ligand bound

β₁- or β₂-adrenergic receptors couple with stimulatory and inhibitory G proteins and non-ligand

bound β₁- or β₂-adrenergic receptors couple with both stimulatory and inhibitory G proteins.

k_{hyd} and k_{reas} are the rates at which alpha subunits of stimulatory and inhibitory G proteins loose

or gain a phosphate. The subscripts *np* refers to the non-phosphorylated fraction and PKA refers to the remaining protein kinase A phosphorylated fraction.

To solve the resulting cubic equation for non-negative roots we normalized the cubic equation to the form:

$$x^3 + px^2 + qx + r = 0; \text{ where } p = \frac{b_{\beta 2,s}}{a_{\beta 2,s}}, \quad q = \frac{c_{\beta 2,s}}{a_{\beta 2,s}}, \text{ and } r = \frac{d_{\beta 2,s}}{a_{\beta 2,s}}.$$

By redefining coefficients to eliminate the quadratic term we obtain:

$$x^3 + Ax = B; \text{ where } A = \frac{1}{3}\left(3q - (p)^2\right) \text{ and } B = \frac{1}{27}\left(2(p)^3 - 9pq + 27r\right)$$

Making Vieta's substitution, $x = w - \frac{A}{3w}$ and then multiplying by w^3 yields an equation which is quadratic in form. The quadratic formula applied to this new equation yields solutions that can be termed as:

$$M = \left(-\frac{B}{2} - \sqrt{D}\right)^{1/3} \text{ and } N = \left(-\frac{B}{2} + \sqrt{D}\right)^{1/3} \text{ where the discriminate } D = \frac{(A)^3}{27} + \frac{(B)^2}{4}.$$

Here, there are four possible cases.

Case 1: $D > 0$. Then $y_1 = M + N$; y_2 and y_3 are complex conjugates.

Case 2: $D = 0$. Then $y_1 = M + N$; $y_2 = y_3 = -(M + N)/2$;

Case 3: $D < 0$ and $B > 0$. Then $\phi = \arccos\left(-\sqrt{\frac{(B)^2/4}{(-A)^3/27}}\right)$ and

$$y_1 = 2\sqrt{-\frac{A}{3}}\cos(\phi); \; y_2 = 2\sqrt{-\frac{A}{3}}\cos(\phi + 2\pi/3); \; y_3 = 2\sqrt{-\frac{A}{3}}\cos(\phi + 4\pi/3)$$

Case 4: $D < 0$ and $B < 0$. Then $\phi = \arccos\left(\sqrt{\frac{(B)^2/4}{(-A)^3/27}}\right)$ and

$$y_1 = 2\sqrt{-\frac{A}{3}}\cos(\phi\ );\ y_2 = 2\sqrt{-\frac{A}{3}}\cos(\phi\ + 2\pi/3);\ y_3 = 2\sqrt{-\frac{A}{3}}\cos(\phi\ + 4\pi/3)$$

The solutions to the cubic equation are then $w_i = y_i - \dfrac{p}{3}, \quad i = 1, 2, 3,$ and

$$[G_s]_f = \max\{w_1, w_3, w_3\}$$

The graphs of the cubic function given by $[G_s]_f$ for 0μM, 1μM and 10μM of the agonist

ligand Isoproterenol is shown in figure 2.2. The maximum solution ensures a positive value.
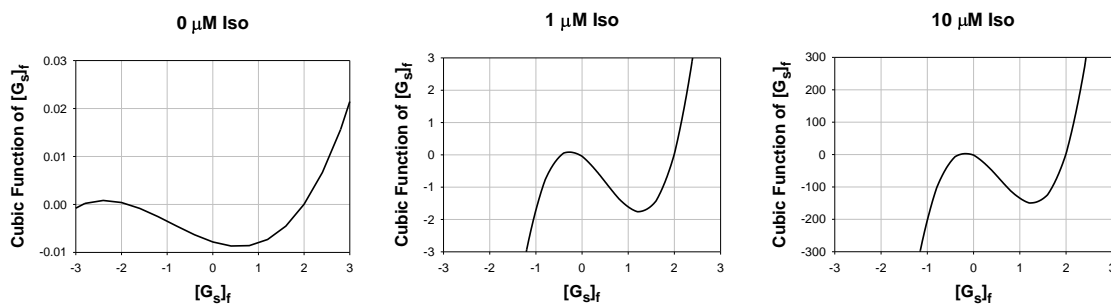
Figure 2.2 The graph of the cubic function given by $[G_s]_f$ for 0μM, 1μM and 10μM of Isoproterenol

Because experimental data[36] shows that interaction of non-phosphorylated β₂-ARs occurs

predominantly with G_s protein and phosphorylated β₂-ARs with G_i protein, we considered the mass

conservation laws for PKA phosphorylated β₂-adrenergic receptors and G_i-protein in the caveolar

compartment (a similar derivation is done for the extracaveolar compartment):

$$[R_{\beta 2}]^{cav}_{PKA,tot} = [LR_{\beta 2}]^{cav}_{PKA} + [LR_{\beta 2}G_i]^{cav}_{PKA} + [R_{\beta 2}G_i]^{cav}_{PKA} + [R_{\beta 2}]^{cav}_{PKA,f}, \tag{2.23}$$

$$[G_i]^{cav}_{\alpha\beta\gamma} = [LR_{\beta 2}G_i]^{cav}_{PKA} + [R_{\beta 2}G_i]^{cav}_{PKA} + [G_i]^{cav}_f, \tag{2.24}$$

where $[R_{\beta 2}]^{cav}_{PKA,tot}$ is the total concentration of PKA-phosphorylated β₂-ARs in the caveolar

compartment, $[LR_{\beta 2}]^{cav}_{PKA}$ is the concentration of β₂-ARs with bound ligand L, $[LR_{\beta 2}G_i]^{cav}_{PKA}$ is the

concentration of β₂-ARs with bound ligand L and inhibitory G-protein G_i, $[R_{\beta2}G_i]^{cav}_{PKA}$ is the concentration of β₂-ARs with bound G_i, $[R_{\beta2}]^{cav}_{PKA,f}$ is the concentration of free PKA-phosphorylated β₂-ARs, $[G_i]^{cav}_{\alpha\beta\gamma}$ is the total concentration of the inhibitory G-protein G_i, and $[G_i]^{cav}_f$ is the concentration of free G_i.

Concentrations of complexes $[LR_{\beta2}]^{cav}_{PKA}$, $[LR_{\beta2}G_i]^{cav}_{PKA}$, and $[R_{\beta2}G_i]^{cav}_{PKA}$ can be obtained from the steady-state approximation for corresponding biochemical reactions:

$$[LR_{\beta2}]_{PKA} = \frac{[L][R_{\beta2}]_{PKA,f}}{K_{\beta2,L}} \tag{2.25}$$

$$[LR_{\beta2}G_i]_{PKA} = \frac{[L][R_{\beta2}]_{PKA,f}[G_i]_f}{K_{\beta2,A}K_{\beta2,F}} \tag{2.26}$$

$$[R_{\beta2}G_i]_{PKA} = \frac{[R_{\beta2}]_{PKA,f}[G_i]_f}{K_{\beta2,A}} \tag{2.27}$$

Substitution of the equations for $[LR_{\beta2}G_i]^{cav}_{PKA}$ and $[R_{\beta2}G_i]^{cav}_{PKA}$ into equation (2.24) yields:

$$[G_i]_{\alpha\beta\gamma} = \frac{[L]\big[R_{\beta2}\big]_{pka,f}[G_i]_f}{K_{\beta2,A}K_{\beta2,F}} + \frac{\big[R_{\beta2}\big]_{pka,f}[G_i]_f}{K_{\beta2,A}} + [G_i]_f \tag{2.28}$$

and solution with respect to $[G_i]^{cav}_f$ results in equation:

$$[G_i]_f = \frac{[G_i]_{\alpha\beta\gamma}}{1 + \big[R_{\beta2}\big]_{pka,f}\left[\dfrac{1}{K_{\beta2,A}} + \dfrac{[L]}{K_{\beta2,A}K_{\beta2,F}}\right]} \tag{2.29}$$

Further substitution of the expressions for $[LR_{\beta2}]^{cav}_{PKA}$, $[LR_{\beta2}G_i]^{cav}_{PKA}$, $[R_{\beta2}G_i]^{cav}_{PKA}$, and $[G_i]^{cav}_f$ into equation (2.23) results in equation:

$$\left[R_{\beta 2}\right]_{pka,tot} = \frac{[L]\left[R_{\beta 2}\right]_{pka,f}}{K_{\beta 2,l}} + \frac{[L]\left[R_{\beta 2}\right]_{pka,f}\left[G_i\right]_{\alpha\beta\gamma}}{K_{\beta 2,A}K_{\beta 2,F}\left[1+\left[R_{\beta 2}\right]_{pka,f}\left[\frac{1}{K_{\beta 2,A}}+\frac{[L]}{K_{\beta 2,A}K_{\beta 2,F}}\right]\right]}$$

$$+\frac{\left[R_{\beta 2}\right]_{pka,f}\left[G_i\right]_{\alpha\beta\gamma}}{K_{\beta 2,A}\left[1+\left[R_{\beta 2}\right]_{pka,f}\left[\frac{1}{K_{\beta 2,A}}+\frac{[L]}{K_{\beta 2,A}K_{\beta 2,F}}\right]\right]} + \left[R_{\beta 2}\right]_{pka,f} \qquad (2.30)$$

Total PKA phosphorylated β2-adrenergic receptors is given by a differential equation, however, here we can obtain an expression for the free PKA phosphorylated β2-adrenergic receptors.

$$\left[R_{\beta 2}\right]_{pka,tot}\left(1+\left[R_{\beta 2}\right]_{pka,f}\left[\frac{1}{K_{\beta 2,A}}+\frac{[L]}{K_{\beta 2,A}K_{\beta 2,F}}\right]\right) = \frac{[L]\left[R_{\beta 2}\right]_{pka,f}}{K_{\beta 2,L}}\left(1+\left[R_{\beta 2}\right]_{pka,f}\left[\frac{1}{K_{\beta 2,A}}+\frac{[L]}{K_{\beta 2,A}K_{\beta 2,F}}\right]\right)$$

$$+\frac{[L]\left[R_{\beta 2}\right]_{pka,f}\left[G_i\right]_{\alpha\beta\gamma}}{K_{\beta 2,A}K_{\beta 2,F}} + \frac{\left[R_{\beta 2}\right]_{pka,f}\left[G_i\right]_{\alpha\beta\gamma}}{K_{\beta 2,A}} + \left[R_{\beta 2}\right]_{pka,f}\left(1+\left[R_{\beta 2}\right]_{pka,f}\left[\frac{1}{K_{\beta 2,A}}+\frac{[L]}{K_{\beta 2,A}K_{\beta 2,F}}\right]\right)$$

$$-\left[R_{\beta 2}\right]_{pka,tot} - \left[R_{\beta 2}\right]_{pka,tot}\left(\frac{1}{K_{\beta 2,A}}+\frac{[L]}{K_{\beta 2,A}K_{\beta 2,F}}\right)\left[R_{\beta 2}\right]_{pka,f} + \frac{[L]}{K_{\beta 2,L}}\left[R_{\beta 2}\right]_{pka,f}$$

$$+\frac{[L]}{K_{\beta 2,L}}\left(\frac{1}{K_{\beta 2,A}}+\frac{[L]}{K_{\beta 2,A}K_{\beta 2,F}}\right)\left[R_{\beta 2}\right]^2_{pka,f} + \frac{[L]\left[G_i\right]_{\alpha\beta\gamma}}{K_{\beta 2,A}K_{\beta 2,F}}\left[R_{\beta 2}\right]_{pka,f} + \frac{\left[G_i\right]_{\alpha\beta\gamma}}{K_{\beta 2,A}}\left[R_{\beta 2}\right]_{pka,f}$$

$$+\left[R_{\beta 2}\right]_{pka,f} + \left(\frac{1}{K_{\beta 2,A}}+\frac{[L]}{K_{\beta 2,A}K_{\beta 2,F}}\right)\left[R_{\beta 2}\right]^2_{pka,f} = 0$$

$$-K_{\beta2,A}K_{\beta2,F}\left[R_{\beta2}\right]_{pka,tot} - \left(K_{\beta2,F}+[L]\right)\left[R_{\beta2}\right]_{pka,tot}\left[R_{\beta2}\right]_{pka,f} + K_{\beta2,A}K_{\beta2,F}\frac{[L]}{K_{\beta2,L}}\left[R_{\beta2}\right]_{pka,f}$$

$$+[L][G_i]_{\alpha\beta\gamma}\left[R_{\beta2}\right]_{pka,f} + [G_i]_{\alpha\beta\gamma}K_{\beta2,F}\left[R_{\beta2}\right]_{pka,f} + K_{\beta2,A}K_{\beta2,F}\left[R_{\beta2}\right]_{pka,f}$$

$$+\left(1+\frac{[L]}{K_{\beta2,L}}\right)\left(K_{\beta2,F}+[L]\right)\left[R_{\beta2}\right]_{pka,f}^{2} = 0 \qquad (2.31)$$

Hence, the free PKA phosphorylated β2-adrenergic receptors is given by a quadratic equation with coefficients:

$$a_{\beta2,i} = \frac{1}{K_{\beta2,L}}\left(K_{\beta2,L}+[L]\right)\left(K_{\beta2,F}+[L]\right)$$

$$b_{\beta2,i} = [G_i]_{\alpha\beta\gamma}\left(K_{\beta2,F}+[L]\right)-\left(K_{\beta2,F}+[L]\right)\left[R_{\beta2}\right]_{pka,tot} + K_{\beta2,A}K_{\beta2,F} + K_{\beta2,A}K_{\beta2,F}\frac{[L]}{K_{\beta2,L}}$$

$$c_{\beta2,i=} -\left[R_{\beta2}\right]_{pka,tot}K_{\beta2,A}K_{\beta2,F}$$

Thus,

$$\left[R_{\beta2}\right]_{pka,f} = \frac{-b_{\beta2,i}+\sqrt{b_{\beta2,i}^{2}-4a_{\beta2,i}c_{\beta2,i}}}{2a_{\beta2,i}} \qquad (2.32)$$

and

$$[G_i]_f = \frac{[G_i]_{\alpha\beta\gamma}}{1+\left[R_{\beta2}\right]_{pka,f}\left(\dfrac{1}{K_{\beta2,A}}+\dfrac{[L]}{K_{\beta2,A}K_{\beta2,F}}\right)} \qquad (2.33)$$

where $[G_i]_{\alpha\beta\gamma}$ is a fraction of $[G_i]_{tot}$ and $\left[R_{\beta2}\right]_{pka,tot}$ is defined by the differential equation:

$$\frac{d[R_{\beta2}]_{PKA,tot}}{dt} = k_{PKA+}\cdot[C]\cdot[R_{\beta2}]_{np,tot} - k_{PKA-}\cdot[R_{\beta2}]_{PKA,tot} \qquad (2.34)$$

2.3   Adenylyl cyclase module

Adenylyl cyclases regulate the synthesis of cAMP from ATP within the β1- and β2-adrenergic signaling systems. Of the 10 isoforms of adenylyl cyclase known to be found in mammalian cells

four of them are prominent in the β_1- and β_2-adrenergic pathway (AC4, AC5, AC6, and AC7) and

thus included in the model. AC5 and AC6, are localized in the caveolar while AC4 and AC7, are

localized in the extracaveolar[37,38]. Adenylyl cyclases AC4-AC7 are activated by the α-subunit of

G-protein, $G_{s\alpha}$, and adenylyl cyclases AC5-AC6 are inhibited by the α-subunit of G-protein,

$G_{i\alpha}$[37,39] (see Appendix). The adenylyl cyclases module for the combined β_1- and β_2-adrenergic

signaling systems is an extension of the adenylyl cyclase module presented in the previous

model[27].

2.4 Electrophysiological part

The action potential of the mouse ventricular myocytes is described by the equation[14,27]:

$$\frac{dV}{dt} = -\frac{1}{C_m}(I_{CaL} + I_{p(Ca)} + I_{NaCa} + I_{Cab} + I_{Na} + I_{Nab} + I_{NaK} + I_{Kto,f}$$
$$+ I_{K1} + I_{Kur} + I_{Kss} + I_{Kr} + I_{Cl,Ca} - I_{stim})$$

where I_{CaL} is the L-type Ca^{2+} current, $I_{p(Ca)}$ is the sarcolemmal Ca^{2+} pump, I_{NaCa} is the Na^+/Ca^{2+}

exchanger, I_{Cab} is the Ca^{2+} background current, I_{Na} is the fast Na^+ current, I_{Nab} is the Na^+

background current, I_{NaK} is the Na^+-K^+ pump, $I_{Kto,f}$ is the rapidly recovering transient outward K^+

current, I_{K1} is the time-independent K^+ current, I_{Kur} is the ultrarapidly activating delayed rectifier

K^+ current, I_{Kss} is the noninactivating steady-state voltage activated K^+ current, I_{Kr} is the rapid

delayed rectifier K^+ current, $I_{Cl,Ca}$ is the Ca^{2+}-activated chloride current, and I_{stim} is the stimulus

current.

Four of the currents (I_{CaL}, I_{Na}, $I_{Kto,f}$, and I_{Kur}) function as the substrates of the β_1- and β_2-

adrenergic signaling systems. In addition, there are three other phosphorylation substrates, which

are the major players in Ca^{2+} dynamics and are affected by the β_1- and β_2-adrenergic signaling

systems: ryanodine receptors, phospholamban, and troponin I. In this chapter we will focus on two major substrates that are affected by β_2-ARs (the L-type Ca^{2+} current and phospholamban) for which experimental data are available.

2.5   Model Simulations

This mathematical model of the combined β_1- and β_2-adrenergic signaling system contains 149 ordinary differential equations, multiple parameters and side conditions. It spans multiple time scales ranging from microseconds (gating of ryanodine receptors) to tens of minutes (cAMP accumulation and protein phosphorylation). Significant portions of the model include stiff differential equations that describe exponentially growing and decaying processes.

We implemented the fourth-order Runge-Kutta method with a fixed time step for solutions of the differential equations. A relatively large time step of 0.1 ms was used for simulations of the model without electrical stimulation. To simulate electrical stimulation with a pulsed stimulus current a time step of 0.0001 ms was used except for the first 10 milliseconds after stimulation, where a time step of 0.000002 ms is used to account for the activation time constants of the ryanodine receptors. This approach allowed us to optimize the accuracy and running time of the simulations. In addition, we performed a sensitivity analysis of the model outputs with respect to major model parameters and the initial conditions, as described below (see Chapter 3.3 Sensitivity Analysis).

Simulations of the model were run under a SUSE Linux 11 single processor platform on a Dell Precision Workstation T3500 and was coded in FORTRAN 90. The workstation is powered by a six-core Intel Xeon CPU with 12 GB RAM and 3.2 GHz. The cellular model is adjusted to a room temperature of 298°K/25°C/77°F.

3 DISTINCT PHYSIOLOGICAL EFFECTS OF β_1- AND β_2-ADRENOCEPTORS IN MOUSE VENTRICULAR MYOCYTES: INSIGHTS FROM A COMPARTMENTALIZED MATHEMATICAL MODEL

3.1 Introduction

Experimental data on stimulation of β_1-ARs from different laboratories consistently shows a robust increase in protein kinase A (PKA) activity; phosphorylation of ion channels, regulatory and contractile proteins; increase or decrease in ionic currents that shape action potential; and a robust increase in intracellular Ca^{2+} transient ($[Ca^{2+}]_i$) (see[27] and refs therein). However, the experimental picture of stimulation of β_2-ARs is less consistent. Some of the experimental data shows that the activation of β_2-ARs does increase cAMP concentration, significantly activates PKA, increase the magnitude of the L-type Ca^{2+} current, and phosphorylation of regulatory proteins (phospholamban) in multiple species[34,40,41,42]. Some other experiments on the stimulation of β_2-ARs do not produce physiological effects, in particular, in mouse ventricular myocytes or mouse hearts[43,44]. Therefore, specific experimental protocols were employed to reveal the physiological effects of β_2-ARs in the mouse hearts to suppress inhibitory G_i-mediated pathway branch or to inhibit phosphodiesterase activity[41,42]. Further, the interpretation of the experimental data on activation of β_2-ARs becomes even more complicated due to the use of different agonists, β_2-AR specific agonist zinterol or combination of isoproterenol and β_1-AR specific inhibitor CGP20712A. In particular, the use of 1 μM zinterol in the experiments, which the half-activation constant for β_1-ARs is around 1 - 3 μM[45,46], can produce significant contribution to the effects of β_1-ARs in addition to the β_2-ARs.

As there is no mathematical model that describes the effects of β_1- and β_2-ARs in mouse ventricular myocytes, we developed and explored a compartmentalized mathematical model of mouse ventricular myocytes that includes both the β_1- and β_2-adrenergic signaling systems to describe the effects of stimulation of β_1- and β_2-ARs on the behavior of cardiac cells. The model is based on the previously developed mathematical model of the β_1-adrenergic signaling system in mouse ventricular cells, which was extensively verified by the experimental data on the activation of β_1-ARs[27,30]. The model[27] was also recently used by Esprito Santo et al.[47] for simulation of the larger susceptibility of the isoproterenol-stimulated mouse cardiac cells to DADs with I_{NaCa} overexpression. We only added β_2-ARs activation module in the β_1- and β_2-adrenergic pathways before the module of cAMP production/degradation and modified adenylyl cyclase module to include the effects of G_i, which were validated by the thorough experimental data on interaction between β_1- and β_2-ARs and cAMP dynamics in different compartments in mice[34] as outlined below. The model was investigated using simultaneous stimulation of both β_1- and β_2-ARs, and separate stimulation of β_1-ARs or β_2-ARs by isoproterenol. The model successfully reproduced existing experimental data on the activation of β_1- and/or β_2-ARs, adenylyl cyclase activity, the effects of G_i and PDE3/PDE4 inhibition on cAMP dynamics, ionic currents, $[Ca^{2+}]_i$ transients. Particular attention is paid to the effects of stimulation of β_2-ARs on cAMP and PKA dynamics, phosphorylation of phospholamban (PLB), the magnitude of the L-type Ca^{2+} current, action potentials, and $[Ca^{2+}]_i$ dynamics. We found that the separate stimulation of the β_2-ARs under normal physiological conditions does not affect action potential and $[Ca^{2+}]_i$ transients. The physiological effects β_2-ARs are revealed upon inhibition of G_i protein (by pertussis toxin (PTX)) or phosphodiesterases of type 3 and 4 (PDE3 and PDE4). The model also made testable predictions on the changes in the action potential, magnitudes of $[Ca^{2+}]_i$ and $[Na^+]_i$ fluxes, the rate of decay of

$[Na^+]_i$ concentration upon both combined and separate stimulation of β_1- and β_2-ARs, and the contribution of phosphorylation of PKA targets to the changes in the action potential and $[Ca^{2+}]_i$ transient. Mechanisms of the changes are disclosed by the simulations, sensitivity of the simulation data to the changes of the concentrations of the major signaling proteins is investigated, and the model limitations are discussed.

3.2   Results

3.2.1   *Adenylyl cyclase activity*

In the combined β_1- and β_2-adrenergic pathways, adenylyl cyclases are responsible for the synthesis of cAMP from ATP. Figure 3.1A shows experimental data on activation of AC5 and AC6 by $G_{s\alpha}$ by Chen-Goodspeed et al.[48] and the corresponding simulation data using our model for AC5/6 activation at different concentrations of $G_{i\alpha}$ (activation of AC4/7 is the same as in the model[27] and is not shown). In Fig 3.1A, simulated data shows a right-handed $G_{i\alpha}$ concentration-dependent shift of the activation curves when AC5/6 activity is normalized to the maximum at $G_{s\alpha}$ = 10 µM. In addition, $G_{i\alpha}$ subunit inhibits maximum AC5/6 activity at $G_{s\alpha}$ = 10 µM when normalized to the maximum activity at $G_{i\alpha}$ = 0 µM (Fig. 3.1B). In Fig. 3.1C, simulation data on inhibition of AC5/6 by $G_{i\alpha}$ is compared to the experimental data for AC6 at different values of $G_{s\alpha}$[48]. The figure demonstrates good agreement between experimental and simulated results.

Adenylyl cyclase activity can also be used as an indicator of desensitization of β_1- or β_2-ARs. Experimental data on AC activity upon stimulation of β_1- or β_2-ARs as functions of isoproterenol concentration were obtained by Freedman et al.[49] at three time moments (at the
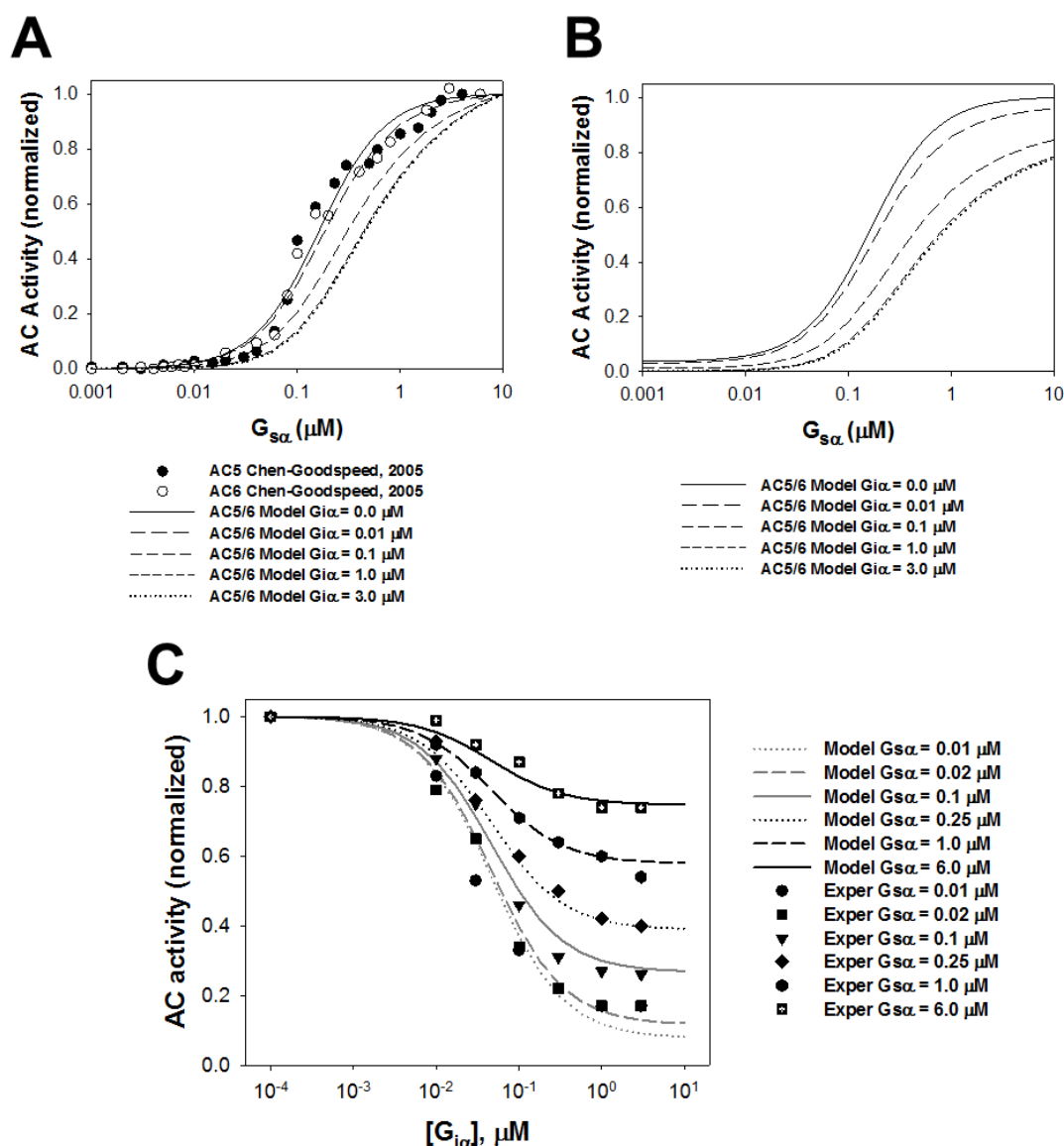
*Figure 3.1 Normalized activity of adenylyl cyclases as functions of $G_{s\alpha}$ and $G_{i\alpha}$. **Panel A**: Experimental normalized activity of AC5 (filled circles) and AC6 (unfilled circles) as functions of $G_{s\alpha}$[48]. Simulated data for normalized activity of AC5/6 for different concentrations of $G_{i\alpha}$ are shown by a solid line ($G_{i\alpha} = 0.0$ μM), long dashed line ($G_{i\alpha} = 0.01$ μM), medium dashed line ($G_{i\alpha} = 0.1$ μM), short dashed line ($G_{i\alpha} = 1.0$ μM), and dotted line ($G_{i\alpha} = 3.0$ μM). Each simulated data on AC5/6 activity for different concentration of $G_{i\alpha}$ is normalized by its maximum value. **Panel B**: Simulated data for normalized activity of AC5/6 for different concentrations of $G_{i\alpha}$ are shown by a solid line ($G_{i\alpha} = 0.0$ μM), long dashed line ($G_{i\alpha} = 0.01$ μM), medium dashed line ($G_{i\alpha} = 0.1$ μM), short dashed line ($G_{i\alpha} = 1.0$ μM), and dotted line ($G_{i\alpha} = 3.0$ μM). Each simulated data on AC5/6 activity for different concentration of $G_{i\alpha}$ is normalized by the maximum AC5/6 activity at $G_{i\alpha} = 0.0$ μM. **Panel C**: Experimental normalized activity of AC6 (symbols) as functions of $G_{i\alpha}$ at different values of $G_{s\alpha}$[48]. Simulated data for normalized activity of AC5/6 for different concentrations of $G_{s\alpha}$ are shown by a gray dotted line ($G_{s\alpha} = 0.01$ μM), gray dashed line ($G_{s\alpha} = 0.02$ μM), gray solid line ($G_{i\alpha} = 0.1$ μM), black dotted line ($G_{s\alpha} = 0.25$ μM), black dashed line ($G_{s\alpha} = 1.0$ μM), and black solid line ($G_{i\alpha} = 6.0$ μM). Each simulated data on AC5/6 activity for different concentration of $G_{s\alpha}$ is normalized by its maximum value.*

maximum activity (from 50th to 75th seconds, depending on isoproterenol concentration), 5th min, and 30th min). It is shown that the AC activity decreases in time, reflecting desensitization of β_1-ARs or β_2-ARs (symbols in Fig. 3.2A and 3.2B). Simulation data also demonstrates the decrease in AC activity as functions of time at different concentrations of isoproterenol (solid, dashed, and dash-dotted lines in Fig. 3.2A and 3.2B). Two mechanisms are responsible for the desensitization of β_1-ARs or β_2-ARs: phosphorylation by PKA and GRK2.

We also simulated the effects of different concentrations of isoproterenol on adenylyl cyclase activity in mouse ventricular myocytes (Fig. 3.2C). Experimental data on total AC activity in mouse ventricles and cardiac cells as a function of isoproterenol concentration after 10-min exposures are shown by unfilled[50] and filled circles[51] with error bars. Simulation data on the total AC activity after a 10-minute exposure to different concentrations of isoproterenol, when both β_1- and β_2-ARs are stimulated are shown by a solid line. Thus, our model was able to reproduce absolute values of the total cellular AC activity as a function of isoproterenol (Fig. 3.2C).

It was also interesting how much inhibition of G_i protein affects AC activity in mouse ventricular cells. For this purpose, Akhter et al.[52] compared AC activity in the cells upon stimulation with 100 µM isoproterenol without and with exposure to PTX. It was shown experimentally (black bars with error marks in Fig. 3.2D) that there is a trend toward an increase in AC activity upon inhibition of G_i. Our simulations reproduced this effect, when both β_1- and β_2-ARs are stimulated by 100 µM isoproterenol (gray bars in Fig. 3.2D).

A β₁-ARs

B β₂-ARs

C

D
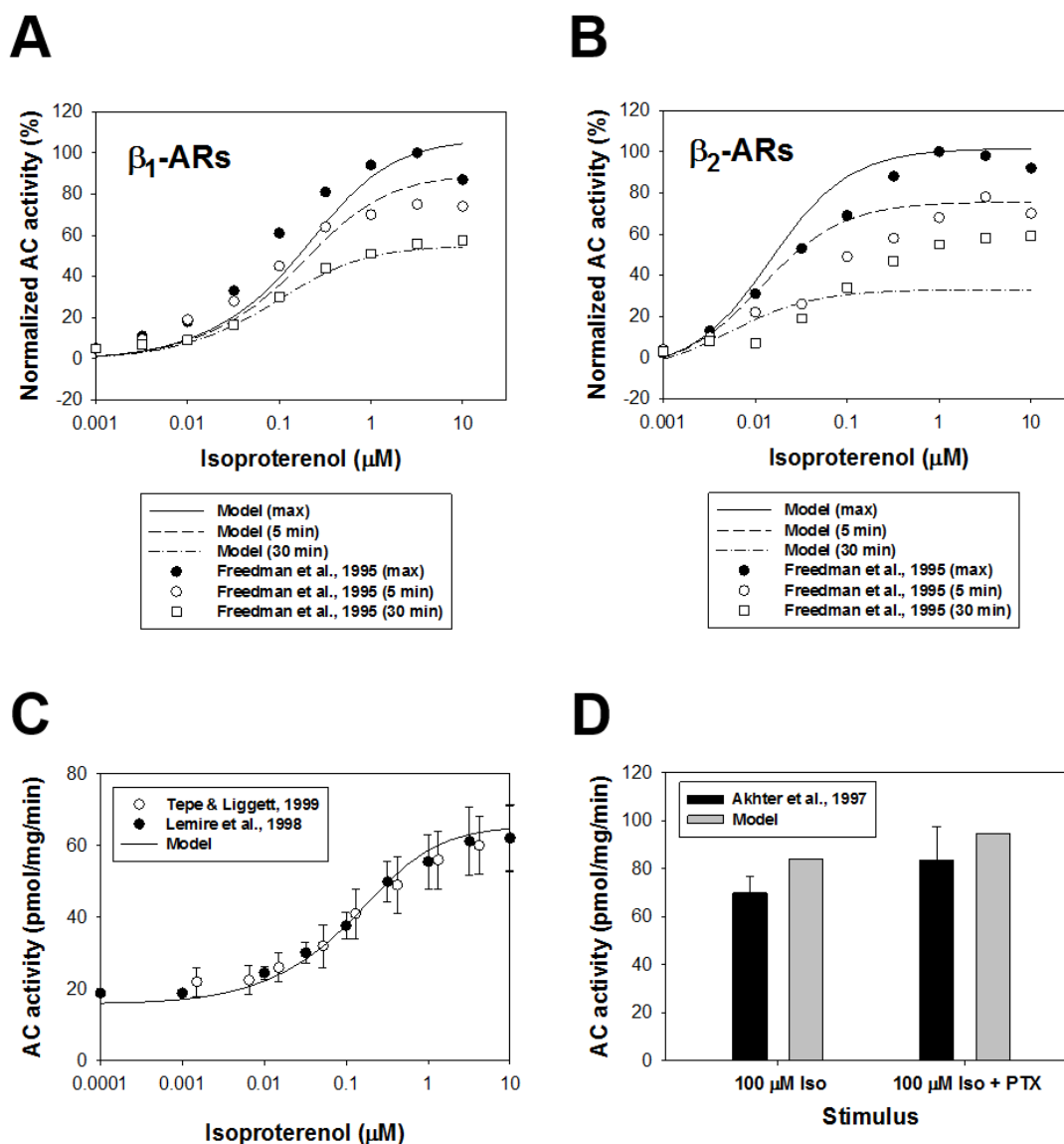
Figure 3.2 Desensitization of β₁- and β₂-adrenoceptors. **Panels A** *and* **B** *show increases in adenylyl cyclase activity above basal level (%) are measured at maximum (from 50th to 75th seconds, control, filled circles) and at two time moments (5 min and 30 min, unfilled circles and unfilled squares, respectively) after exposure to different concentrations of isoproterenol[49]. The corresponding simulated data on the normalized AC activity for the maximum, 5-minute, and 30-minute delays are shown by solid, dashed, and dash-dotted lines, respectively. Data for β₁-ARs and β₂-ARs are obtained with the block of β₂-ARs and β₁-ARs, respectively.* **Panel C**: *Adenylyl cyclase activity as a function of isoproterenol. Experimental data on AC activity (in pmol/mg/min) in mouse hearts and ventricular myocytes obtained after 10-minutes exposure to isoproterenol are shown by unfilled circles[50] and filled circles[51]. The solid line shows corresponding simulated AC activity at different concentrations of isoproterenol upon activation of both β₁-ARs and β₂-ARs.* **Panel D**: *The effects of PTX on adenylyl cyclase activity. Experimental data on AC activity (in pmol/mg/min) in myocardial membranes are obtained after 15-minutes exposure to 100 μM isoproterenol without and with application of PTX and are shown by black bars with error bars[52]. The corresponding simulated data are shown by gray bars when both β₁-ARs and β₂-ARs are activated.*

3.2.2 Protein kinase A activation

Generated by adenylyl cyclases, cAMP molecules activate protein kinase A, a major signaling molecule in the β_1- and β_2-adrenergic signaling system which phosphorylates signaling proteins, ion channels, and proteins regulating Ca^{2+} dynamics. Figure 3.3A shows PKAI (circles) and PKAII (squares) activity as functions of cAMP concentrations obtained from experimental data[53,54]. Our simulations displayed by a solid (PKAI) and a dashed (PKAII) line, respectively, fit well to the experimental data. We also simulated the cellular PKA activity ratio in control and upon stimulation of the combined β_1- or β_2-adrenergic signaling system, separate stimulation of the β_1- or β_2-adrenergic signaling, and the β_2-adrenergic signaling in the cells pretreated by PTX with 1 µM isoproterenol (Fig. 3.3B). We performed four simulations for this figure: no isoproterenol/basic cAMP level (−cAMP), no isoproterenol/3 µM cAMP (+cAMP), 1 µM isoproterenol/no externally applied cAMP (−cAMP), and 1 µM isoproterenol/3 µM cAMP (+cAMP). Then, the corresponding PKA(−cAMP)/PKA(+cAMP) ratios were calculated. The simulations of the stimulation of the combined β_1- or β_2-adrenergic signaling system and a separate stimulation of the β_1-adrenergic signaling compare well to the experimental data for similar experimental conditions in the rabbit hearts (black bars[55]). However, separate stimulation of the β_2-adrenergic signaling system with 1 µM isoproterenol alone lead to very little activation of PKA (10% increase compared to control). A significantly larger increase in PKA activation (39% increase) is observed upon stimulation by 1 µM isoproterenol plus PTX (Fig. 3.3B). This simulation result explains one of the mechanisms by which the effects of the β_2-adrenergic signaling system are revealed in the experiments - by the inhibition of G_i protein.
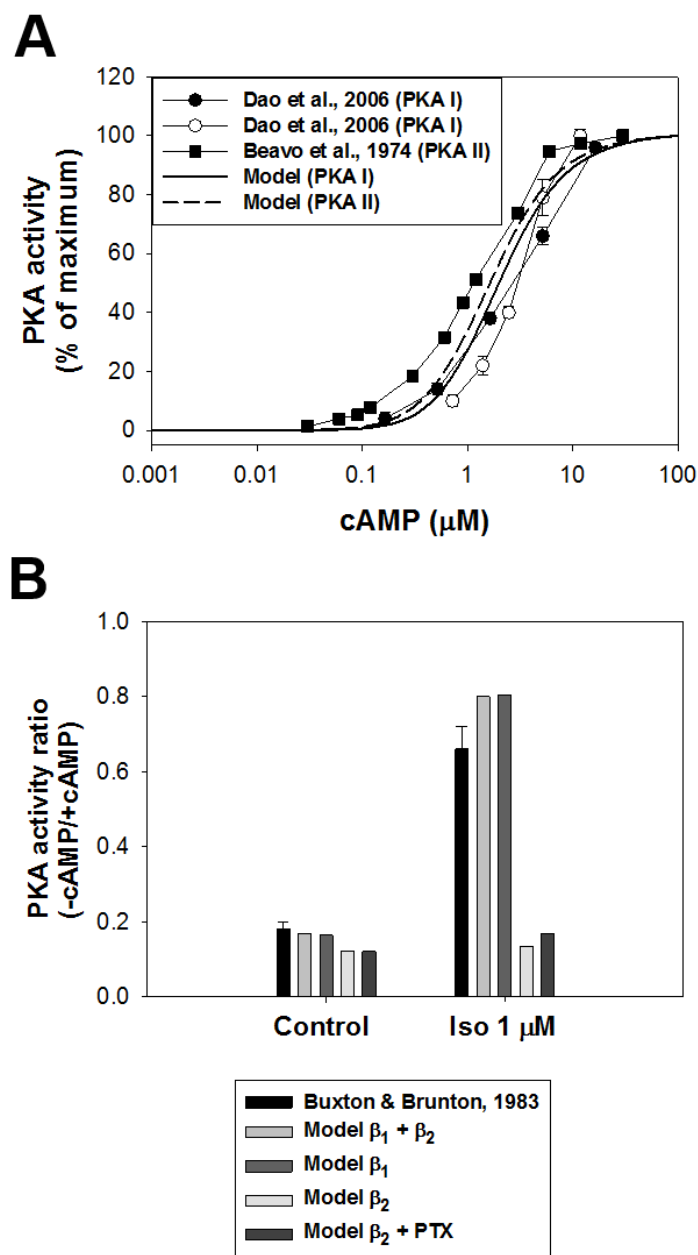
Figure 3.3 Protein kinase A activity. **Panel A**: PKA I and PKA II activity as functions of cAMP. Experimental data for PKA I are obtained by two methods by Dao et al.[54] and are shown by filled and unfilled circles; data for PKA II is obtained by Beavo et al.[53]. The corresponding simulated data are shown by a solid (PKA I) and a dashed (PKA II) line. **Panel B**: PKA activity ratio. Experimental data (black bars with error) were obtained without (−cAMP) and with (+cAMP) an externally applied 3 μM cAMP, both without and with 1 μM isoproterenol (black bars[55]). We also performed four simulations: no isoproterenol/basic level cAMP (−cAMP), no isoproterenol/3 μM cAMP (+cAMP), 1 μM isoproterenol/no externally applied cAMP (−cAMP), and 1 μM isoproterenol/3 μM cAMP (+cAMP). Then, the corresponding PKA ratios were calculated. Simulations were performed for four cases: activation of both β_1-ARs and β_2-ARs, activation of β_1-ARs alone, activation of β_2-ARs alone, and activation of β_2-ARs alone with the inhibition of G_i (PTX).

3.2.3 Compartmentalized cAMP and PKA dynamics

cAMP concentration displays different dynamics in the three major cellular compartments. It is determined by the balance between cAMP production by adenylyl cyclases, cAMP degradation by phosphodiesterases, and cAMP diffusion between intracellular compartments. Figure 3.4 shows the simulated time courses of cAMP concentrations in different subcellular compartments in response to 1 μM isoproterenol under four different conditions: stimulation of the combined β_1- and β_2-adrenergic signaling systems, β_1-adrenergic signaling system alone, β_2-adrenergic signaling system alone, or β_2-adrenergic signaling system alone with prior exposure to PTX. Stimulation of the combined β_1- and β_2-adrenergic signaling systems or β_1-adrenergic signaling system alone results in a significant and similar increase of cAMP production by adenylyl cyclases and cAMP degradation by phosphodiesterases in the caveolar, extracaveolar, and cytosolic compartments, as well as in the whole cardiac cell (Fig. 3.4 A-D, red and green lines). Stimulation of the β_2-adrenergic signaling system alone shows a smaller but significant increase only in the caveolar compartment with virtually no change in the extracaveolar and cytosolic compartments and the whole cell (Fig. 3.4A-D, cyan lines). However, a much larger increase in cAMP production is obtained during stimulation of β_2-ARs with PTX (Fig. 3.4A-D, blue lines). The greatest, multifold increase is observed in the caveolar compartment (Fig. 3.4A), and a smaller, but noticeable increase is found in the extracaveolar and cytosolic compartments and the whole cell (Fig. 3.4B-D).

The behavior of the catalytic subunit of PKA is similar to that for cAMP (Fig. 3.5). Stimulation of the combined β_1- and β_2-adrenergic signaling systems or β_1-adrenergic signaling system alone lead to a large similar increase of PKA activity in all three compartments and in the whole cardiac cell (Fig. 3.5A-D, red and green lines). Stimulation of β_2-ARs alone produces quite a significant

effect on PKA activity only in the caveolar compartment (Fig. 3.5A-D, cyan lines). Inhibition of

G_i by PTX upon stimulation of β_2-ARs significantly enhances the response in the caveolar, but the

effects in other compartments are still quite small (Fig. 3.5A-D, blue lines).
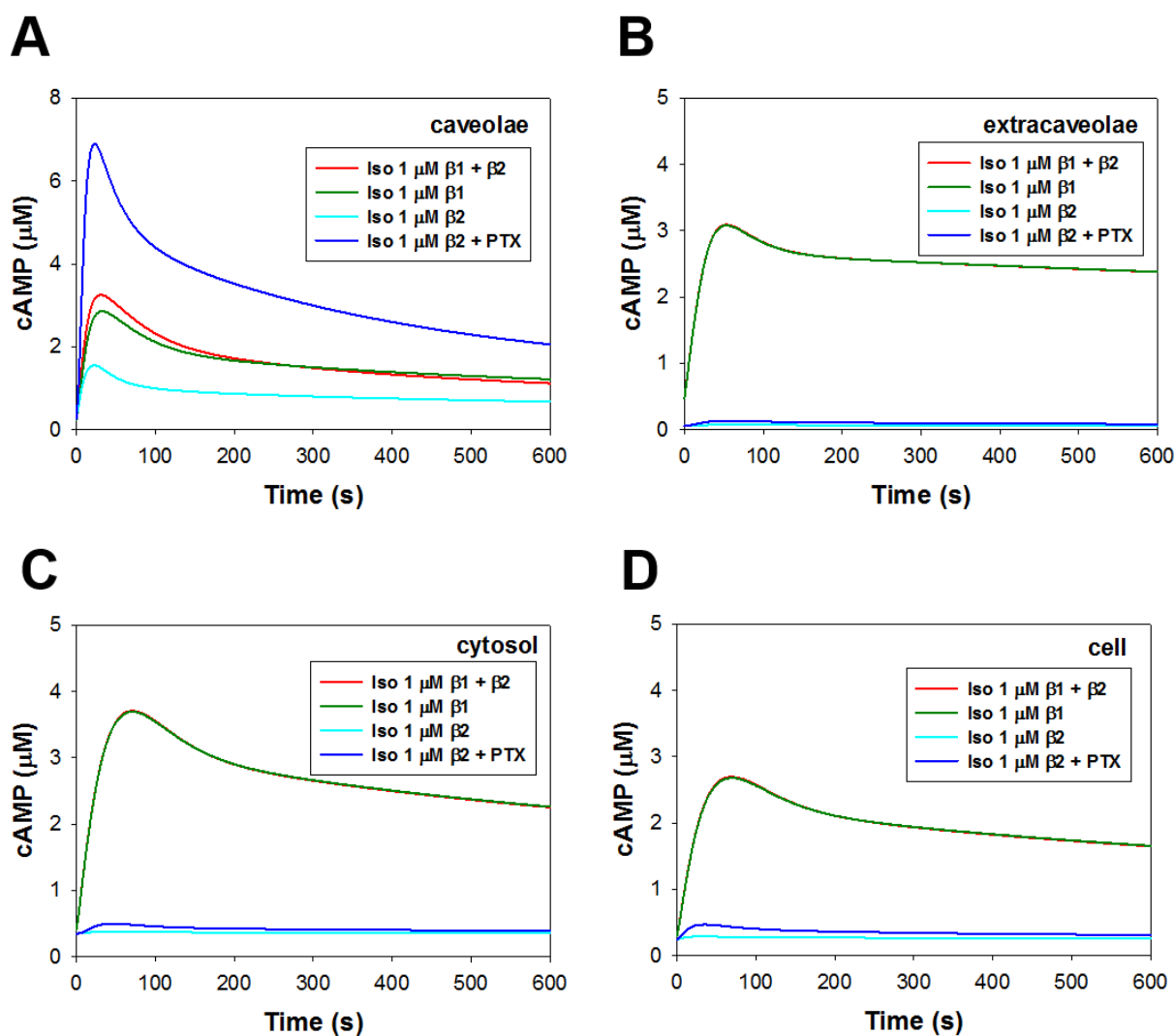
*Figure 3.4 cAMP dynamics in mouse ventricular myocytes. Simulated cAMP concentrations are shown as functions of time in the caveolar (**Panel A**), extracaveolar (**Panel B**), and cytosolic compartments (**Panel C**), as well as in the whole cell (**Panel D**). Simulations were performed for four cases: activation of both β1-ARs and β2-ARs, activation of β1-ARs alone, activation of β2-ARs alone, and activation of β2-ARs alone with the inhibition of Gi (PTX). Data in **Panels A-D** are obtained upon application of 1 μM isoproterenol.*
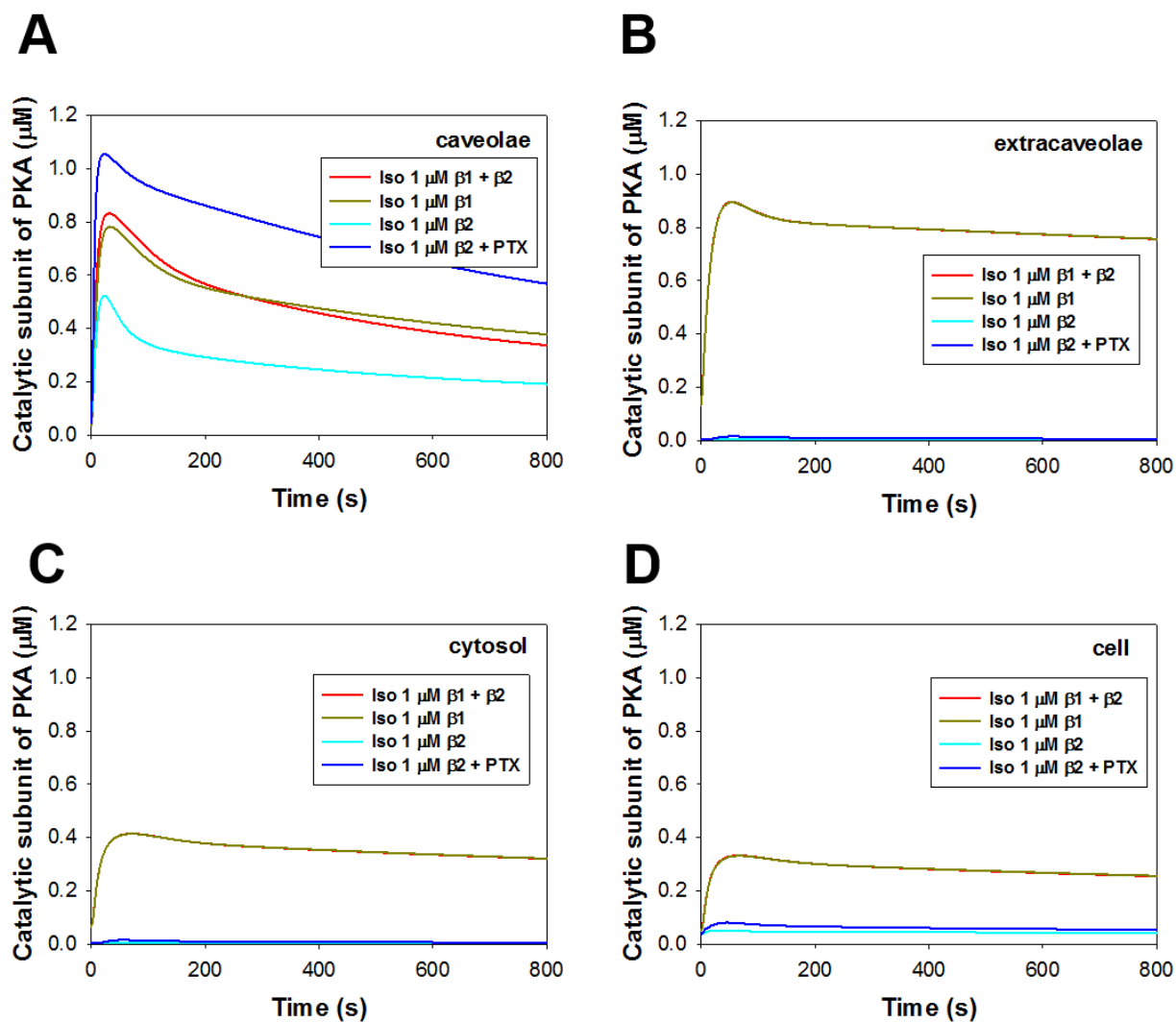
*Figure 3.5 PKA catalytic subunit dynamics in mouse ventricular myocytes. Simulated PKA catalytic subunit concentrations are shown as functions of time in the caveolar (**Panel A**), extracaveolar (**Panel B**), and cytosolic compartments (**Panel C**), as well as in the whole cell (**Panel D**). Simulations were performed for four cases: activation of both β_1-ARs and β_2-ARs, activation of β_1-ARs alone, activation of β_2-ARs alone, and activation of β_2-ARs alone with the inhibition of G_i (PTX). Data in **Panels A-D** was obtained upon the application of 1 µM isoproterenol.*

We compared simulated cAMP production in different compartments and in the whole cell with the experimental data by Nikolaev et al.[34]. Nikolaev et al.[34] used a fluorescence resonance energy transfer (FRET) based cAMP sensor to measure local cAMP concentrations in different regions of the ventricular myocytes upon stimulation of the β_1- and β_2-adrenergic signaling systems. Figure 3.6A shows a comparison of the simulated and the experimental data on cAMP

production upon separate stimulation of β_1-ARs and β_2-ARs in caveolar and extracaveolar compartments. It is seen that the stimulation of β_1-ARs in both compartments significantly increases cAMP production; however, the stimulation of β_2-ARs demonstrates only a tiny increase of cAMP in the extracaveolar and a significant, but smaller than for β_1-ARs, increase in cAMP in the caveolar compartment. On the whole cell level, simultaneous stimulation of β_1-ARs and β_2-ARs or β_1-ARs alone produces quite a large magnitude of cAMP transient, while the effect of the stimulation of β_2-ARs alone is quite small (Fig. 3.6B). Simulation results satisfactorily reproduced the experimental observations (Fig. 3.6A, B).

3.2.4   *The effects on the L-type Ca^{2+} current*

Experimental data on mouse ventricular myocytes shows that the application of 1 µM isoproterenol, which stimulates both β_1-ARs and β_2-ARs, robustly increases the magnitude of the L-type Ca^{2+} current by about 2 folds[41,56,57,58]. Stimulation of β_1-ARs alone with 1 µM isoproterenol and a block of β_2-ARs by 50 nM ICI-118551 results in a similar increase in the magnitude of I$_{CaL}$[41]. Further, application of 1 µM of isoproterenol with β_1-ARs blocked with 0.3 µM of CGP-20712A[41] or application of PTX without stimulation of β_1-ARs or β_2-ARs[43,58,59] does not show any effect on I$_{CaL}$, demonstrating silence of the β_2-adrenergic signaling system under these experimental conditions. However, the small effects of β_2-ARs can be revealed by stimulating β_2-ARs with 1 µM isoproterenol and additional application of PTX[58] or with inhibition of PDE3 and PDE4[41]. Figure 3.7 shows simulations of these experimental findings. Application of PTX does not demonstrate any effect on I$_{CaL}$ when both β_1-ARs and β_2-ARs are intact (compare solid line for
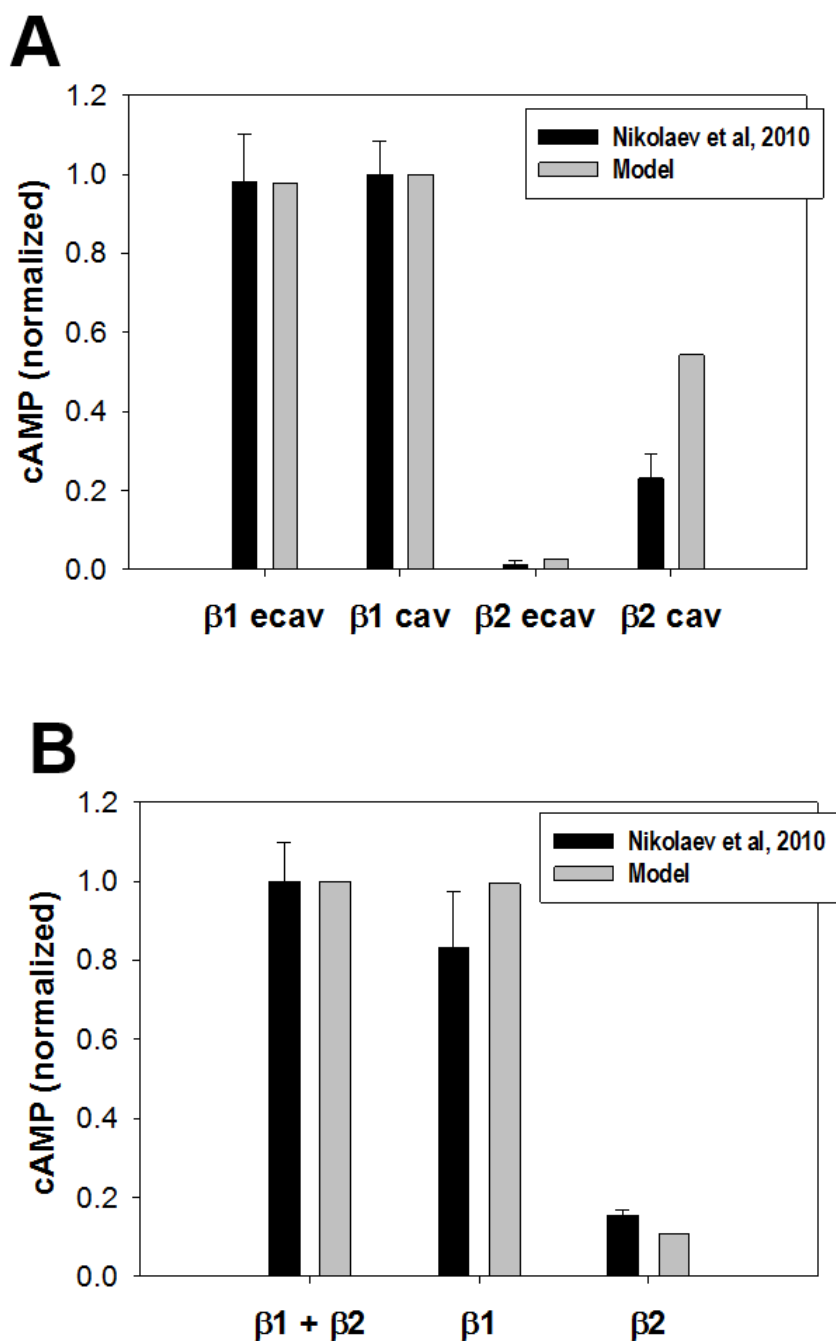
Figure 3.6 Compartmentalization of cAMP dynamics in mouse ventricular myocytes. **Panel A**: Experimental data on normalized cAMP concentration in mouse ventricular myocytes in caveolar and extracaveolar compartments upon selective stimulation of β_1-ARs and β_2-ARs are shown by black bars[34]; the corresponding simulation data is shown by gray bars. **Panel B**: Experimental data on normalized cAMP concentration in mouse ventricular myocytes (whole cell concentrations) upon stimulation of both β_1-ARs and β_2-ARs, β_1-ARs alone, or β_2-ARs alone are shown by black bars[34]; the corresponding simulation data is shown by gray bars.

control and long-dashed line for PTX in Fig. 3.7A). Stimulation of both β_1-ARs and β_2-ARs by 1 µM isoproterenol increases the magnitude of I_{CaL} by 1.9 folds (compare solid line for control and small-dashed line for 1 µM isoproterenol in Fig. 3.7A and Fig. 3.8C for the experimental data). An additional application of PTX to 1 µM isoproterenol slightly increases the amplitude of I_{CaL} to reflect the effects of β_2-ARs (dotted line in Fig. 3.7A). Finally, the magnitude of I_{CaL} shows a larger increase upon application of 1 µM isoproterenol with inhibition of PDE3 and PDE4 (dashed-dotted line in Fig. 3.7A). To reveal the contribution of β_1-ARs and β_2-ARs to the total effects, we performed simulations with the same protocols, but with inhibition of β_2-ARs or β_1-ARs. The results are shown in Figs. 3.7, B and C). The effects of stimulation of β_1-ARs with 1 µM isoproterenol and a block of β_2-ARs are very similar to those when both β_1-ARs and β_2-ARs are intact (Fig. 3.7B). The only difference is that no effects of PTX are observed.

In contrast, only small increases in the magnitudes of I_{CaL} are observed upon stimulation of β_2-ARs when β_1-ARs are blocked under different experimental conditions (Fig. 3.7C). The application of PTX did not change the magnitude of I_{CaL} (compare solid line for control and long-dashed line for PTX in Fig. 3.7C). Stimulation of β_2-ARs when β_1-ARs are blocked with 1 µM isoproterenol leads to a tiny increase in I_{CaL} (3% increase), which virtually cannot be detected in the experiments (compare solid line for control and small-dashed line for 1 µM isoproterenol in Fig. 3.7C). Application of 1 µM isoproterenol in the presence of PTX results in a larger increase in I_{CaL} (12% increase, dotted line in Fig. 3.7C). Even larger effects of stimulation of β_2-ARs are obtained upon application of 1 µM isoproterenol and inhibition of PDE3 and PDE4 (22% increase, dashed-dotted line in Fig. 3.7C).
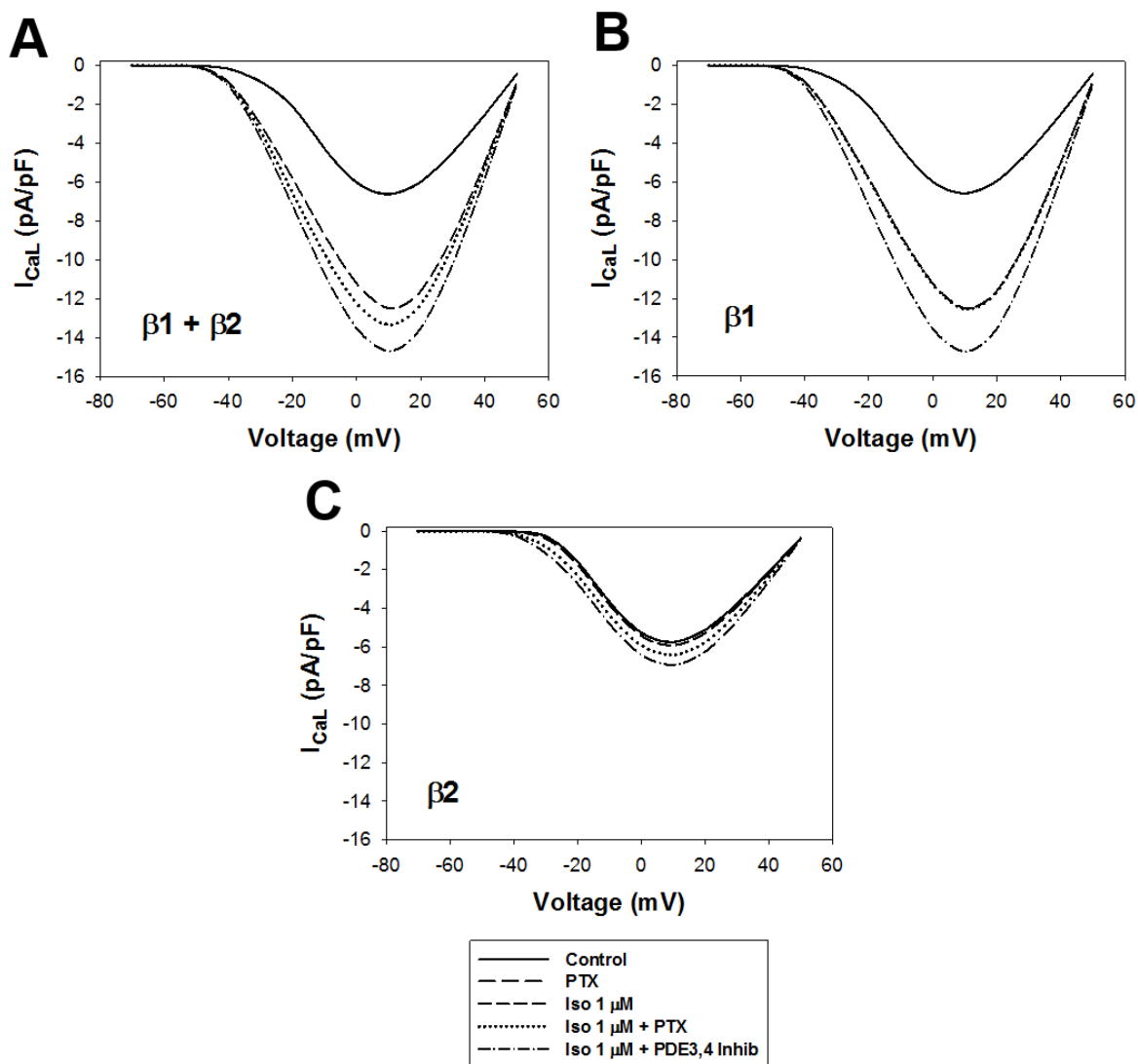
*Figure 3.7 The effects of stimulation of β_1-ARs and β_2-ARs on the L-type Ca^{2+} current. Simulated current-voltage relationships obtained upon the stimulation of both β_1-ARs and β_2-ARs (**Panel A**), β_1-ARs alone (**Panel B**), and β_2-ARs alone (**Panel C**). Currents are obtained by voltage pulses from -70 mV to $+50$ mV (in 10-mV increments) from a holding potential of -80 mV and without Ca^{2+}-induced Ca^{2+} release to account for heavy buffering conditions. Simulations were performed for several physiological conditions: control (solid lines), inhibition of G_i without isoproterenol (long dashed lines, they are almost invisible in figures due to very tiny effects), after application of 1 μM isoproterenol (medium dashed lines), after application of 1 μM isoproterenol with inhibition of G_i (dotted lines), or after application of 1 μM isoproterenol with inhibition of PDE3 and PDE4 (dash-dotted lines).*

Comparisons of the simulated and experimental data under different experimental conditions is shown in Fig. 3.8. No effect is observed in simulations and in the experiments[43,59] upon application of PTX (Fig. 3.8A). A small increase in the magnitude of I_{CaL} is observed upon

application of 1 µM isoproterenol without and with PTX in simulations and in the experiment by Xu et al.[58] (Fig. 3.8B). The statistically significant effects of stimulation of β_2-ARs alone (37%±13% increase) is observed upon application of 1 µM isoproterenol and inhibition of PDE3 and PDE4 (by cilostamide and rolipram, respectively), which is close to our simulated effect under similar experimental conditions (third set of bars in Fig. 3.8C). However, as expected, stimulation of β_1-ARs alone with 1 µM isoproterenol and inhibition of PDE3 and PDE4 results in a much larger increase in I_{CaL} (two last bars in Fig. 3.8C), which was also predicted by our simulations.

Thus, our model for the first time provides non-contradictive simulated data on the effects of β_1-ARs and β_2-ARs on the L-type Ca^{2+} current in mouse ventricular myocytes. Simulations show that the effects of β_2-ARs on the L-type Ca^{2+} current can be revealed by stimulation with isoproterenol with additional inhibition of G_i or PDE3 and PDE4.

3.2.5 *The effects on phospholamban*

Similar to the L-type Ca^{2+} current, stimulation of both β_1-ARs and β_2-ARs or β_1-ARs alone with 10 µM isoproterenol results in a multifold increase of the relative phosphorylation level of phospholamban (which regulates SERCA pump activity) compared to control levels in both simulations (4.9 and 5.6-fold increase) and in the experiment with β_2-AR knockout mice (3.6-fold increase) (Fig. 3.9A). This isoproterenol concentration is chosen to compare simulations with corresponding experimental data by Soto et al.[60], for which simulation data are similar to the experimental findings. Inhibition of G_i, which mimics application of PTX, does not affect the
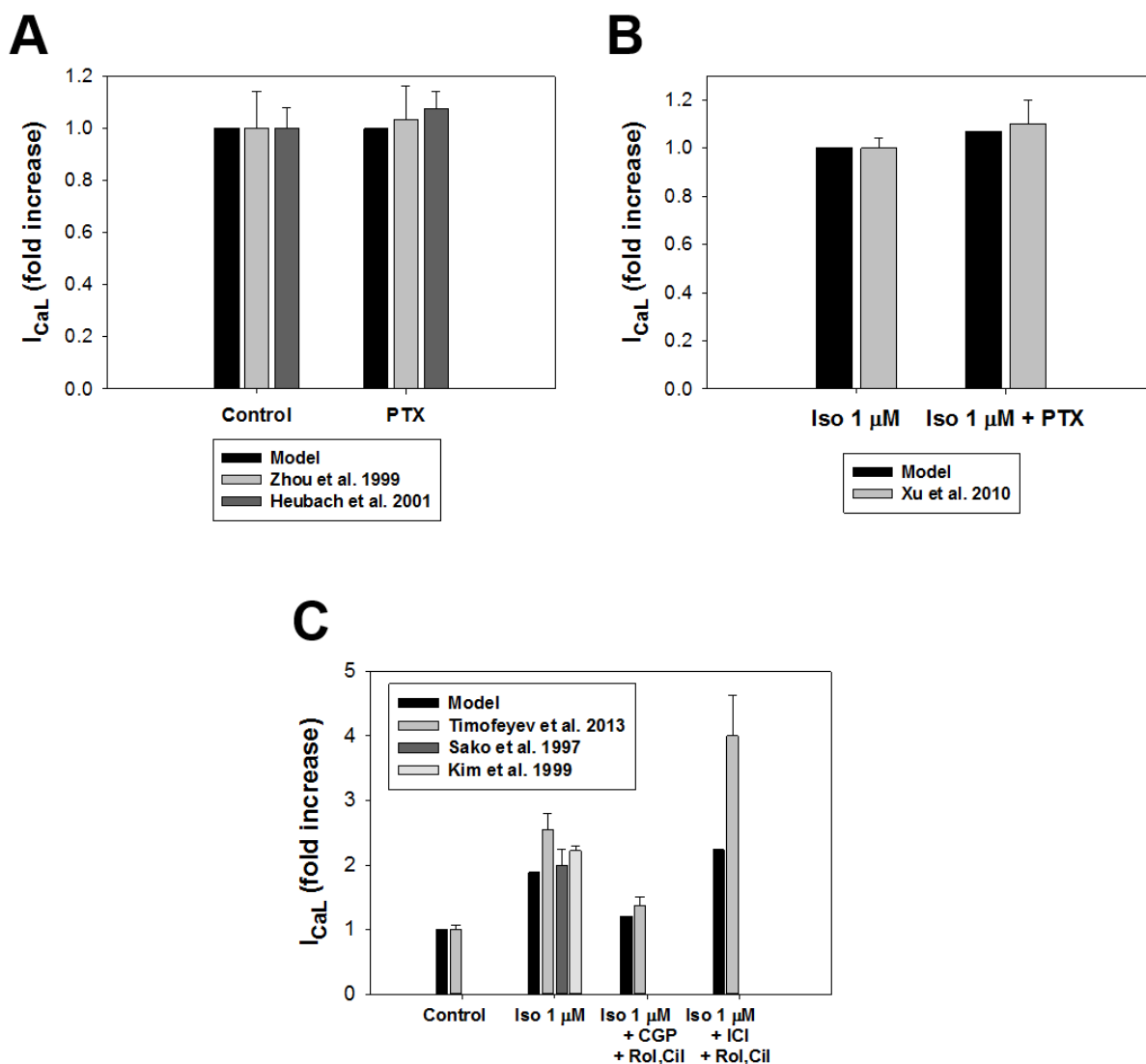
*Figure 3.8 A comparison of the experimental and simulated data on the L-type Ca²⁺ current. A comparison of the experimental and simulated data on the L-type Ca²⁺ current at different physiological conditions in mouse ventricular myocytes upon stimulation of both β₁-ARs and β₂-ARs. **Panel A:** PTX (inhibition of Gᵢ) does not cause any effect on the magnitude of the L-type Ca²⁺ current in the simulation (black bar) and in experiments (gray bars by Zhou et al.⁵⁹ and dark gray bars by Heubach et al.⁴³). **Panel B:** The increase in magnitude of the L-type Ca²⁺ current upon stimulation with 1 μM isoproterenol without and with the inhibition of Gᵢ by PTX. Simulated data are shown with black bars; experimental data by Xu et al.⁵⁸ are shown by gray bars with errors. **Panel C:** An increase in peak IₐₐL under different physiological conditions (control, application of 1 μM isoproterenol, application of 1 μM isoproterenol with inhibition of β₁-ARs and PDE3 and PDE4, or application of 1 μM isoproterenol with inhibition of β₂-ARs and PDE3 and PDE4). Experimental data on the application of 1 μM isoproterenol are obtained from Sako et al.⁵⁷, Kim et al.⁵⁶, and Timofeev et al.⁴¹; experimental data on application of 1 μM isoproterenol with inhibition of β₁-ARs and PDE3 and PDE4 and application of 1 μM isoproterenol with inhibition of β₂-ARs and PDE3 and PDE4 are obtained from Timofeev et al.⁴¹.*

phosphorylation level of phospholamban. An application of 10 µM isoproterenol with inhibition of G_i demonstrates similar effects as without G_i inhibition (Fig. 3.9A). This phospholamban behavior is different from the L-type Ca^{2+} current (the last is affected by G_i inhibition) and is explained by the localization of phospholamban in the cytosolic compartment, where the effects of β_1-ARs are predominant.

Activation of β_2-ARs alone, with inhibition of β_1-ARs, shows a different behavior (Fig. 3.9B). Inhibition of G_i with PTX and without application of isoproterenol does not affect PLB phosphorylation in simulations and in the experiments with β_1-AR knockout mice[60,61]. Simulations also show a 57% increase in PLB phosphorylation upon stimulation of β_2-ARs alone with 10 µM isoproterenol. This is in line with the trend in the experimental data, where PLB phosphorylation increased by 1.8-2.3 times upon application of 10 µM isoproterenol in β_1-AR knockout mice; however, experimental data did not conclude a significant difference. Finally, stimulation of β_2-ARs alone with 10 µM isoproterenol and upon inhibition of G_i results in a multifold increase of PLB phosphorylation both in simulations (9-fold increase comparing to control) and in the experiments with β_1-AR knockout mice (3-3.7-fold increase) (Fig. 3.9B). Note that even larger relative increase in PLB phosphorylation are obtained upon stimulation of β_2-ARs with zinterol in rats[62] (Fig. 3.9B). While the stimulation of β_2-ARs alone leads to a larger relative increase in PLB phosphorylation compared to the stimulation of β_1-ARs alone, the absolute level of PLB phosphorylation is significantly larger during stimulation of β_1-ARs (100% PLB phosphorylation) than β_2-ARs (35% PLB phosphorylation).

Therefore, our model demonstrated that the effects of β_2-ARs on phospholamban can be revealed by stimulation with isoproterenol with an additional inhibition of G_i.
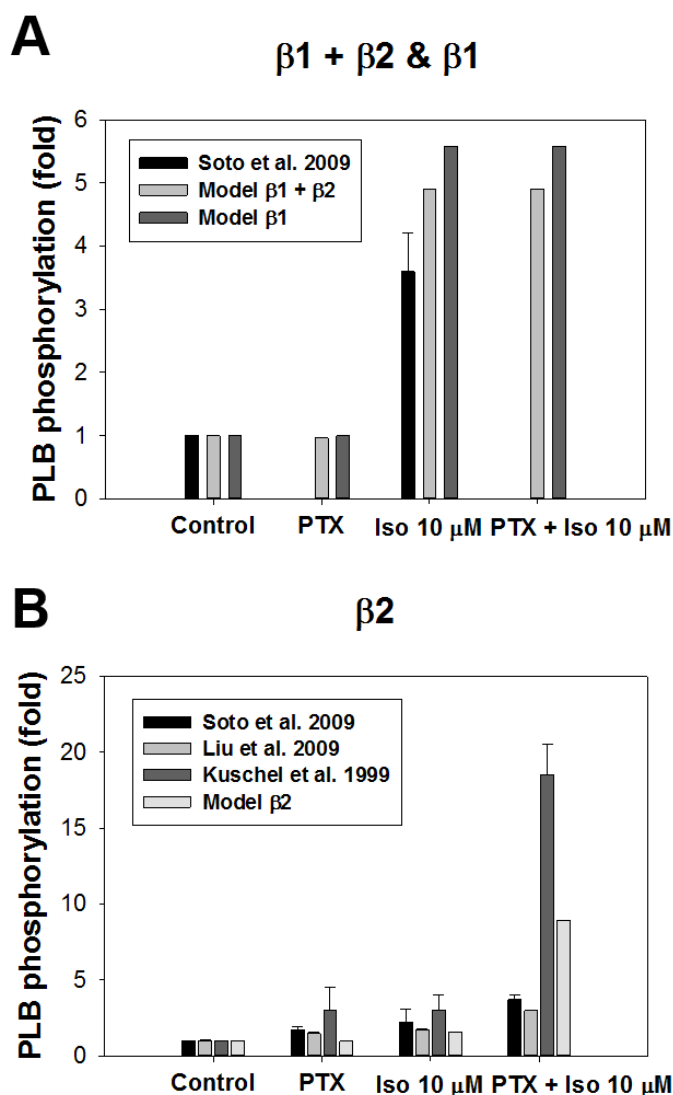
Figure 3.9 Phosphorylation of phospholamban in mouse ventricular myocytes upon stimulation of β₁-ARs and β₂-ARs. **Panel A:** *Activation of both β₁-ARs and β₂-ARs or β₁-ARs alone. Experimental data on PLB phosphorylation by Soto et al.[60] (black bars with errors) are obtained upon application of 10 μM isoproterenol. Simulation of activation of both β₁-ARs and β₂-ARs (gray bars) or β₁-ARs alone (dark gray bars) are shown for control, after inhibition of Gᵢ by PTX, after application of 10 μM isoproterenol, or application of 10 μM isoproterenol with inhibition of Gᵢ by PTX.* **Panel B:** *Activation of β₂-ARs alone. Experimental data on PLB phosphorylation by Soto et al.[60] (black bars with errors) and Liu et al.[61] (gray bars with errors are obtained in mice for control, after incubation with PTX, upon application of 10 μM isoproterenol, and upon application of 10 μM isoproterenol and incubation with PTX. Experimental data on PLB phosphorylation by Kuschel et al.[62] (dark gray bars with errors) are obtained in rats for control, after incubation with PTX, upon application of 10 μM zinterol, and upon application of 10 μM zinterol and incubation with PTX. Simulation of activation of β₂-ARs alone (light gray bars) are shown for control, after inhibition of Gᵢ by PTX, after application of 10 μM isoproterenol, or application of 10 μM isoproterenol with inhibition of Gᵢ by PTX.*

3.2.6 The effects on mouse action potential and ionic currents

Experimental data obtained from mouse ventricular myocytes shows that the application of near-saturating doses of isoproterenol (1 to 2 µM) results in prolongation of the action potential duration at 50% and 90% repolarization[27]. To simulate these and other effects, we stimulated the model cell with current pulses (I_{stim} = 80 pA/pF, τ_{stim} = 1.0 ms) with the frequency 1 Hz for 300 s when both β_1-ARs and β_2-ARs are available, or β_2-ARs blocked, or β_1-ARs blocked. Simulations were performed under several physiological conditions: control; application of 1 µM isoproterenol; inhibition of G_i (PTX application); application of 1 µM isoproterenol and PTX; PDE3 and PDE4 inhibition; and application of 1 µM isoproterenol and PDE3 and PDE4 inhibition. The effects of 1 µM isoproterenol on the APDs when both β_1-ARs and β_2-ARs are stimulated or only β_1-ARs are stimulated are very similar, and the effects of the stimulation of β_1-ARs are studied in detail previously (see Fig. 23 and Table 1 in Ref. 27). They demonstrated that the application of 1 µM isoproterenol affected APDs at all levels of repolarization (25%, 50%, 75%, and 90%; see also Table 1 in this paper). In contrast, the stimulation of β_2-ARs with 1 µM isoproterenol, when β_1-ARs are blocked, affects mostly the later phases of repolarization (APD_{75} and APD_{90}), and the effects of β_2-ARs can be revealed upon application of PTX or inhibition of PDE3,4 (see Fig. 1A and Table 1).

Figure 3.10 shows mouse action potentials for control conditions and after application of 1 µM isoproterenol in the PTX-pretreated myocytes when $\beta1$-ARs are blocked. In this case, APD_{25} does not change at all, and the

Table 1 Action potential durations (in ms) upon stimulation of both β_1-ARs and β_2-ARs, β_1-ARs alone, and β_2-ARs alone under different physiological conditions

	APD_{25}	APD_{50}	APD_{75}	APD_{90}
β_1- & β_2-ARs				
Control	1.7	3.3	9.35	26.15
Isoproterenol 1 µM	1.8	3.8	11.1	30.00
PTX	1.7	3.2	9.35	26.15
PTX + Isoproterenol 1 µM	1.8	3.8	11.6	32.35
PDE3,4 inhibition	1.85	3.95	12.1	33.25
PDE3,4inhibition+Isoproterenol 1µM	1.8	3.9	11.45	32.30
β_1-ARs				
Control	1.7	3.2	9.3	25.95
Isoproterenol 1 µM	1.7	3.85	11.1	30.15
PTX	1.7	3.2	9.35	25.95
PTX + Isoproterenol 1 µM	1.85	3.85	11.1	30.15
PDE3,4 inhibition	1.9	3.95	11.9	32.85
PDE3,4 inhibition + Isoproterenol 1 µM	1.8	3.9	11.5	31.65
β_2-ARs				
Control	1.6	3.1	8.55	24.05
Isoproterenol 1 µM	1.6	3.0	8.9	25.35
PTX	1.6	3.05	8.55	24.05
PTX + Isoproterenol 1 µM	1.6	3.05	10.1	29.4
PDE3,4 inhibition	1.6	3.1	9.9	29.65
PDE3,4 inhibition + Isoproterenol 1 µM	1.6	3.15	10.7	31.8
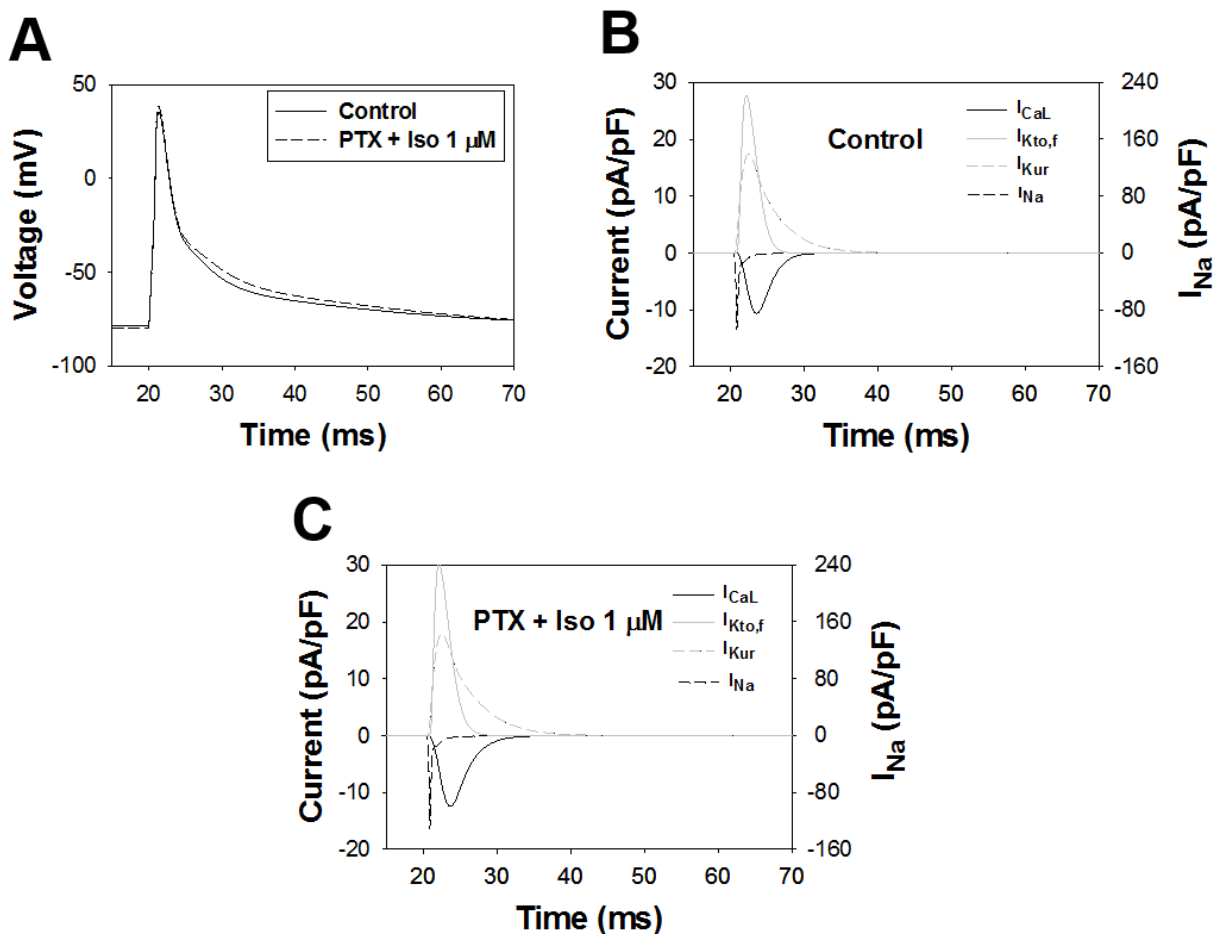
Figure 3.10 Mouse action potential and underlying major ionic currents upon activation of β_2-ARs with the inhibition of G_i. **Panel A:** Simulated mouse action potentials for control (solid line) and upon activation of β_2-ARs alone (β_1-ARs are blocked) with the inhibition of G_i (dashed line). **Panel B:** Simulated major ionic currents underlying mouse action potential in control. **Panel C:** Simulated major ionic currents underlying mouse action potential after the application of 1 μM isoproterenol and the inhibition of G_i with PTX. In **Panels A-C**, action potentials and ionic currents are shown after 300 s stimulation with 1 Hz.

APD$_{50}$ change is less than 2%. However, prolongations of APD$_{75}$ and APD$_{90}$ are quite significant, 18% and 22%, respectively, suggesting a strong effect of stimulation of β_2-ARs (see also Table 1). The effect of an application of 1 μM isoproterenol without PTX is significantly smaller and increases APD$_{75}$ and APD$_{90}$ by ~5% only (Table 1). Even larger increases in APD$_{75}$ and APD$_{90}$ are observed upon application of 1 μM isoproterenol and inhibition of PDE3 and PDE4 (25% and 32%, respectively, Table 1). Thus, stimulation of β_2-ARs with blocked β_1-ARs can

produce significant physiological effects on APDs upon stimulation with 1 µM isoproterenol and additional inhibition of G_i or PDE3 and PDE4.

Our mathematical model allows for exposing the mechanisms of APD changes at different levels of repolarization after stimulation of β_2-ARs with 1 µM isoproterenol in the PTX-pretreated myocytes. Figure 3.10B and C plot the behavior of the major repolarization currents at early phases of repolarization (APD_{25} and APD_{50}). The lack of changes in APD_{25} and APD_{50} are explained by a relatively small increase in the inward currents I_{Na} and I_{CaL}, which is balanced by a similarly small increase in the outward current $I_{Kto,f}$. The changes in APD_{75} and APD_{90} are determined predominantly by the changes in the inward current I_{CaL} and the outward current I_{Kur}: I_{CaL} increased by ~1.8 pA/pF and I_{Kur} increased by only ~0.5 pA/pF, suggesting prolongation of APD_{75} and APD_{90}.

Figure 3.11 shows changes in the major ionic currents upon stimulation of both β_1-ARs and β_2-ARs, β_1-ARs alone, or β_2-ARs alone. Stimulation of both β_1-ARs and β_2-ARs, or β_1-ARs alone demonstrate similar patterns of changes in ionic currents under different physiological conditions (Fig. 3.11A and B). Without isoproterenol, an application of PTX does not affect current magnitudes, while inhibition of PDE3 and PDE4 increases I_{Na}, I_{CaL} (both caveolar, I_{CaLc}, and extracaveolar, I_{CaLe}, fractions), and I_{Kur}, and decreases $I_{Kto,f}$, leading to APD prolongation in the latter case. The application of 1 µM isoproterenol without other interventions and the application of 1 µM isoproterenol with inhibition of G_i or PDE3 and PDE4 result in larger increases in I_{Na}, I_{CaL}, and I_{Kur}, and decreases $I_{Kto,f}$, which also promote APD prolongation at all repolarization levels.
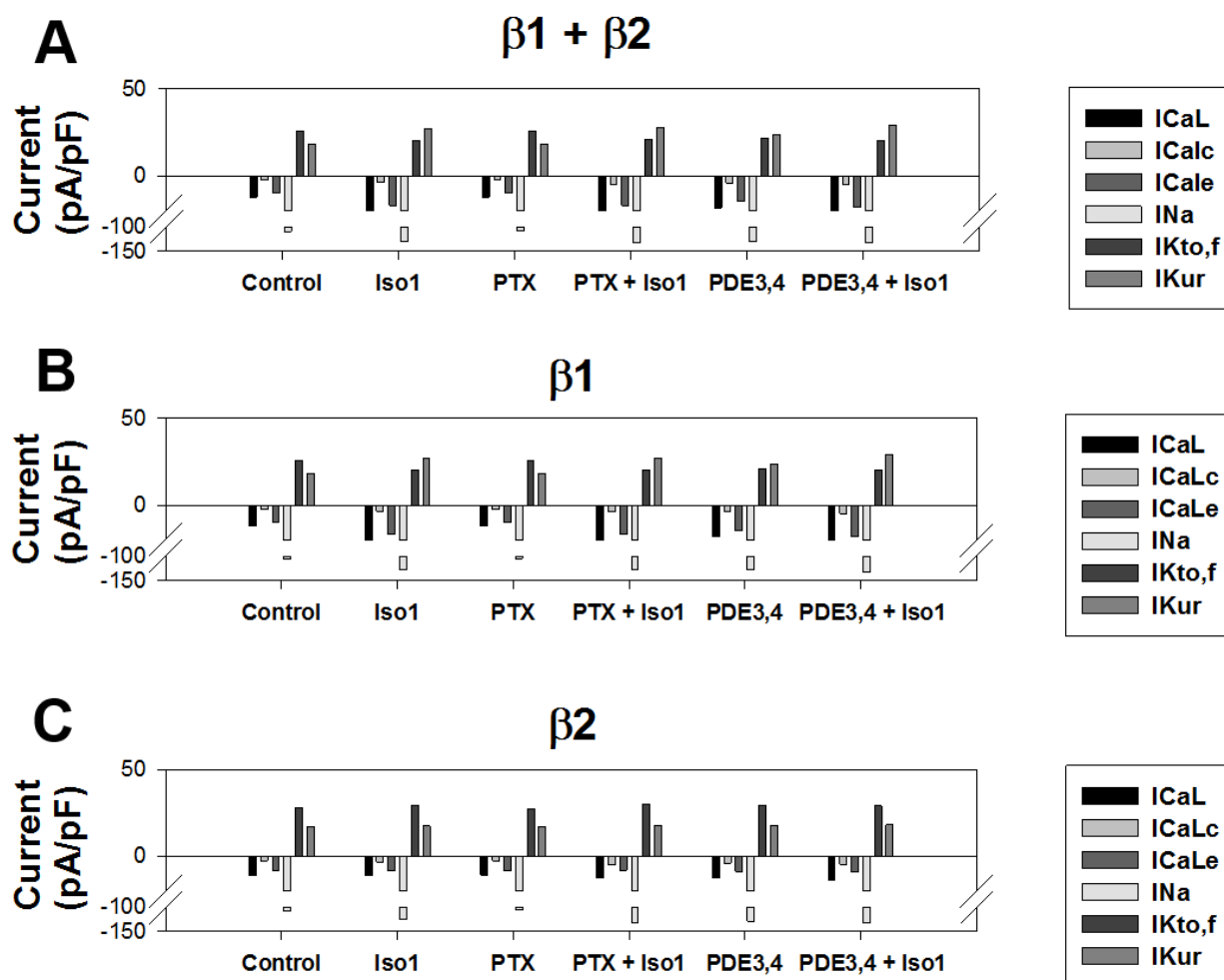
*Figure 3.11 Simulated magnitudes of major ionic currents in mouse ventricular myocytes upon stimulation of β₁-ARs and β₂-ARs under different physiological conditions. **Panel A:** Activation of both β₁-ARs and β₂-ARs. **Panel B:** Activation of β₁-ARs alone. **Panel C:** Activation of β₂-ARs alone. In **Panels A-C**, simulated data are shown for control (control), upon application of 1 μM isoproterenol (Iso1), with the inhibition of G_i (PTX), upon application of 1 μM isoproterenol with the inhibition of G_i (PTX + Iso1), with inhibition of PDE3 and PDE4 (PDE3,4), and upon application of 1 μM isoproterenol with the inhibition of PDE3 and PDE4 (PDE3,4 + Iso1); ionic currents are shown after 300 s stimulation with 1 Hz.*

A different picture is observed during stimulation of β₂-ARs alone (Fig. 3.11C). Without isoproterenol, the application of PTX does not affect current magnitudes. Other interventions do not affect APD_{25} and APD_{50} significantly as well (Table 1). The application of 1 μM isoproterenol without other interventions increases mostly I_{Na}, I_{CaL}, and $I_{Kto,f}$, which balance each other, resulting

in relatively small changes in APD_{75} and APD_{90} (~5% increase of both). However, more significant changes are observed in APD_{75} and APD_{90} (15% - 32% increase) upon stimulation of β_2-ARs with 1 μM isoproterenol and inhibition of G_i and PDE3 and PDE4 (Table 1). While there is no experimental data on the effects of stimulation of β_2-ARs in wild type mouse ventricular myocytes, the data on APD_{50} and APD_{90} in transgenic (TG) β_2-AR overexpressing mouse ventricular myocytes do not show significant change in APD_{50} compared to WT littermates, but APD_{90} is significantly prolonged in TG mice[63]. In all cases, these prolongations are due to non-balanced increase in I_{CaL} and I_{Kur}, with the larger increase in the inward I_{CaL} compared to the outward I_{Kur} (Fig. 3.11C). In contrast to stimulation of both β_1-ARs and β_2-ARs, or β_1-ARs alone, stimulation of β_2-ARs alone predominately increases the caveolar fraction of I_{CaL}, I_{CaLc}. The model predictions on the changes in action potentials and underlying mechanisms can be verified by the future experiments.

3.2.7 *The effects on $[Ca^{2+}]_i$ transients*

Experimental data shows that stimulation of both β_1-ARs and β_2-ARs, β_1-ARs alone, or β_2-ARs alone with isoproterenol enhances $[Ca^{2+}]_i$ transients in mouse ventricular myocytes, however, to different magnitudes. Micro molar concentrations of isoproterenol lead to a significant (up to 5-fold) increase in intracellular $[Ca^{2+}]_i$ transients obtained from mouse ventricular myocytes when both β_1-ARs and β_2-ARs are intact[64,65]. Experimental stimulation of β_2-ARs alone with 0.1 - 1.0 μM zinterol in PTX-pretreated ventricular myocytes increases $[Ca^{2+}]_i$ transients to a lesser extent, up to 2-fold[66,67] (data on stimulation of β_2-ARs alone with isoproterenol are not available). Our simulations show similar behavior; however, we simulated stimulation with isoproterenol and a corresponding block of β_1-ARs or β_2-ARs, because zinterol is not a specific agonist for β_2-ARs

and can affect both β_1-ARs or β_2-ARs, which create difficulties in the separation of the effects on these receptors[43].

Figure 3.12A demonstrates $[Ca^{2+}]_i$ transients for control conditions and after application of 1 µM isoproterenol in the presence of G_i and β_1-ARs block. It is seen that the peak value of $[Ca^{2+}]_i$ increases by about 1.4 fold, which is close to the experimental data[66,67]. Figure 3.12B demonstrates simulations of the effects of both β_1-ARs and β_2-ARs, β_1-ARs alone, and β_2-ARs alone under different physiological conditions and their comparisons with experimental data. Stimulation of both β_1-ARs and β_2-ARs with 1 µM isoproterenol (no G_i inhibition) results in a 3.8-fold increase in $[Ca^{2+}]_i$, which is in line with the experimental data[64,65]. The same result (3.8-fold increase in $[Ca^{2+}]_i$) is obtained in the simulation of the stimulation of β_1-ARs alone. However, stimulation of β_2-ARs alone with 1 µM isoproterenol without inhibition of G_i does not affect $[Ca^{2+}]_i$. Inhibition of G_i by PTX does not change $[Ca^{2+}]_i$ transients for all three patterns of β-ARs. However, stimulation of both β_1-ARs and β_2-ARs with 1 µM isoproterenol plus PTX slightly increases $[Ca^{2+}]_i$ as compared with 1 µM isoproterenol alone (4.3-fold increase). Stimulation of β_1-ARs alone increases $[Ca^{2+}]_i$ to the same degree as the stimulation of both β_1-ARs and β_2-ARs without inhibition of G_i (3.8-fold increase). Stimulation of β_2-ARs alone increases $[Ca^{2+}]_i$ only by 1.4-fold (Fig. 3.12B).

$[Ca^{2+}]_i$ transients are also affected by the inhibition of PDE3 and PDE4. Our simulation data shows an increase in $[Ca^{2+}]_i$ upon inhibition of PDE3 and PDE4 without isoproterenol application when both β_1-ARs and β_2-ARs are available, β_2-ARs are blocked, or β_1-ARs are

blocked by 3.0-, 2.9-, or 1.7-folds, respectively. An additional application of 1 µM isoproterenol
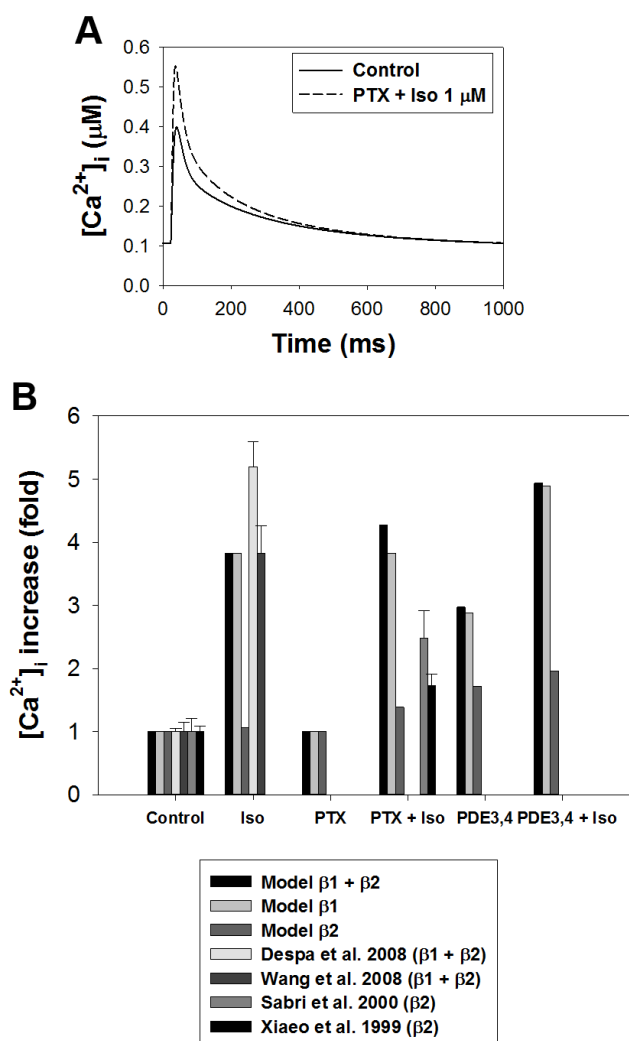
leads to a

Figure 3.12 $[Ca^{2+}]_i$ transients in mouse ventricular myocytes upon stimulation of β_1-ARs and β_2-ARs under different physiological conditions. **Panel A:** *Simulated $[Ca^{2+}]_i$ transients obtained for control and after application of 1 µM isoproterenol with the inhibition of G_i (PTX).* **Panel B:** *Experimental and simulated data on a relative increase in $[Ca^{2+}]_i$ transients. Experimental data by Despa et al.[64] and Wang et al.[65] are obtained upon stimulation of both β_1-ARs and β_2-ARs; experimental data by Sabri et al.[66] and Xiao et al.[67] are obtained upon stimulation of β_2-ARs with zinterol (0.1 µM and 1.0 µM, respectively). Simulations are performed for stimulation of both β_1-ARs and β_2-ARs, β_1-ARs alone, and β_2-ARs alone under different physiological conditions: control (control), upon application of 1 µM isoproterenol (Iso), upon the inhibition of G_i (PTX), upon application of 1 µM isoproterenol with the inhibition of G_i (PTX + Iso), with the inhibition of PDE3 and PDE4 (PDE3,4), or upon application of 1 µM isoproterenol with the inhibition of PDE3 and PDE4 (PDE3,4 + Iso). $[Ca^{2+}]_i$ transients are shown after 300 s stimulation with 1 Hz.*

larger increase in $[Ca^{2+}]_i$ transients when both β_1-ARs and β_2-ARs are available, β_2-ARs are blocked, or β_1-ARs are blocked, by 4.9-, 4.9-, or 2.0-folds, respectively (Fig. 3.12B).

Thus, stimulation of both β_1-ARs and β_2-ARs or β_1-ARs alone results in strong increases in $[Ca^{2+}]_i$ transients, while the effects of stimulation of β_2-ARs alone can be revealed only upon stimulation with isoproterenol during inhibition of G_i or PDE3 and PDE4.

3.2.8 *The effects on Ca^{2+} and Na^+ fluxes*

Our model allows for evaluation of various Ca^{2+} and Na^+ integral fluxes and their modifications by stimulations of β_1-ARs and β_2-ARs by isoproterenol under different experimental conditions (Figs. 3.13-3.15), which can be verified by future experiments. The effects of β_1-ARs were investigated in detail in Ref. 27 and they are similar to the effects of β_1-ARs and β_2-ARs together (compare Fig. 3.14A and Fig. 3.14B, Fig. 3.15A and Fig. 3.15B).

Stimulation of both β_1-ARs and β_2-ARs or β_1-ARs alone with 1 µM isoproterenol results in ~1.5- to 2.0-fold increase in major integral Ca^{2+} fluxes (through the L-type Ca^{2+} channels, I_{CaL}, Ca^{2+} release influx, J_{rel}, Ca^{2+} uptake influx minus Ca^{2+} leak from the SR, J_{up} - J_{leak}, Ca^{2+} efflux through the Na^+/Ca^{2+} exchanger, J_{NaCa}, and Ca^{2+} amount bound to troponin, J_{trpn}). The effects of stimulation of β_2-ARs alone is smaller and can be only revealed with inhibition of G_i. Figure 3.13, A and B, demonstrates the effects of stimulation of β_2-ARs alone with 1 µM isoproterenol and inhibition of G_i by PTX. It is seen that stimulation of β_2-ARs leads to an increase in Ca^{2+} influx through the L-type Ca^{2+} channels from 1.23 µM to 1.67 µM (36% increase) during cardiac cycles
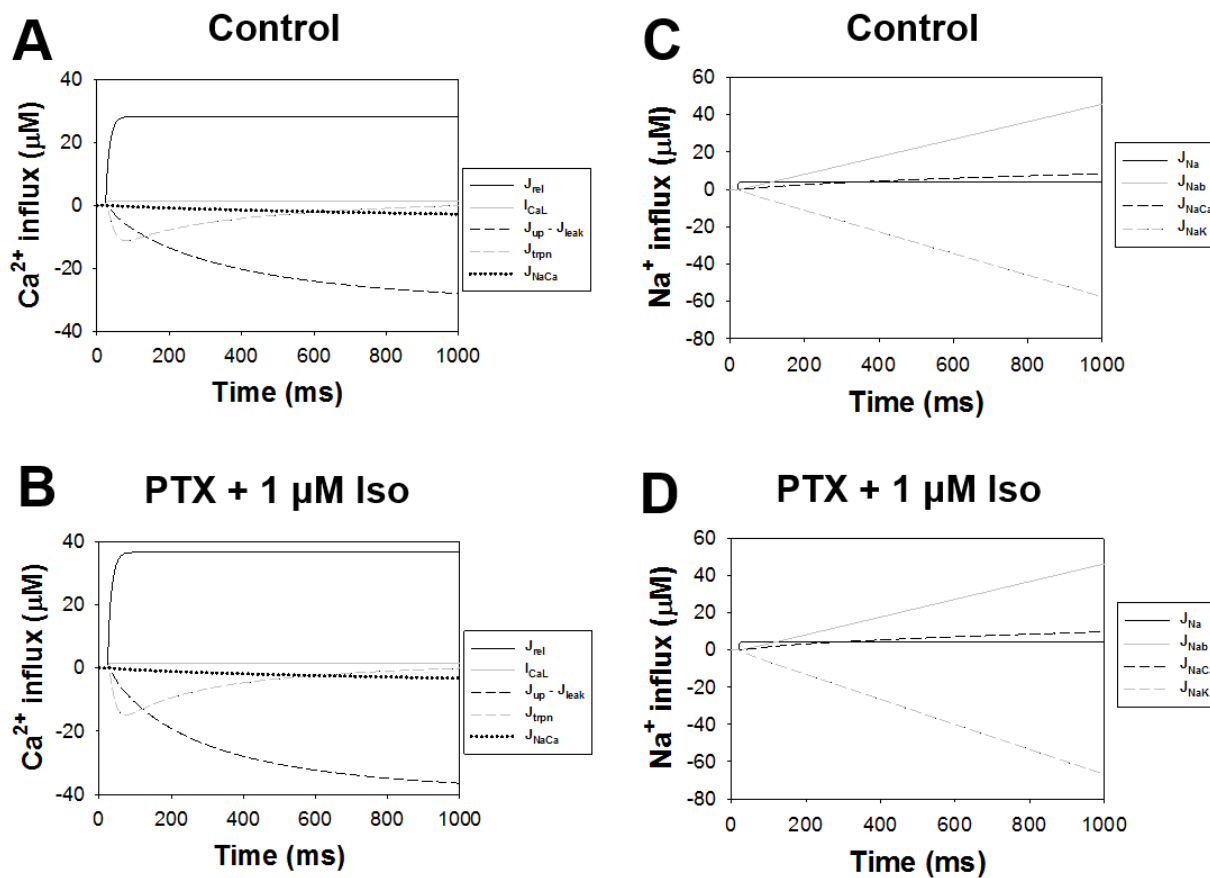
Figure 3.13 Integrated Ca^{2+} and Na$^+$ fluxes (influxes). *Simulation of the selective activation of β_2-ARs with 1 μM isoproterenol (β_1-ARs are blocked) and inhibition of G_i by PTX on the integrated Ca^{2+} and Na$^+$ fluxes (influxes) in isolated mouse ventricular myocyte model cell during one cardiac cycle. Simulated Ca^{2+} influxes are shown in **Panels A** and **B**. Simulated Na$^+$ influxes are shown in **Panels C** and **D**. Simulations for control conditions are shown in **Panels A** and **C**. Simulations for 1 μM isoproterenol and inhibition of G_i by PTX are shown in **Panels B** and **D**. Ca^{2+} and Na$^+$ fluxes are shown after 300 s of stimulation with 1 Hz.*

Figure 3.14 Magnitudes of the integral Ca^{2+} fluxes. *Simulated magnitudes of the integral Ca^{2+} fluxes in mouse ventricular myocytes upon stimulation of β$_1$-ARs and β$_2$-ARs under different physiological conditions. **Panel A:** Activation of both β$_1$-ARs and β$_2$-ARs. **Panel B:** Activation of β$_1$-ARs alone. **Panel C:** Activation of β$_2$-ARs alone. In **Panels A-C**, simulated data on Ca^{2+} release from the sarcoplasmic reticulum (Jrel), Ca^{2+} influx through the L-type Ca^{2+} channels (JCaL), difference between Ca^{2+} uptake and Ca^{2+} leak from the SR (Jup - Jleak), and Ca^{2+} flux through the Na$^+$/Ca^{2+} exchanger (JNaCa) are shown for control (control), upon application of 1 μM isoproterenol (Iso), with the inhibition of G$_i$ (PTX), upon application of 1 μM isoproterenol with the inhibition of G$_i$ (PTX + Iso), with the inhibition of PDE3 and PDE4 (PDE3,4), or upon application of 1 μM isoproterenol with the inhibition of PDE3 and PDE4 (PDE3,4 + Iso). Integral Ca^{2+} fluxes are shown after 300s stimulation with 1 Hz.*

(1 Hz stimulation). Increases in Ca^{2+} influx results in an increase in Ca^{2+}-induced Ca^{2+} release, from 28 μM to 37 μM (30% increase; similar increase is observed for J_{up} - J_{leak}). An increase in intracellular [Ca^{2+}]$_i$ transients after an application of isoproterenol also increases Ca^{2+} extrusion from the cytosol by the Na$^+$/Ca^{2+} exchanger, J_{NaCa}, from 2.78 μM to 3.23 μM (16% increase). The

Ca^{2+} amount bound to troponin during one cardiac cycle (1000 ms, 1 Hz), which is important for cardiac cell contraction, is also increased by ~33%, from 11.2 µM to 14.9 µM.

Stimulation of β_2-ARs alone with 1 µM isoproterenol and inhibition of G_i by PTX also affects the Na^+ integral fluxes (Fig. 3.13, C and D). The Na^+ influx by the fast Na^+ current, J_{Na}, increases by 14%, from 3.89 µM to 4.44 µM. A little change is seen for the background Na^+ influx, J_{Nab}, from 45.6 µM to 46.3 µM (1.5% increase); however, Na^+ influx through the Na^+/Ca^{2+} exchanger, J_{NaCa}, increases by 16%, from 8.3 µM to 9.7 µM, and Na^+ extrusion by Na^+-K^+ pump, J_{NaK}, is also increased from 57.6 µM to 66.9 µM (16% increase).

Cumulative simulated data on the effects of both β_1-ARs and β_2-ARs, β_1-ARs alone, or β_2-ARs alone on the Ca^{2+} and Na^+ integral fluxes under different interventions are shown in Figs. 3.14 and 3.15. Figure 3.14 plots the data on Ca^{2+} fluxes. Stimulation of both β_1-ARs and β_2-ARs or β_1-ARs alone under different physiological conditions results in similar changes in Ca^{2+} fluxes. Stimulation of both β_1-ARs and β_2-ARs with 1 µM isoproterenol increases J_{CaL} from 1.6 µM to 3.3 µM (109% increase), J_{rel} from 35 µM to 61 µM (75% increase; similar increase is in J_{up} - J_{leak}), and J_{NaCa} from 3.1 µM to 4.7 µM (51% increase). Very similarly, stimulation of β_1-ARs alone with 1 µM isoproterenol increases J_{CaL} from 1.5 µM to 3.3 µM (112% increase), J_{rel} from 35 µM to 62 µM (75% increase; similar increase is in J_{up} - J_{leak}), and J_{NaCa} from 3.1 µM to 4.6 µM (52% increase). In contrast, stimulation of β_2-ARs alone with 1 µM isoproterenol only slightly increases Ca^{2+} influxes: J_{CaL} from 1.2 µM to 1.4 µM (10% increase), J_{rel} from 28 µM to 30 µM (5% increase; similar increase is in J_{up} - J_{leak}), and J_{NaCa} from 2.8 µM to 2.9 µM (5% increase). Inhibition of G_i with PTX does not change Ca^{2+} fluxes in all three cases. G_i inhibition only slightly changes the
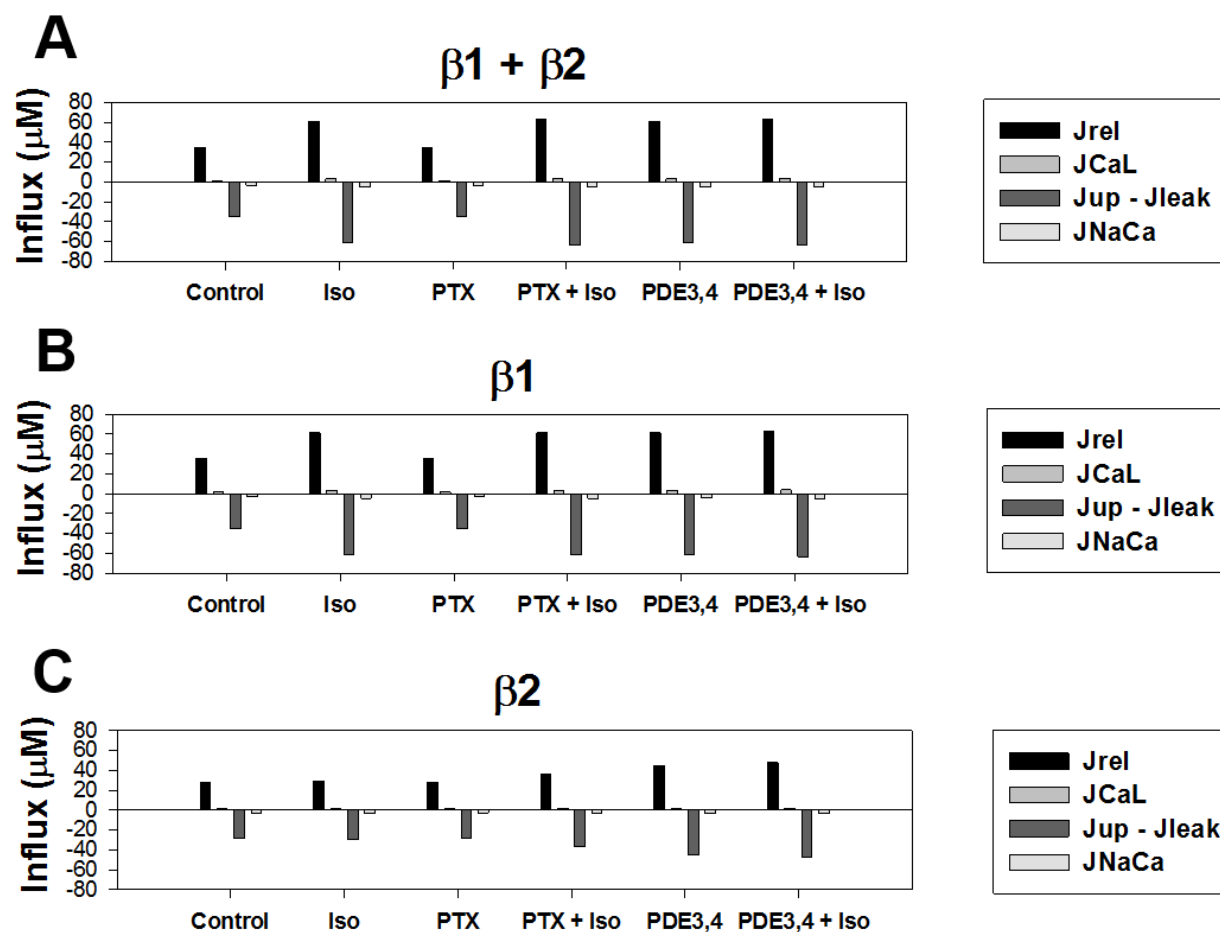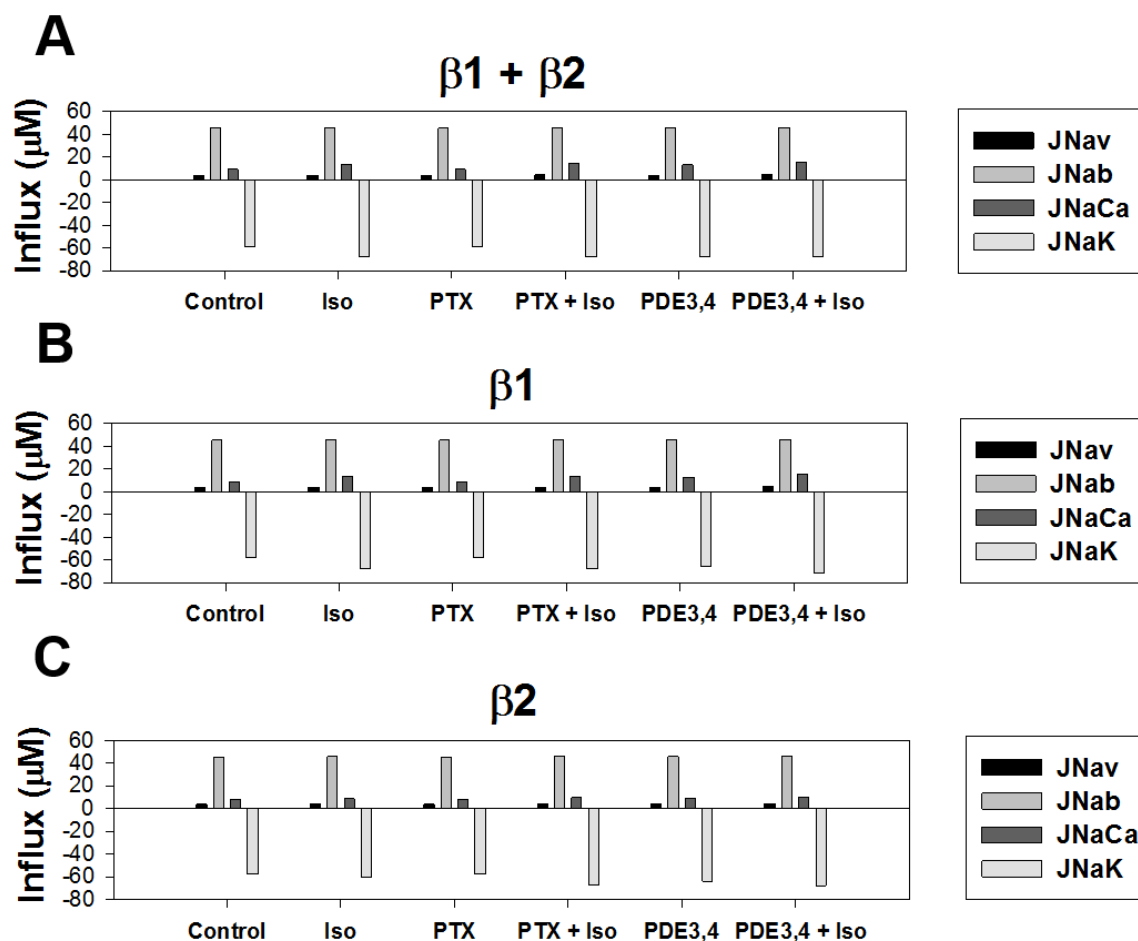
Figure 3.15 Magnitudes of integral Na$^+$ fluxes. *Simulated magnitudes of integral Na$^+$ fluxes in mouse ventricular myocytes upon stimulation of β$_1$-ARs and β$_2$-ARs under different physiological conditions.* **Panel A:** *Activation of both β$_1$-ARs and β$_2$-ARs.* **Panel B:** *Activation of β$_1$-ARs alone.* **Panel C:** *Activation of β$_2$-ARs alone. In* **Panels A-C**, *simulated data on Na$^+$ influx through the fast Na$^+$ channels (JNav), background Na$^+$ influx (JNab), Na$^+$ flux through the Na$^+$/Ca^{2+} exchanger (JNaCa), and Na$^+$ flux through the Na$^+$-K$^+$ pump (JNaK) are shown for control (control), upon application of 1 μM isoproterenol (Iso), with the inhibition of G$_i$ (PTX), upon application of 1 μM isoproterenol with the inhibition of G$_i$ (PTX + Iso), with the inhibition of PDE3 and PDE4 (PDE3,4), or upon application of 1 μM isoproterenol with the inhibition of PDE3 and PDE4 (PDE3,4 + Iso). Integral Na$^+$ fluxes are shown after 300 s stimulation with 1 Hz.*

results of stimulation of both β$_1$-ARs and β$_2$-ARs with 1 μM isoproterenol: increases J$_{CaL}$ from 1.6 μM to 3.6 μM (128% increase), J$_{rel}$ from 35 μM to 63 μM (80% increase), and J$_{NaCa}$ from 3.1 μM to 4.9 μM (60% increase). Inhibition of G$_i$ during stimulation of β$_1$-ARs alone with 1 μM isoproterenol produces the same effect as stimulation without inhibition of G$_i$. However,

stimulation of β_2-ARs alone with 1 µM isoproterenol plus G_i inhibition dramatically changes the results obtained without inhibition of G_i: it increases J_{CaL} from 1.2 µM to 1.7 µM (36% increase), J_{rel} from 28 µM to 37 µM (30% increase), and J_{NaCa} from 2.8 µM to 3.2 µM (16% increase). These data suggest that the effects of stimulation of β_2-ARs alone on Ca^{2+} fluxes can be revealed upon inhibition of G_i. Figure 3.14 also demonstrates the effects of inhibition of PDE3 and PDE4 without and with stimulation by 1 µM isoproterenol. Quite a large effect on Ca^{2+} fluxes occurs upon inhibition of PDE3 and PDE4, when both β_1-ARs and β_2-ARs are intact or β_2-ARs are blocked, which is similar to the effect of stimulation by 1 µM isoproterenol alone. More interesting are the effects of PDE3 and PDE4 inhibition without and with 1 µM isoproterenol on Ca^{2+} integral fluxes when β_2-ARs are stimulated alone. In the case of PDE3 and PDE4 inhibition alone, J_{CaL} increases from 1.2 µM to 1.6 µM (33% increase), J_{rel} from 28 µM to 45 µM (61% increase), and J_{NaCa} from 2.8 µM to 3.2 µM (14% increase). An additional application of 1 µM isoproterenol only slightly increases Ca^{2+} fluxes: J_{CaL} from 1.6 µM to 1.9 µM (14% increase), J_{rel} from 45 µM to 48 µM (6% increase), and J_{NaCa} from 3.2 µM to 3.4 µM (8% increase).

Figure 3.15 shows cumulative simulated data on the effects of both β_1-ARs and β_2-ARs, β_1-ARs alone, or β_2-ARs alone on the Na^+ integral fluxes under different interventions. As in the case of Ca^{2+} fluxes, stimulation of both β_1-ARs and β_2-ARs or β_1-ARs alone under different physiological conditions results in similar changes in Na^+ fluxes. Stimulation of both β_1-ARs and β_2-ARs with 1 µM isoproterenol increases J_{Na} from 3.9 µM to 4.2 µM (8% increase), J_{Nab} from 45.6 µM to 46.0 µM (1% increase), J_{NaCa} from 9.3 µM to 14.0 µM (51% increase), and J_{NaK} from 58.5 µM to 67.7 µM (16% increase). Similarly, stimulation of β_1-ARs alone with 1 µM isoproterenol increases J_{Na} from 3.8 µM to 4.1 µM (9% increase), J_{Nab} from 45.4 µM to 45.8 µM (1% increase), J_{NaCa} from 9.2 µM to 13.9 µM (52% increase), and J_{NaK} from 58.1 µM to 67.5 µM

(16% increase). In contrast, stimulation of β_2-ARs alone with 1 µM isoproterenol leads to significantly smaller increases of Na^+ influxes, except for J_{Na}: J_{Na} from 3.9 µM to 4.2 µM (9% increase), J_{Nab} from 45.6 µM to 45.8 µM (0.5% increase), J_{NaCa} from 8.3 µM to 8.8 µM (5% increase), and J_{NaK} from 57.6 µM to 60.4 µM (5% increase). Inhibition of G_i with PTX does not change Na^+ fluxes in all three cases. Stimulation of both β_1-ARs and β_2-ARs or β_1-ARs alone with 1 µM isoproterenol plus inhibition of G_i show Na^+ fluxes increase, which is similar to the effects of 1 µM isoproterenol alone. However, stimulation of β_2-ARs alone with 1 µM isoproterenol plus G_i inhibition remarkably changes the results: J_{Na} increases from 3.9 µM to 4.4 µM (14% increase), J_{Nab} from 45.6 µM to 46.3 µM (1.6% increase), J_{NaCa} from 8.3 µM to 9.7 µM (16% increase), and J_{NaK} from 57.6 µM to 66.9 µM (16% increase).

Thus, simulation data suggest that the effects of stimulation of β_2-ARs alone on Na^+ fluxes can be more reliably revealed upon inhibition of G_i. Na^+ fluxes upon inhibition of PDE3 and PDE4 without and with 1 µM isoproterenol do not differ significantly from those obtained upon stimulation with the same amount of isoproterenol and inhibition of G_i for all three case of β_1-ARs and β_2-ARs availability. In terms of revealing the effects of β_2-ARs, the differences in changes of Na^+ fluxes upon inhibition of PDE3 and PDE4 without and with 1 µM isoproterenol are rather small compared to the usage of inhibition of G_i.

3.2.9   *The effects on the Na^+-K^+ pump and $[Na^+]_i$ decline*

The Na^+-K^+ pump, which is regulated by phospholemman, is one of the important players in the sympathetic stimulation of cardiac cells[64,68]. Experimental data demonstrates that increased activity in the Na^+-K^+ pump upon stimulation with isoproterenol results in $[Na^+]_i$ decline in cardiac cells[68]. Such a decline in $[Na^+]_i$ was suggested to be a protective mechanism against cellular Ca^{2+}

overload and pro-arrhythmic events. However, the contribution of different types of β-ARs to [Na⁺]ᵢ decrease was not studied experimentally.

Therefore, we simulated the effects of the stimulation of $β_1$-ARs and $β_2$-ARs on the dynamics of intracellular [Na⁺]ᵢ concentration under different physiological conditions (Fig. 3.16). When both $β_1$-ARs and $β_2$-ARs are intact, stimulation of the cell with 1 μM isoproterenol leads to a reduction of [Na⁺]ᵢ to a new steady-state value within ~600 seconds (black solid line in Fig. 3.16). Additional inhibition of G_i with PTX results in a significantly faster decline in [Na⁺]ᵢ (red solid line in Fig. 3.16). To reveal the major contributors to the decline in [Na⁺]ᵢ, we performed simulations when
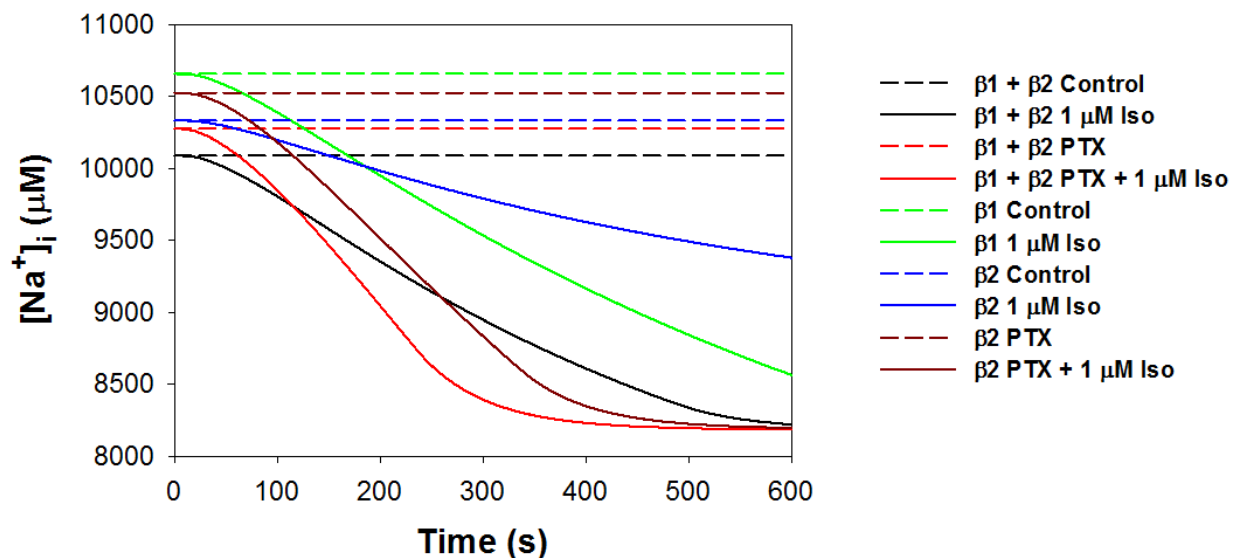
Figure 3.16 [Na⁺]ᵢ concentration as function of time. *Simulated [Na⁺]ᵢ concentration as function of time in mouse ventricular myocytes upon stimulation of β₁-ARs and β₂-ARs under different physiological conditions. Data are shown for control (Control), upon application of 1 μM isoproterenol (1 μM Iso), with the inhibition of Gᵢ (PTX), and upon application of 1 μM isoproterenol with the inhibition of Gᵢ (PTX + Iso). Dashed lines plot steady state [Na⁺]ᵢ concentrations in the cell in control and during inhibition of Gᵢ; solid lines plot [Na⁺]ᵢ concentrations after application of 1 μM isoproterenol. Simulations were performed for the case, when both β₁-ARs and β₂-ARs are intact (black lines for control and red lined for the inhibition of Gᵢ), when β₂-ARs are inhibited (green lines, data with and without inhibition of Gᵢ are identical), and when β₁-ARs are inhibited (blue lines for control and dark red lined for the inhibition of Gᵢ).*

only one type of β-ARs was present. In the case when β_2-ARs are blocked, an application of 1 μM isoproterenol results in a $[Na^+]_i$ decline (green solid line in Fig. 3.16), the rate of which is similar to the case when both β_1-ARs and β_2-ARs are intact without inhibition of G_i. Additional G_i inhibition does not affect the simulation results (data not shown). In the case when β_1-ARs were blocked, an application of 1 μM isoproterenol results in a relatively slow $[Na^+]_i$ decline (blue solid line in Fig. 3.16). Additional inhibition of G_i with PTX dramatically accelerates the isoproterenol-induced $[Na^+]_i$ decline (dark red line in Fig. 3.16), with a rate similar to the case of inhibition of G_i when β_1-ARs and β_2-ARs are intact (red solid line in Fig. 3.16). Thus, our simulations suggest an important role of the stimulation of β_2-ARs in $[Na^+]_i$ removal in the presence of PTX (inhibition of G_i). This interesting simulation result is supported by the experimental observations of the stronger coupling of β_2-ARs to G_s protein than of β_1-ARs[69], the primary localization of β_2-ARs in the caveolar compartment[20,31], and that most of I_{NaK} activity is localized in the caveolar compartment[70]. However, direct experimental observation of the important role of β_2-ARs in this case is currently absent and can be verified by future experiments.

3.2.10 The contribution of phosphorylation of PKA targets to the changes in the action potential and $[Ca^{2+}]_i$ transients

Phosphorylation of the proteins involved in intracellular signaling systems plays an important role in healthy and diseased hearts. Stimulation of the β_1- and β_2-adrenergic signaling systems results in the phosphorylation of several PKA target proteins that affect action potential and $[Ca^{2+}]_i$ transients. Therefore, it is of significant interest to reveal the major PKA targets that contribute to the changes in the action potential and $[Ca^{2+}]_i$ transients upon stimulation. The experimental investigation of individually eliminating PKA target protein phosphorylation is quite challenging

whether using biochemical methods, due to the complex effects of the interventions (e.g., activation of phosphatases), or molecular biology methods, due to the difficulties in the generation of transgenic mice with mutations of the phosphorylation sites of the target proteins.

We used our mathematical model to simulate the effects of elimination of protein phosphorylation on the changes in the action potential and $[Ca^{2+}]_i$ transient upon stimulation of mouse ventricular myocytes with 1 µM isoproterenol for the two most interesting cases: 1) both β_1- and β_2-ARs are intact; 2) β_1-ARs are blocked and G_i is inhibited. We performed simulations for control conditions without application of isoproterenol, for control conditions with application of 1 µM isoproterenol, and for the conditions with application of 1 µM isoproterenol when the phosphorylation of phospholamban, troponin I, phospholemman (regulates Na^+-K^+ pump), ryanodine receptors, the L-type Ca^{2+} channels, or the channels responsible for the transient outward K^+ current $I_{Kto,f}$ and the ultrarapidly activating K^+ current I_{Kur} is removed. To eliminate phosphorylation, the rate of phosphorylation of the particular protein investigated was decreased by factor of 1000 and the dissociation constant for phosphorylation was increased by 1000. The model was then run for 10,000 seconds to ensure equilibrium. As a result, protein phosphorylation levels became negligible. Finally, starting from these initial conditions, 1 µM isoproterenol was applied for 300 seconds to the electrically stimulated cell ($I_{stim} = 80$ pA/pF, $\tau_{stim} = 1.0$ ms), and the action potential and $[Ca^{2+}]_i$ transient during the 300th period was analyzed. The changes in the shape of the action potential and $[Ca^{2+}]_i$ transient are shown in Fig. 3.17, and the changes in quantitative measures (APD_{50}, APD_{90}, and $[Ca^{2+}]_i$ transient magnitude) are shown in Fig. 3.18.

When both β_1- and β_2-ARs are intact, the most notable changes in the action potential shape are seen upon phosphorylation removal in proteins encoding ionic currents I_{CaL}, $I_{Kto,f}$, and I_{Kur} (Fig. 3.17A). These changes are also evident in Fig. 3.18, A and B, for APD_{50} and APD_{90}, except for

$I_{Kto,f}$, which phosphorylation removal does not affect APD_{90}. The removal phosphorylation of the L-type Ca^{2+} channels significantly shortened APD_{50} from 3.8 ms (control with 1 μM isoproterenol) to 3.1 ms and APD_{90} from 30.0 ms to 14.7 ms. The removal of phosphorylation of the channels responsible for the ultrarapidly activating K^+ current I_{Kur} significantly prolonged APD_{50} from 3.8 ms to 4.8 ms and APD_{90} from 30.0 ms to 42.4 ms. The removal of phosphorylation of the channels
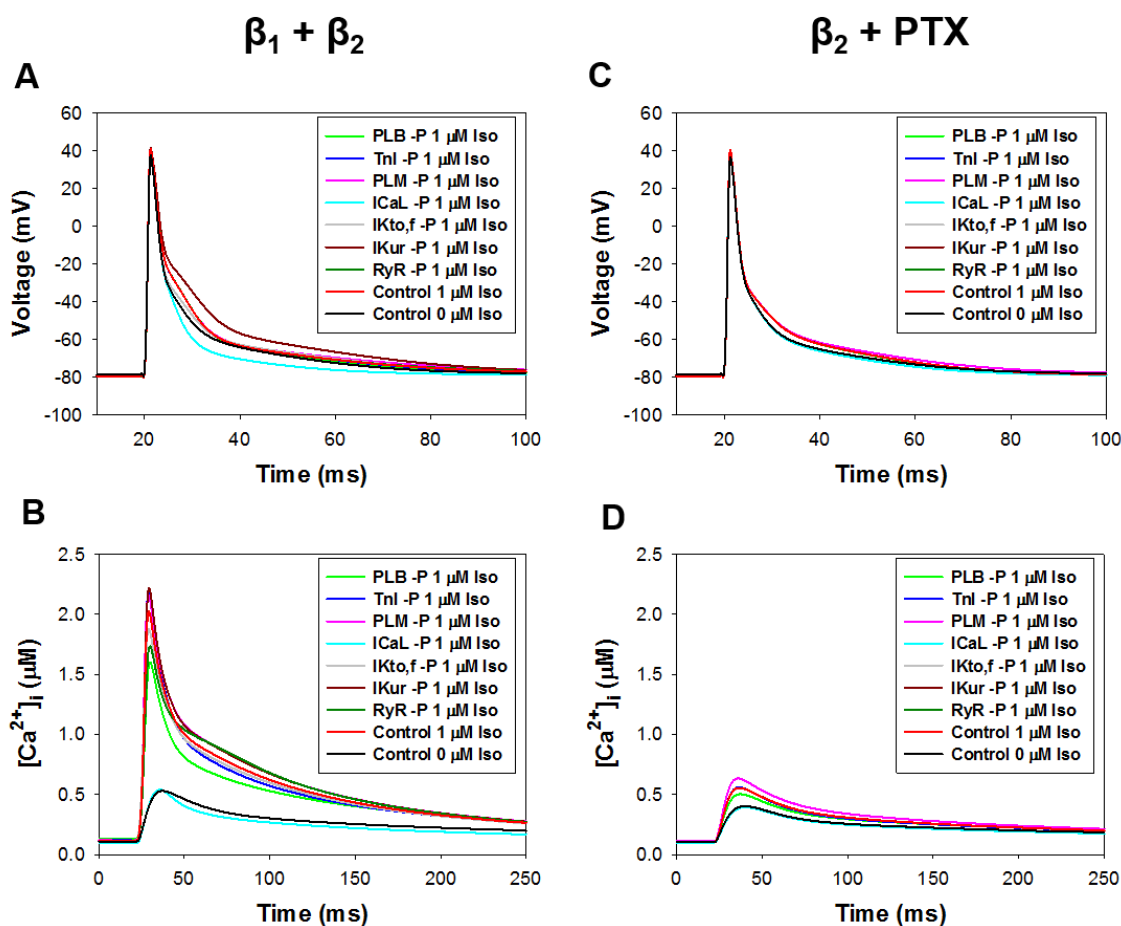
Figure 3.17 Simulated action potentials and $[Ca^{2+}]_i$ transients. *Simulated action potentials (**Panels A and C**) and $[Ca^{2+}]_i$ transients (**Panels B and D**) obtained upon stimulation of both β_1-ARs and β_2-ARs without inhibition of G_i (**Panels A and B**) and β_2-ARs with inhibition of G_i by PTX (**Panels C and D**). Data are shown for control without isoproterenol (black lines), control with 1 μM isoproterenol (red lines), and upon stimulation with 1 μM isoproterenol and removal of phosphorylation of phospholamban (green lines), troponin I (blue lines), phospholemman (which regulates Na^+-K^+ pump, magenta lines), the L-type Ca^{2+} channels (cyan lines), the channels responsible for $I_{Kto,f}$ (gray lines), the channels responsible for I_{Kur} (dark red lines), and ryanodine receptors (dark green lines). The action potential and $[Ca^{2+}]_i$ transients are shown during the 300th stimulation period with 1 Hz.*

responsible for the transient outward K^+ current $I_{Kto,f}$ significantly shortened only APD_{50} from 3.8 ms to 3.2 ms. When only β_2-ARs were selectively stimulated with 1 μM isoproterenol along with G_i inhibition (β_1-ARs are blocked), significant shortening of APD_{90} from 29.4 ms (control with 1 μM isoproterenol) to 22.7 ms is obtained only upon removal of phosphorylation in the L-type Ca^{2+} channels (Fig. 3.17C and Fig. 3.18, A and B).

The picture of the contribution of the phosphorylation of different PKA targets on $[Ca^{2+}]_i$ transient is more complex. When both β_1- and β_2-ARs are intact, the most notable changes in the magnitude of isoproterenol-stimulated $[Ca^{2+}]_i$ transient is seen upon phosphorylation removal of proteins encoding I_{CaL} (Fig. 3.17B and Fig. 3.18C). Phosphorylation removal of phospholamban, ryanodine receptors, and the channels responsible for the transient outward K^+ current, $I_{Kto,f}$, tend to reduce and phosphorylation removal of phospholemman, troponin I, and the channels responsible for the ultrarapidly activating K^+ current I_{Kur} tend to increase isoproterenol-stimulated $[Ca^{2+}]_i$ transient. We suggest that the availability of multiple regulation factors for $[Ca^{2+}]_i$ transient upon stimulation of the β-adrenergic signaling system ensures reliable control of Ca^{2+} dynamics under different physiological conditions. When only β_2-ARs were selectively stimulated with 1 μM isoproterenol along with G_i inhibition (β_1-ARs are blocked), the largest effect (decrease) on $[Ca^{2+}]_i$ transient is obtained upon phosphorylation removal in the L-type Ca^{2+} channels (Fig. 3.17D and Fig. 3.18C). Phosphorylation removal in only two other proteins affected $[Ca^{2+}]_i$ transient: phospholemman and phospholamban. Phosphorylation removal in phospholemman increased $[Ca^{2+}]_i$ transient and phosphorylation removal in phospholamban decreased $[Ca^{2+}]_i$ transient as compared to the isoproterenol-stimulated $[Ca^{2+}]_i$ under control (Fig. 18D).
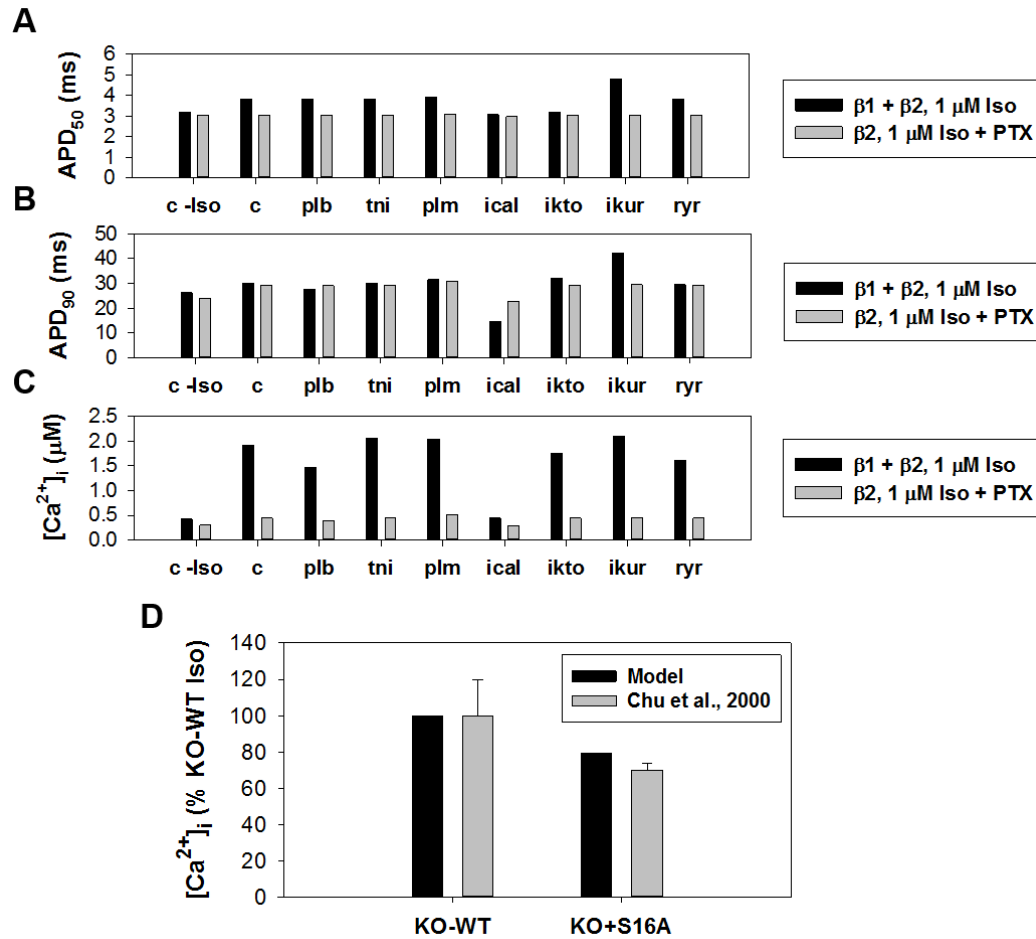
Figure 3.18 Changes in APD_{50}, APD_{90}, and $[Ca^{2+}]_i$ transient magnitudes. *Simulated changes in APD_{50} (**Panel A**), APD_{90} (**Panel B**), and $[Ca^{2+}]_i$ transient magnitudes (**Panel C**) obtained upon stimulation of both β_1-ARs and β_2-ARs without inhibition of G_i (black bars) and β_2-ARs with inhibition of G_i by PTX (gray bars). Data are shown for control without isoproterenol (c -Iso), control with 1 μM isoproterenol (c), and upon stimulation with 1 μM isoproterenol and removal of phosphorylation of phospholamban (PLB), troponin I (tni), phospholemman (PLM), the L-type Ca^{2+} channels (Ical), the channels responsible for $I_{Kto,f}$ (Ikto), the channels responsible for I_{Kur} (Ikur), and ryanodine receptors (ryr). The characteristics of the action potential and $[Ca^{2+}]_i$ transients are calculated during the 300th stimulation period with 1 Hz. **Panel D** shows the experimental $[Ca^{2+}]_i$ transients (gray bars with errors) in isoproterenol-stimulated mouse ventricular myocytes from phospholamban-knockout mice with reintroduced wild type phospholamban (KO-WT) and phospholamban with S16A mutation (KO-S16A). Experimental data were obtained by Chu et al.[71]. Corresponding simulated data are obtained for $[Ca^{2+}]_i$ transients in control and upon removal of phospholamban phosphorylation, both stimulated with 1 μM isoproterenol (black bars). Data are shown in % to the control (wild type) case.*

While most of these simulations with phosphorylation removal of PKA target proteins require verification by future experiments, we found one experiment that confirms our simulations. Chu

et al.[71] investigated the effects of phospholamban PKA phosphorylation site S16 on $[Ca^{2+}]_i$ transient in mouse ventricular myocytes. They reintroduced both wild type PLB and PLB with S16A mutation into PLB-knockout mouse hearts and measured $[Ca^{2+}]_i$ transients in corresponding ventricular myocytes. The measurements have shown a significant decrease in $[Ca^{2+}]_i$ transient in myocytes with mutant PLB compared to those with wild type PLB (gray bars with errors in Fig. 3.18D)[71]. Our model demonstrated a similar decrease in $[Ca^{2+}]_i$ transient upon removal PLB phosphorylation (black bars in Fig. 3.18D).

Thus, our mathematical model is capable of revealing the major factors affecting the action potential and $[Ca^{2+}]_i$ transient upon stimulation of β_1- and β_2-ARs through phosphorylation of specific PKA target proteins. The simulations suggest an alternative to the ion channel blockers method of regulation of the action potential and $[Ca^{2+}]_i$ transient upon selective actions on the phosphorylation sites of the proteins involved in the β_1- and β_2-adrenergic signaling systems.

3.3 Sensitivity analysis

To estimate the mathematical model's stability and major contributing factors to the changes in the action potential and $[Ca^{2+}]_i$ transient, we performed a sensitivity analysis. In the previous paper[30], where the mathematical model included only the β_1-adrenergic signaling system, a sensitivity analysis was carried out with respect to the major repolarization currents. With the model presented in this chapter, we obtained very similar results. In addition, we performed a sensitivity analysis with respect to the concentrations of major signaling proteins included in the model of the combined β_1- and β_2-adrenergic signaling system. As the interbeat changes in the concentrations of signaling proteins did not produce measurable effects on the action potential and $[Ca^{2+}]_i$ transient, we explored a method of analysis different from[30]. We ran the model cell for 300

s for the control set of the model parameters and for the case, when one protein concentration increased by 5%. Then the differences between APD_{25}, APD_{50}, APD_{75}, APD_{90}, action potential amplitudes, and magnitudes of $[Ca^{2+}]_i$ transients were calculated during the 300th period. The results are shown in Fig. 3.19. It is seen that the largest contribution to APDs and $[Ca^{2+}]_i$ transients come from the total concentrations of β_2-ARs, adenylyl cyclases, and phosphodiesterase of type 4. In addition, the total concentration of PDE3 is one of the major contributing factors to the action potential amplitude.
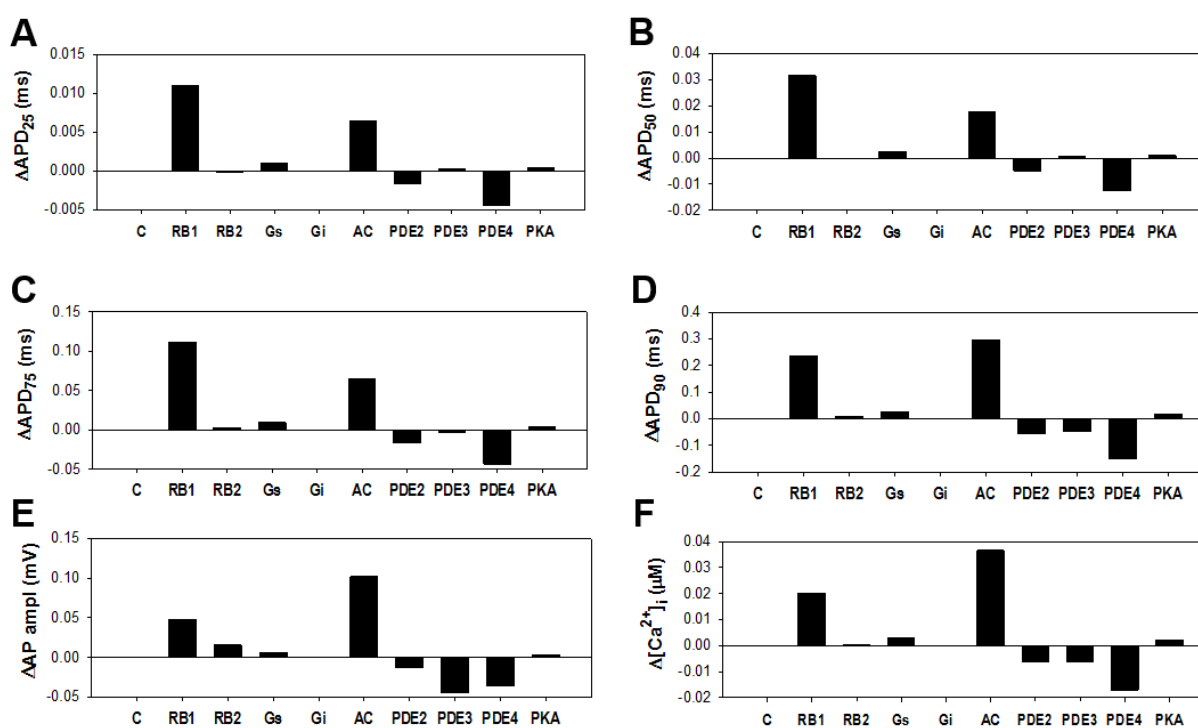
Figure 3.19 Absolute changes in APD_{25}, APD_{50}, APD_{75}, APD_{90}, action potential amplitudes, and magnitudes of $[Ca^{2+}]_i$ transients. *Simulated absolute changes of action potential durations at 25% (**Panel A**), 50% (**Panel B**), 75% (**Panel C**), and 90% repolarization (**Panel D**), action potential amplitude (**Panel E**), and $[Ca^{2+}]_i$ transient (**Panel F**) after 5% increase in concentrations of the major signaling proteins in the combined β_1-and β_2-adrenergic signaling system. A 5% increase in concentrations of the major proteins were set at time t = 0, and changes in action potential characteristics and $[Ca^{2+}]_i$ transient compared to those at original protein concentrations are measured after 300-second stimulation at 1 Hz. Notations are for control (C) and the changes of concentrations of β_1-ARs (RB1), β_2-ARs (RB2), stimulatory G protein (G_s), inhibitory G protein (G_i), adenylyl cyclases, total (AC), phosphodiesterase of type 2 (PDE2), phosphodiesterase of type 3 (PDE3), phosphodiesterase of type 4 (PDE4), and protein kinase A (PKA).*

We also performed a sensitivity analysis with respect to the changes in the initial conditions. For this purpose, we run the model for 300 s with the steady-state initial conditions and the model with increased values of all initial conditions by 5%. In this case, the differences in the transmembrane voltage and $[Ca^{2+}]_i$ concentration at the end of the 300-second simulations were only 1.66% and 0.92%, respectively.

3.4   Discussion

Thus, in the previous chapters of this dissertation, a new compartmentalized model for the combined β_1- and β_2-adrenergic signaling system in mouse ventricular myocytes is developed. The model is an extension of the previously published model of the β_1-adrenergic signaling system[27], which includes compartmentalization and the effects on the action potential, ionic currents, and Ca^{2+} and Na^+ dynamics. The new model was explored to investigate the contribution of each receptor type (β_1-ARs and β_2-ARs) to the regulation of electrical activity and ionic homeostasis in cardiac cells upon stimulation with isoproterenol under several physiological conditions which are commonly used in experiments. We found that the major inotropic, lusitropic, and chronotropic effects are due to the activation of β_1-ARs. The β_2-ARs are silent under control conditions or upon inhibition of G_i, and cause tiny effects upon stimulation with nearly saturating concentrations of isoproterenol. The effects of β_2-ARs can be revealed upon application of isoproterenol in PTX-pretreated mouse ventricular myocytes or in the cells with inhibited PDE3 and PDE4. The model allows for determination of the mechanisms of action potential prolongation and increase in $[Ca^{2+}]_i$ transients upon stimulation of β_1-ARs and/or β_2-ARs. The model also made testable predictions on the changes of Ca^{2+} and Na^+ fluxes, $[Na^+]_i$ decline, and the contribution of phosphorylation of

different PKA targets to the changes in action potential and $[Ca^{2+}]_i$ transients during stimulation of β_1-ARs and/or β_2-ARs.

3.4.1   *Differential effects of the β₁- and β₂-adrenergic signaling systems in the heart*

β_1- and β_2-adrenergic receptors have different physiological roles in regulation of the action potential, ionic currents, and Ca^{2+} and Na^+ dynamics in cardiac myocytes. Stimulation of β_1-ARs activates G_s-mediated signaling pathway, which is characterized by a relatively large production of the major signaling molecule, cAMP. β_2-ARs, in contrast, activates both G_s- and G_i-mediated signaling systems, resulting in less pronounced effects[42]. In addition, β_1- and β_2-adrenergic receptors have different cellular localization. Experimental data shows that β_1-adrenergic receptors are mostly distributed outside of the caveolar compartment, while β_2-adrenergic receptors are predominantly localized in the caveolar compartment[20,31]. In accordance with the experimental findings, our model includes only 1% of β_1-adrenergic receptors in the caveolar compartment, with the majority of them distributed between the extracaveolar and cytosolic compartments. In contrast, 99% of β_2-adrenergic receptors in the model are localized in the caveolar compartment[20,34]. Differential localization and coupling to G_s and G_i proteins results in different functional consequences: selective activation of β_1-adrenergic receptors in mouse ventricular myocytes under control conditions both in experiments and in our simulations leads to a significant increase in $[Ca^{2+}]_i$ transient and myocyte contraction, while selective activation of β_2-adrenergic receptors does not have any effect on myocyte contractility[67]. Stimulation of β_1-adrenergic receptors also leads to phosphorylation of phospholamban, while stimulation of β_2-adrenergic receptors does not produce this effect under control conditions[72].

While, in general, the physiological effects of β_1-ARs are stronger than those of β_2-ARs, they are different in different species. In some cases, the effects of β_2-ARs are not seen at all under normal physiological conditions, which produces discussion about their physiological importance for cardiac function[42,44]. For example, in human ventricular myocytes, coupling of β_2-ARs to the changes in cardiac function (systolic tension response) was observed upon application of β_2-ARs agonist zinterol[73]. In contrast, application neither β_2-ARs agonist zinterol nor isoproterenol with β_1-ARs block elicited functional response in mouse ventricular myocytes, in particular, to the effects on the L-type Ca^{2+} current[41,43]. In addition, experiments on stimulation of β_2-ARs with isoproterenol in β_1-AR knockout mice did not produce a significant effect on phospholamban phosphorylation[60]. Similar data are obtained for rat ventricular myocytes, where activation of β_2-ARs caused an increase in cAMP production, but did not affect Ca^{2+} dynamics, cardiac contraction, and phospholamban phosphorylation[74]. On the other hand, experimental data shows that the stimulation of β_2-ARs in canine ventricular myocytes enhanced the L-type Ca^{2+} current and myocyte contraction, but did not affect phospholamban phosphorylation[40].

Such different experimental results on the physiological effects of β_2-ARs in cardiac cells are due not only to species differences, but also due to the usage of zinterol as a specific agonist of β_2-ARs beyond its specificity concentrations. Experimental data shows that zinterol affinity for β_2-ARs and β_1-ARs is ~40 nM and ~$1 - 3$ μM, respectively[45,46]. It means that the effects of 1 μM zinterol are non-specific for β_2-ARs and can activate significant portion of β_1-ARs. This issue was studied in detail by Heubach et al.[47], who has shown that 1 μM zinterol causes an increase in the L-type Ca^{2+} current, but this effect is suppressed by 300 nM CGP 20712A, a selective β_1-AR antagonist. Therefore, throughout this study, we used isoproterenol as a β_1-AR and β_2-AR agonist, but its action was simulated in the presence of selective antagonists, CGP 20712A for β_1-ARs and

ICI 118551 for β_2-ARs. As result, we obtained non-contradictory simulation data, which explained most of the experimental data obtained under similar physiological conditions. In particular, we have shown that the physiological effects of inhibition of G_i by PTX or stimulation of β_2-ARs with 1 µM isoproterenol without PTX are virtually absent. The effects of stimulation of β_2-ARs with 1 µM isoproterenol can be revealed only with the additional inhibition of G_i by PTX or inhibition of PDE3 and PDE4 by cilostamide and rolipram, respectively. Specifically, such effects of β_2-ARs are obtained for the L-type Ca^{2+} current, $[Ca^{2+}]_i$ transients, and phosphorylation of phospholamban, which is similar to the experimental findings.

3.4.2 The effects of the β_1- and β_2-adrenergic signaling system on action potential and Ca^{2+} and Na^+ dynamics

Our simulation data suggest differential effects of β_1-ARs and β_2-ARs on the mouse action potential. Selective stimulation of β_1-ARs or both β_1-ARs and β_2-ARs prolongs APDs at all levels of repolarization, 25%, 50%, 75%, and 90%. This prolongation moderate and is similar to the experimental observations and simulations obtained before[27]. However, simulation of the selective activation of β_2-ARs shows the effects mostly on APD_{75} and APD_{90} in mouse ventricular myocytes only when G_i is blocked. The simulations also reveal major players in the prolongation of APDs at 75% and 90% repolarization: the L-type Ca^{2+} current, I_{CaL}, and the ultrarapidly activating K^+ current, I_{Kur}. A significant portion of I_{CaL} is localized in the caveolar compartment, which is mostly affected by β_2-ARs, and mainly diffusive fluxes of cAMP affects PKA and I_{Kur} in the extracaveolar compartment, where only 1% of β_2-ARs are located, leading to a significantly larger increase in the inward I_{CaL} as compared to the outward I_{Kur}. There is no experimental data on the effects of β_2-ARs on the wild type mouse action potential, and the experimental verification of these simulation

predictions will be of great interest. However, an increase in APD_{90} and no change in APD_{50} in mouse ventricular myocytes overexpressing β_2-ARs compared to wild type littermates[63] favors our modeling predictions.

As found experimentally, activation of the β_1- and β_2-adrenergic signaling systems significantly increases the magnitude of intracellular $[Ca^{2+}]_i$ transients, however, to different extents and depending on species and the concentration of agonist[64,65,66,67,75,76]. The effects of stimulation of both β_1-ARs and β_2-ARs or β_1-ARs alone is more pronounced than that for β_2-ARs alone, in particular in rodent ventricular cells where the increase can reach up to 5 times[64,65]. In larger species, such as rabbits and dogs, the increase is only by a factor of $2^{[75,76]}$. Stimulation of β_2-ARs alone with application of PTX results in a relatively moderate increase in $[Ca^{2+}]_i$ transients, from 40% to 150% in rodents[66,67,77] and up to 40% increase in dogs[78]. No significant increase in $[Ca^{2+}]_i$ transients without PTX are observed in rats[77] and in rabbits[79]. Our simulations with mouse ventricular myocytes show similar results. Stimulation of both β_1-ARs and β_2-ARs or β_1-ARs alone with 1 µM isoproterenol results in a 3.8-fold increase in $[Ca^{2+}]_i$ transients, but stimulation of β_2-ARs alone with the same concentration of isoproterenol does not produce any effect (Fig. 3.12). Inhibition of G_i (effects of PTX) does not alter the effects of both β_1-ARs and β_2-ARs or β_1-ARs alone, but it uncovers the effects of stimulation of β_2-ARs alone, where a 39% increase in $[Ca^{2+}]_i$ transient is obtained (Fig. 3.12).

The simulations also demonstrate differences in integral Ca^{2+} and Na^+ fluxes upon stimulation of both β_1-ARs and β_2-ARs, β_1-ARs alone, or β_2-ARs alone. The integral Ca^{2+} fluxes increase to much larger values, when both β_1-ARs and β_2-ARs or β_1-ARs alone are activated than when β_2-ARs alone are activated (Fig. 3.14). What is remarkable is that the relative percentage contribution of each Ca^{2+} influx mechanism does not change too much upon different physiological conditions,

shown in Fig. 3.14. For example, 4%-5% of the total Ca^{2+} entry into cytosol is due to the L-type Ca^{2+} channels, which triggers Ca^{2+}-induced Ca^{2+} release from the SR (91%-93% of the total Ca^{2+} entry into cytosol); 7%-8% of Ca^{2+} entry is extruded by the Na^+/Ca^{2+} exchanger; and ~0.5% Ca^{2+} is extruded by the sarcolemmal Ca^{2+} pump. The differences in integral Na^+ fluxes increases between stimulations of both β_1-ARs and β_2-ARs or β_1-ARs alone, on the one hand, and β_2-ARs alone, on the other hand, are less pronounced (Fig. 3.15). About 7% of Na^+ enters the cell through the fast Na^+ channels, ~16% enters through the Na^+/Ca^{2+} exchanger, and ~77% enters through different background mechanisms (large transmembrane Na^+ gradient, the Na^+/H^+ exchanger, the Na^+/HCO^-_3 co-transporter, etc.[64]). These influxes are counterbalanced by Na^+ extrusion by the Na^+-K^+ pump. The fractions differ from those evaluated for rabbits[64], where about 22% of Na^+ enter the cell through the fast Na^+ channels, 60% through the Na^+/Ca^{2+} exchanger, and 18% through the background mechanisms, suggesting the Na^+/Ca^{2+} exchanger to be the major player in the Na^+ transport into the cell. Further experiments are necessary to verify the predicted Na^+ fluxes in mouse ventricular cells.

3.4.3   *The role of signaling proteins phosphorylation in the healthy and diseased cardiac cells*

Phosphorylation of signaling proteins is one of the major mechanisms of biochemical signal transduction in cardiac cells. Upon stimulation or inhibition of the β_1- and β_2-adrenergic signaling system, phosphorylation regulates ionic currents, pumps, transporters, as well as other intracellular proteins involved in Ca^{2+} and Na^+ dynamics and cellular contraction[80,81]. In healthy hearts, activation of the β-adrenergic signaling system is a natural response to the increased heart load during exercises, which leads to increased phosphorylation of PKA target proteins and ultimately

to the changes in the action potential and Ca^{2+} dynamics. Diseased states, such as heart failure, are accompanied by significant modifications of the β-adrenergic signaling: decreased expression of the $β_1$-adrenergic receptors, increased activity of G_i proteins, increased phosphorylation of the L-type Ca^{2+} channels and ryanodine receptors, decreased phosphorylation of phospholamban[82,83,84]. Therefore, the pharmacological effects on the β-adrenergic signaling system or its components are among those methods for the treatment of heart failure[83].

To better understand mechanisms of adaptive changes in the β-adrenergic signaling system in human heart failure, mouse models of heart diseases were developed that recapitulate those found in human subjects[85,86]. In particular, several strategies were developed to improve cardiac function by affecting the $β_1$- and $β_2$-adrenergic signaling and its components in mice. Inhibition of cardiac β-adrenergic receptor kinase 1 (βARK1, currently named GRK2), the cause of desensitization of the β-adrenergic receptors in the failing hearts, significantly prolonged survival and β blocker therapy in mice with severe heart failure[87]. Deletion of the phospholamban gene dramatically enhanced survival of transgenic mice overexpressing $β_1$-adrenoceptors[88]. Transgenic mice with knock-in non-phosphorylated ryanodine receptors (S2808A mutant) were able to protect rolipram-treated mice from arrhythmias[89].

Our simulations of selective removal of phosphorylation of PKA targets demonstrated remarkable changes in the action potential duration due to dephosphorylation of the L-type Ca^{2+} channels and the channels responsible for I_{Kur} resulting both in increase and decrease of the action potential duration (Figs. 3.17 and 3.18). These ion channels can be potential new targets for the regulation of the electrical activity in the heart through modification of their phosphorylation. We also found that $[Ca^{2+}]_i$ transients are significantly modified by all investigated PKA targets in

mouse ventricular myocytes that provides a flexibility in the choice of potential drug targets or genetic modifications of phosphorylation sites (Figs. 3.17 and 3.18).

3.4.4   Model limitations

While the developed model of the combined β_1- and β_2-adrenergic signaling system was extensively verified by experimental data and simulated numerous experimental effects of stimulation of β_1-ARs and β_2-ARs under different physiological conditions, it has some limitations. One of the limitations comes from the low accuracy of biochemical and physiological experiments, which can vary by multiple folds, up to an order of magnitude. The second is that not all model parameters were measured directly in the experiments, and were adjusted numerically to fit the experimental data. These adjustable parameters are: 1) background currents, which were adjusted in the previous model[27]; 2) activation rates for G_s and G_i proteins, which are not directly measured or measured with low accuracy, but adjusted to fit the experimental data on kinetics of phosphorylation and dephosphorylation of the key signaling proteins, as well as the magnitude and kinetics of cAMP and protein kinase A under different physiological conditions; 3) basal adenylyl cyclase activities, which are responsible for background cAMP concentration without interventions. The third limitation is the possible effects of the CaMKII-mediated signaling system, which are not taken into account in the present model. However, the model of the combined β_1- and β_2-adrenergic signaling system describes quite well significant portions of the available experimental data obtained for mouse ventricular myocytes. In particular, it gives a non-contradictory description of the physiological effects of β_2-ARs in wild type mice. The authors consider this model as an intermediate step in the development of a more comprehensive

mathematical model of the mouse ventricular myocytes, which will include multiple signaling systems.

3.5   Conclusions

We developed a comprehensive experimentally-based compartmentalized mathematical model of the combined β_1- and β_2-adrenergic signaling system in mouse ventricular myocytes. The model describes the dynamics of major signaling molecules in different subcellular compartments; kinetics and magnitudes of phosphorylation of ion channels, transporters, and Ca^{2+} handling proteins; modifications of action potential shape and duration; and $[Ca^{2+}]_i$ and $[Na^+]_i$ dynamics upon simultaneous stimulation of β_1- and β_2-adrenergic receptors, or during separate stimulation of β_1- or β_2-ARs. The simulation results are compared to the experimental data obtained upon stimulation of the β_1- and β_2-adrenergic signaling systems in mouse ventricular myocytes. Simulations demonstrate that the separate stimulation of the β_2-ARs under normal physiological conditions does not affect action potential and $[Ca^{2+}]_i$ transients, which is also observed in experiments. The physiological effects of β_2-ARs are revealed in simulations upon the inhibition of G_i proteins or PDE3 and PDE4. The model also made testable predictions of the changes of the action potential, magnitudes of $[Ca^{2+}]_i$ and $[Na^+]_i$ fluxes, the rate of decay of $[Na^+]_i$ concentration upon both combined and separate stimulation of β_1- and β_2-ARs, and the contribution of phosphorylation of different PKA targets to the changes in the action potential and $[Ca^{2+}]_i$ transient.

4   MATHEMATICAL MODELING PHYSIOLOGICAL EFFECTS OF THE OVEREXPRESSION OF β₂-ADRENOCEPTORS IN MOUSE VENTRICULAR MYOCYTES

4.1   Introduction

Mice are important animals for studies of human disease. Multiple transgenic (TG) mice were generated during the last decades for this purpose. These include overexpressions, knock-outs, knock-ins, and genetic modifications of ion channels, transporters, and signaling proteins in mouse hearts, brains, and other organs[90]. Such modifications have allowed for revealing major mechanisms of generation of specific disease states in mice, with subsequent translation to human subjects[90].

Specifically, transgenic mice were generated with modifications of the β₁- and β₂-adrenergic signaling systems and their components, to demonstrate their different roles in the heart. Experimental investigations by Engelhardt et al.[28] have shown that heart-specific overexpression of β₁-adrenoceptors leads to a progression of hypertrophy and heart failure. In this study, the overexpression level of β₁-adrenoceptors of TG mice was only 15 times the normal expression of wild type (WT) mice. Such an overexpression resulted in progressive development of cardiac hypertrophy, clinical signs of heart failure and premature deaths before the age of 14 months. On the other hand, a study by Milano et al.[29] demonstrated that cardiac-specific overexpression of β₂-adrenoceptors (195 fold) resulted in improved cardiac function. This resulted in increased basal adenylyl cyclase activity, enhanced atrial contractility, and increased ventricular function *in vivo*. More detailed studies of different levels of overexpression of β₂-adrenoceptors (60-, 100-, 150-,

and 350-fold) conducted by Liggett et al.[91] concluded that cardiac function was dependent on the level of overexpression. Their data have shown that mouse hearts tolerated enhanced cardiac function without detriment for a period of more than 1 year only for 60-fold overexpression of β_2-adrenoceptors; other levels of overexpression resulted in cardiomyopathy.

Experimental data demonstrates interesting and intriguing differences in the response of the WT mouse ventricular myocytes and ventricular myocytes from TG mice overexpressing β_2-adrenergic receptors to β-adrenergic stimulation. WT mice show a large response to stimulation with β_1- and β_2-adrenoceptor agonist isoproterenol[42]. Blocking β_1-adrenoceptors (β_1-ARs) in WT mice basically eliminate this response, demonstrating that the role of β_2-adrenoceptors (β_2-ARs) is minimal. Indeed, the response of WT mouse cardiac cells to stimulation of β_2-adrenoceptors is absent under normal physiological conditions and can be only revealed after application of pertussis toxin (PTX, G_i inhibitor) or after inhibition of phosphodiesterases of type 3 and 4 (PDE3 and PDE4)[41,42]. On the other hand, ventricular myocytes from TG mice overexpressing β_2-ARs do not show notable responses to stimulation with β_1-AR agonist norepinephrine without and with application of PTX, and to stimulation with β_2-AR agonist zinterol without application of PTX. However, myocytes from TG mice demonstrate quite a significant response to stimulation with β_2-AR agonist zinterol in the presence of PTX[67]. In addition, this response can be inhibited by specific β_2-AR inhibitor ICI 118,551[67].

Our model for the combined β_1- and β_2-adrenergic signaling system in mouse ventricular myocytes was able to explain only experimental data on WT mice[92]. It showed the primary role of β_1-ARs in inotropic response to stimulation with β_1- and β_2-adrenoceptor agonist isoproterenol. The model also demonstrated that the response to β_2-AR stimulation was only notable with the application of PTX or upon inhibition of PDE3 and PDE4[92]. However, it is interesting whether our

model can simulate the experimental data obtained from TG mice overexpressing β_2-adrenoceptors after modifications and can the model reveal different responses of WT and TG mice to β-adrenergic stimulation.

Therefore, we developed and explored a compartmentalized mathematical model of ventricular myocytes from TG mice overexpressing β_2-adrenoceptors. The model is based on the previously developed mathematical model of the combined β_1- and β_2-adrenergic signaling system in mouse ventricular cells, which was extensively verified by experimental data[92]. In the new model, we implemented differences in the model parameters between WT mice and TG mice overexpressing β_2-adrenoceptors and simulated different myocyte behavior found experimentally. We have shown that β_2-AR overexpression does not significantly affect action potential shape and duration, but the effect is most notable upon stimulation of β_2-ARs with zinterol in the presence of PTX. Significant effects of zinterol on the L-type Ca^{2+} current in TG mice were also achieved with the model by stimulation with zinterol plus PTX. We also found that $[Ca^{2+}]_i$ transients are larger in TG mice as compared to WT mice without any stimulation, and a significant increase in $[Ca^{2+}]_i$ transients was observed upon stimulation with zinterol after the application of PTX. Mechanisms of the changes are disclosed by the simulations and the model limitations are discussed.

4.2   Methods

4.2.1   Model development

A mathematical model for TG mouse ventricular myocytes overexpressing β_2-ARs is obtained from our previously published model of the combined β_1- and β_2-adrenergic signaling system[92]. We incorporated the following changes of the model parameters that correspond to the differences between WT and TG mice found experimentally (shown in green in Fig. 4.1 and in Table 2).

In TG mice overexpressing β_2-ARs, we increased the concentration of β_2-ARs by 200 fold according to the experimental data by Milano et al.[29]. In addition, we reduced the concentration of β_1-ARs by a factor of 0.0001, as these receptors are in inactive states and do not respond to epinephrine and zinterol[67,93]. We also increased the expression of inhibitory G protein G_i in TG mouse hearts by 70% according to the experimental finding by Gong et al.[94].

Experimental data with TG mice overexpressing β_2-ARs demonstrate a 44% reduction of the expression of phospholamban (PLB)[95]. This should result in a smaller inhibition of the SERCA pump in TG mice. To estimate the change in the pumping rate of the SERCA pump due to smaller PLB expression, we used experimental data by Luo et al.[96] and Kadambi et al.[97]. Luo et al.[96] measured the dissociation constant for the SERCA pump, $K_{m,up}$, in WT and PLB-knockout mice (0.24±0.02 µM and 0.11±0.01 µM for $[Ca^{2+}]_i$, respectively). Kadambi et al.[97] measured $K_{m,up}$ in WT mice and mice with a two-fold overexpression of PLB, which were equal to 0.27±0.01 µM and 0.48±0.04 µM for $[Ca^{2+}]_i$, respectively. Our interpolation of these data resulted in ~20% reduction of $K_{m,up}$ for TG mice overexpressing β_2-ARs, which was implemented in the new mathematical model.

Further, most experimental data shows a decrease in the magnitude of the L-type Ca^{2+} current I_{CaL} in TG mice overexpressing β_2-ARs (~40% reduction[98], ~32% reduction[43], ~26% reduction[99], and no change[63]). In our mathematical model we implemented the average value of these experimental data which corresponds to a 24% reduction in I_{CaL}.
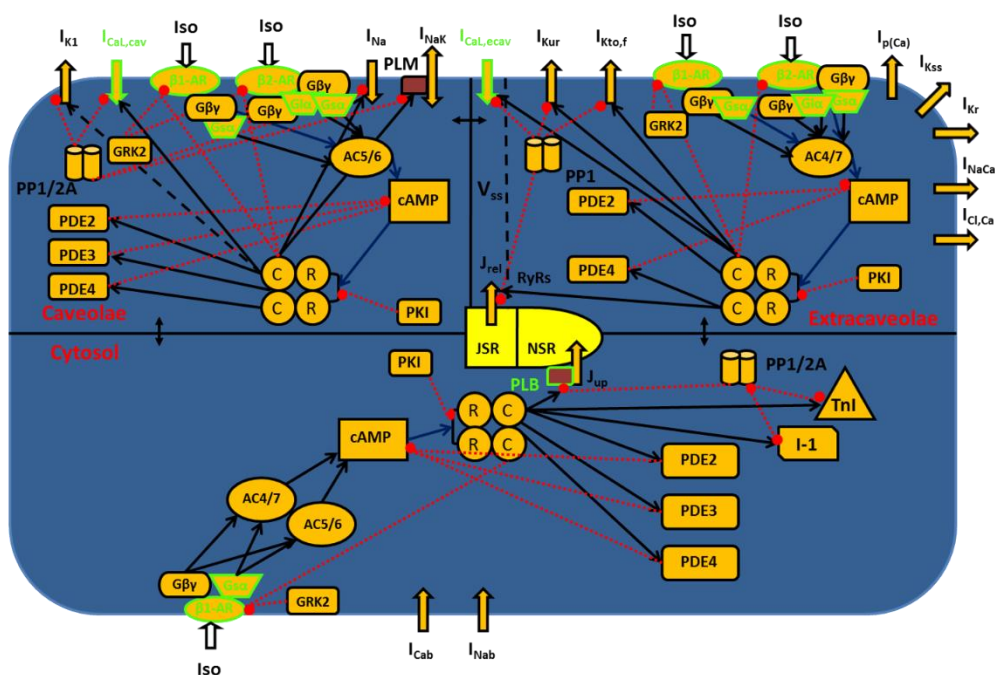
Figure 4.1 A schematic representation of the combined β₁- and β₂-adrenergic signaling systems in mouse ventricular myocytes overexpressing β₂-adrenergic receptors. *The cell consists of three compartments (caveolar, extracaveolar, and cytosol) related to the combined β₁- and β₂-adrenergic signaling systems. The subspace volume (V_{ss}) is localized in the extracaveolar compartment. The biochemical portions of the combined β₁- and β₂-adrenergic signaling systems are the β₁-adrenergic receptors (β1-AR), the β₂-adrenergic receptors (β2-AR), the α-subunit of stimulatory G-protein ($G_{s\alpha}$), the α-subunit of inhibitory G-protein ($G_{i\alpha}$), the βγ-subunit of G_s and G_i ($G_{\beta\gamma}$), the adenylyl cyclases of type 5/6 or 4/7 (AC5/6 or AC4/7, respectively), the phosphodiesterases of type 2, 3, or 4 (PDE2, PDE3, or PDE4, respectively), the cyclic AMP (cAMP), regulatory (R) and catalytic (C) subunits of protein kinase A holoenzyme, the protein kinase A inhibitor (PKI), the G-protein-coupled receptor kinase of type 2 (GRK2), the protein phosphatases of type 1 and 2A (PP1 and PP2A, respectively), the inhibitor-1 (I-1). Targets of the combined β₁- and β₂-adrenergic signaling systems are in the caveolar (the fast Na^+ current (I_{Na}), the L-type Ca^{2+} current ($I_{CaL,cav}$), the Na^+/K^+ pump (I_{NaK}) which is regulated by phospholemman (PLM), phosphodiesterases PDE2-PDE4, and the time-independent K^+ current (I_{K1})), the extracaveolar (the L-type Ca^{2+} current ($I_{CaL,ecav}$), the rapidly recovering transient outward K^+ current ($I_{Kto,f}$), the ultrarapidly activating delayed rectifier K^+ current (I_{Kur}), ryanodine receptors (RyRs), and phosphodiesterases (PDE2, PDE4)), and cytosol (phospholamban (PLB) and troponin I (TnI)). Stimulatory links are shown by black arrows and inhibitory links are shown by red dashed lines with balls. Other transmembrane currents are the sarcolemmal Ca^{2+} pump ($I_{p(Ca)}$), the Na^+/Ca^{2+} exchanger (I_{NaCa}), the rapid delayed rectifier K^+ current (I_{Kr}), the noninactivating steady-state voltage activated K^+ current (I_{Kss}), the Ca^{2+} and Na^+ background currents (I_{Cab} and I_{Nab}), which are not affected by the combined β₁- and β₂-adrenergic signaling systems. The Ca^{2+} fluxes are uptake of Ca^{2+} from the cytosol to the network sarcoplasmic reticulum (NSR) (J_{up}) by the SERCA pump and Ca^{2+} release from the junctional sarcoplasmic reticulum (JSR) (J_{rel}) through the ryanodine receptors. $[Ca^{2+}]_i$, $[Na^+]_i$, and $[K^+]_i$ are the intracellular Ca^{2+}, Na^+, and K^+ concentrations in the caveolar, extracaveolar, and cytosol; $[Ca^{2+}]_o$, $[Na^+]_o$, and $[K^+]_o$ are the extracellular Ca^{2+}, Na^+, and K^+ concentrations. Proteins which characteristics are modified in transgenic mouse overexpressing β₂-adrenergic receptors are shown in green.*

As most experimental data on TG mice were obtained with stimulation by zinterol, we changed the affinity constants of the ligand L for β_1-ARs and β_2-ARs. The new constants are $K_{\beta1,L} = 1.0$ μM and $K_{\beta1,H} = 1.0\,\mu$M for β_1-ARs and $K_{\beta2,H} = 0.04\,\mu$M and $K_{\beta2,F} = 0.04\,\mu$M for β_2-ARs[46]. Finally, we adjusted the activation rate constants for G_s and G_i proteins to reflect their changes in affinities. To simulate the effects of isoproterenol, we used the values of affinities and rate constants as in the original model[92]. All changes made to the model by Rozier and Bondarenko[92] are shown in Table 2.

PKA target proteins are located in different compartments in the same manner as in reference 92. The fast Na$^+$ current, I_{Na}, 20% of the L-type Ca^{2+} channels (the L-type Ca^{2+} current, I_{CaL}), phospholemman (PLM), which regulates the Na$^+$-K$^+$ pump, I_{NaK}, and the time-independent K$^+$ current, I_{K1}, are localized in the caveolar compartment; the ultra-rapidly activating delayed rectifier K$^+$ current, I_{Kur}, the rapidly inactivating transient outward K$^+$ current, $I_{Kto,f}$, 80% of the L-type Ca^{2+} channels, and the ryanodine receptors, RyRs, are localized in the extracaveolar compartment; and phospholamban and troponin I are localized in the cytosolic compartment. Detailed model descriptions can be found in the previously published papers[27, 92].

4.2.2 Method of simulation

The mathematical model consists of 149 ordinary differential equations, which were solved by a fourth-order Runge-Kutta method, with two different time steps. A relatively small time step of 0.000002 ms was used during a 10 millisecond interval after the initiation of the stimulus current; for all other times we used the time step 0.0001 ms. Simulation of the cellular behavior without electrical stimulation was performed with time step of 0.1 ms. The model equations were implemented in FORTRAN 90. All simulations were performed on a single processor under SUSE

Table 2 Differences between current TG mouse model and the WT mouse model by Rozier and Bondarenko[92].

	Parameter definition	WT cell model Rozier and Bondarenko [2017]	Current TG cell model
	β-adrenergic receptor module		
$[R_{\beta 1}]_{tot}$	Total β_1-adrenergic receptor concentration	0.0103 μM	0.00000103 μM
$K_{\beta 1,L}$	Low affinity constant of β_1-adrenoceptor for zinterol	N/A	1.0 μM
$K_{\beta 1,H}$	High affinity constant of β_1-adrenoceptor for zinterol	N/A	1.0 μM
$k_{act1,Gs\beta 1}$	Activation rate for G_s by β_1-ARs high affinity complex	4.9 s^{-1}	0.98 s^{-1}
$[R_{\beta 2}]_{tot}$	Total β_2-adrenoceptor concentration	0.0053 μM	1.06 μM
$[G_i]_{tot}$	Total concentration of G_i protein	10.086 μM	17.1462 μM
$K_{\beta 2,H}$	High affinity constant of β_2-adrenoceptor for zinterol	N/A	0.04 μM
$K_{\beta 2,F}$	High affinity constant of phosphorylated β_2-adrenoceptor/ligand	0.0189 μM	0.04 μM
$k_{act1,Gi}$	Activation rate for G_i by high affinity complex	2.0 s^{-1}	0.26 s^{-1}
$k_{act2,Gi}$	Activation rate for G_i by low affinity complex	0.050 s^{-1}	0.0065 s^{-1}
	L-type Ca^{2+} current module		
G_{CaL}	Specific maximum conductivity for L-type Ca^{2+} channel (non-phosphorylated)	0.3772 mS/μF	0.2791 mS/μF
G_{CaLp}	Specific maximum conductivity for L-type Ca^{2+} channel (phosphorylated)	0.7875 mS/μF	0.5828 mS/μF
	Phospholamban module		
$K_{m,up}^{np}$	Half-saturation constant for SR Ca^{2+}-ATPase pump (non-phosphorylated)	0.41 μM	0.328 μM
$K_{m,up}^{p}$	Half-saturation constant for SR Ca^{2+}-ATPase pump (phosphorylated)	0.31 μM	0.248 μM

Linux 11 on a Dell Precision Workstation T3500 with a six-core Intel Xeon CPU W3670 (3.2 GHz, 12 GB RAM). The model is developed for a room temperature of 25ºC (T = 298ºK). Initial conditions were obtained by running the program code without electrical stimulations for about 10,000 seconds to ensure quasi-steady-state. Action potentials were initiated by a stimulus current (I_{stim} = 80 pA/pF, τ_{stim} = 1 ms) with the frequency 0.5 Hz (electrical stimulation).

4.3 Results

In this chapter, we developed a mathematical model of the ventricular myocyte from TG mice overexpressing β2-adrenergic receptors. The model includes three major subcellular compartments, caveolar, extracaveolar, and cytosol, and β2-ARs are localized in the membranes of caveolar (99%) and extracaveolar (1%) compartments. In the model, we inhibited β1-ARs according to the experimental finding that they are inactive[100]. The model was explored to investigate the effects of stimulation of β2-ARs with zinterol under different physiological conditions, such as control, inhibition of G_i by PTX or inhibition of β2-ARs by ICI 118,551. Under these multiple physiological conditions, we investigated: 1) compartmentalization of cAMP generation and PKA activation; 2) the effects on the L-type Ca^{2+} current; 3) the alterations of the action potentials and ionic currents; 4) the effects on $[Ca^{2+}]_i$ transients; and 5) the effects of ICI 118,551 on the cellular activity.

4.3.1 Adenylyl cyclase activity, cAMP and PKA dynamics

Experimental data consistently shows an increased level of the background adenylyl cyclase activity in TG mice overexpressing β2-ARs as compared to WT mice (~150-200 level of overexpression, Fig. 4.2A)[29,91]. Upon stimulation with isoproterenol, the total AC activity increases in both WT and TG mice, however, to different degrees at maximum stimulation with

100 µM isoproterenol. The experimental maximum AC activity is larger for WT mice than that for TG mice overexpressing β_2-ARs[91] (however, see data by Milano et al.[29], where total AC activity is somewhat larger in TG mice). Our model reproduced this dependence of AC activity as functions of isoproterenol in WT and TG mice (Fig. 4.2B). Our simulations show larger AC activity in TG mice without application of isoproterenol, and this relation reversed at high dose of isoproterenol (100 µM).

Figure 2C demonstrates the comparison of the absolute total AC activities in WT and TG mice in control (0 µM isoproterenol) and after stimulation with 100 µM isoproterenol. Our simulation data for WT mice corresponds well to the data by Lemire et al.[51], which was normalized (experimentally measured AC activities can vary substantially, we have chosen the most frequently occurring values for fitting our simulations). The experimental data on the total AC activities by Liggett et al.[91] for WT mice is somewhat larger, but demonstrates a similar tendency to increase. For TG mice, our simulations demonstrate larger values of AC activity in control and smaller values at maximum stimulation with isoproterenol (Fig. 4.2C).

An interesting feature of TG mice overexpressing β_2-ARs is that the high level of overexpression results in the appearance of a constitutively active (phosphorylated) fraction of β_2-ARs[100]. This fraction is quite high and approaches 100% of the concentration of β_2-ARs even at low doses of isoproterenol[100]. We estimated fractions of phosphorylated β_2-ARs using our models for WT and TG mice under different physiological conditions (Fig. 4.2D). For WT mice, the estimations for control conditions and upon inhibition of G_i demonstrated ~57% and ~78% of phosphorylated β_2-ARs. For TG mice, the fraction of phosphorylated β_2-ARs is larger for control and upon inhibition of G_i (~77% and ~82%, respectively). This fraction does not change

dramatically upon stimulation with 1 µM zinterol (81.5% and 84% for 1 µM zinterol and PTX + 1 µM zinterol, respectively, Fig. 4.2D).

cAMP concentrations in TG mice display different dynamics in the three major cellular compartments under different physiological conditions. cAMP dynamics is defined by cAMP production by adenylyl cyclases, cAMP degradation by phosphodiesterases, and cAMP diffusion
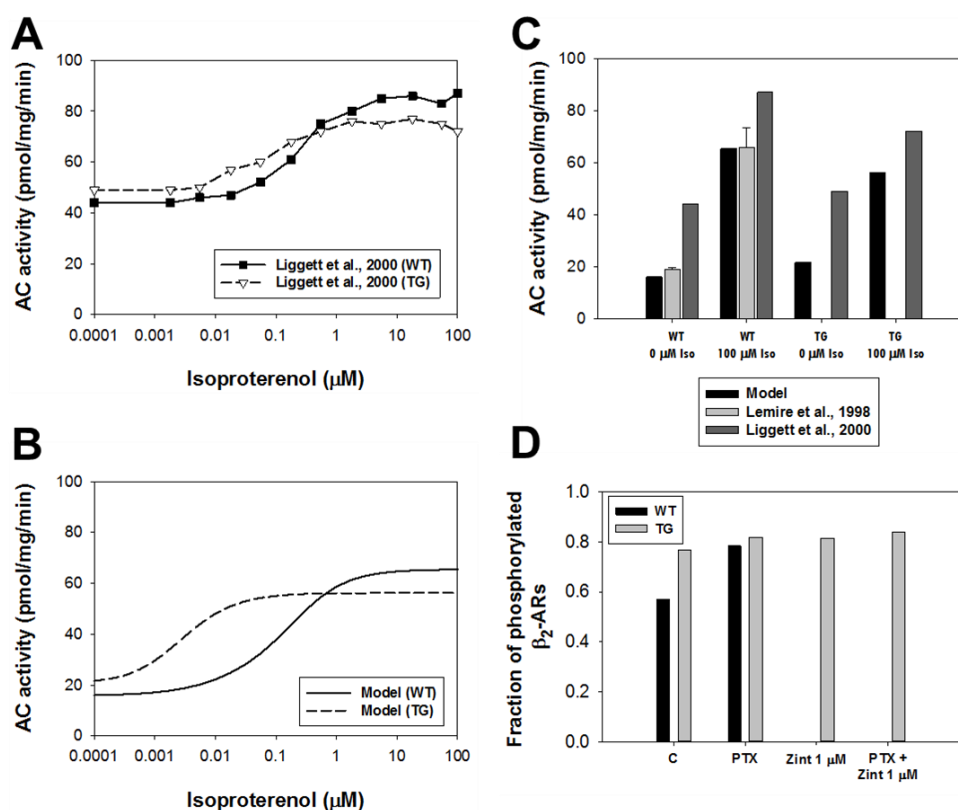
Figure 4.2 Adenylyl cyclase activities and phosphorylation of β_2-adrenoceptors. **Panel A**: *Experimental total adenylyl cyclase activities in WT mice (filled squares) and TG mice overexpressing β_2-adrenoceptors (unfilled triangles) as functions of isoproterenol concentration[91]. **Panel B**: Simulated total adenylyl cyclase activities in WT mice (solid line) and TG mice overexpressing β_2-adrenoceptors (dashed line) as functions of isoproterenol concentration. **Panel C**: Simulated and experimental total AC activities in WT and TG mice for control (0 µM isoproterenol) and after application of 100 µM isoproterenol. Experimental data for WT mice are from[51]; experimental data for WT and TG mice are from[91]. **Panel D**: Simulated fractions of phosphorylated β_2-adrenoceptors in WT (black bars) and TG (gray bars) mice under different physiological conditions. Data are simulated for control (C), after application of PTX (PTX), after application of 1 µM zinterol (Zint 1 µM), and after application of PTX and 1 µM zinterol (PTX + Zint 1 µM).*

between intracellular compartments. Figure 4.3 shows the simulated time courses of cAMP concentrations in different subcellular compartments in control (red lines), upon inhibition of G_i with PTX (cyan lines), upon stimulation with 1 µM zinterol (green lines), and upon stimulation with 1 µM zinterol in the presence of PTX (blue lines). The modeling data shows different levels of cAMP in different compartments in control. The largest level of cAMP is in the caveolar compartment where most (99%) β_2-ARs are localized. Inhibition of G_i with PTX increases cAMP levels in all compartments. Simulated cAMP concentration on the cellular level increases as well from 0.36 µM to 0.78 µM (2-fold increase) (Fig. 4.3D). Myocyte stimulation with 1 µM zinterol increases cAMP level by about two-fold on the cellular level, with the significantly larger increase in the caveolar compartment (Fig. 4.3A). The most significant cAMP increase was obtained with 1 µM zinterol in the presence of PTX in all compartment. In this case, the cAMP transient achieves ~2.5 µM at the cellular level, which is close to the cAMP concentrations obtained with 1 µM isoproterenol in WT mice[27]. Note that in TG mice, cAMP production is due to the activation of β_2-ARs, because β_1-ARs are silent[100], while in WT mice cAMP is mostly produced by the activation of β_1-ARs, because β_2-ARs are silent. Such a behavior of cAMP is reproduced by our model for TG mice and by the Bondarenko model[27] for WT mice.

The time behavior of the catalytic subunit of PKA is similar to that for cAMP (Fig. 4.4). Significantly higher concentration of the catalytic subunit of PKA is generated by the TG mouse model in the caveolar compartment even in control due to a significantly higher concentration of
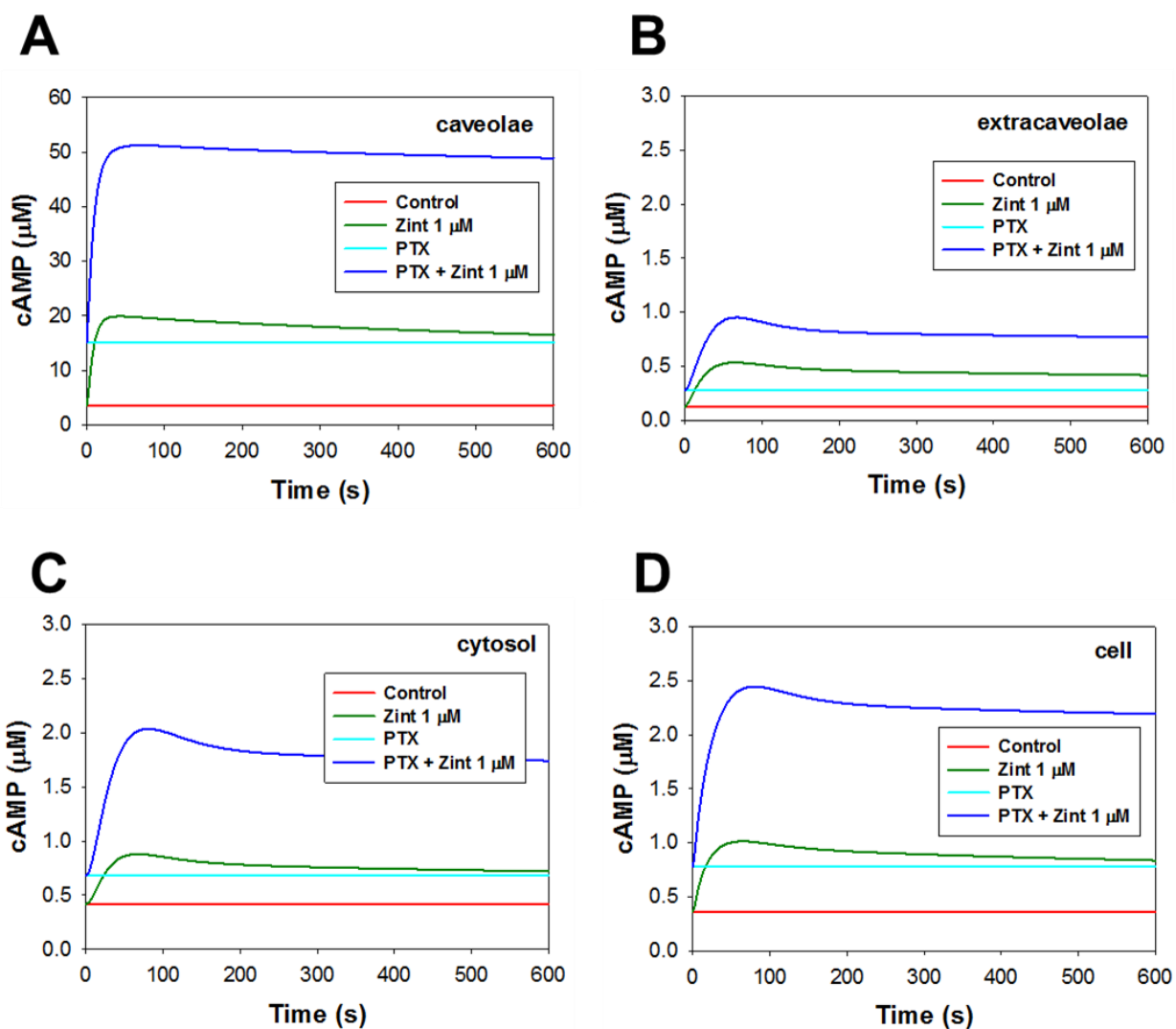
Figure 4.3 cAMP dynamics in mouse ventricular myocytes overexpressing β₂-adrenoceptors. *(**Panel A**), extracaveolar (**Panel B**), and cytosolic (**Panel C**) compartments, as well as in the whole cell (**Panel D**). Simulations were performed for four cases: control, application of 1 μM zinterol, application of PTX, and application of PTX + 1 μM zinterol.*
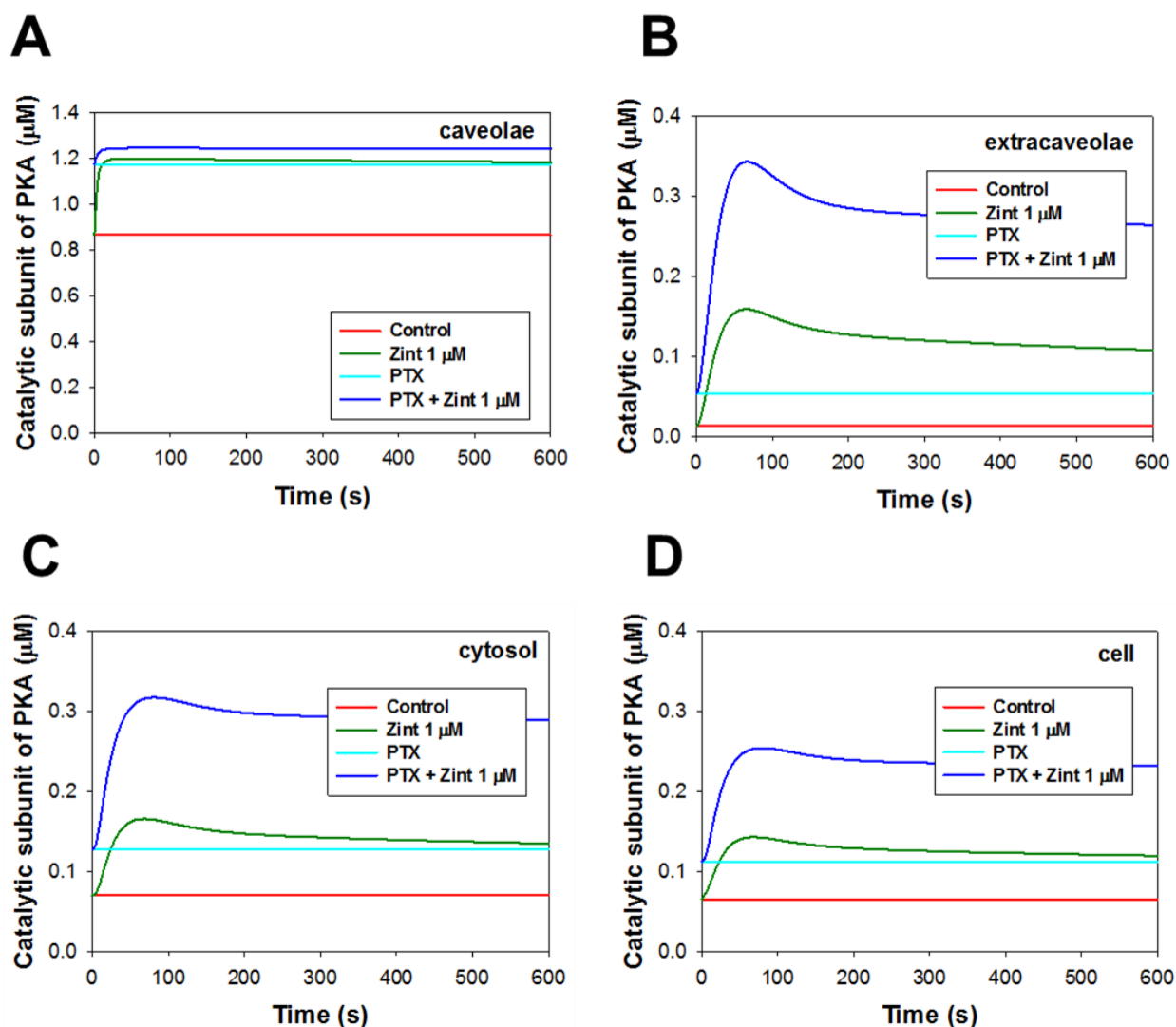
Figure 4.4 PKA catalytic subunit dynamics in mouse ventricular myocytes overexpressing β_2-adrenoceptors. *Simulated PKA catalytic subunit concentrations are shown as functions of time in the caveolar (**Panel A**), extracaveolar (**Panel B**), and cytosolic (**Panel C**) compartments, as well as in the whole cell (**Panel D**). Simulations were performed for four cases: control, application of 1 μM zinterol, application of PTX, and application of PTX + 1 μM zinterol.*

cAMP in that compartment (Fig. 4.4A). In addition, the concentration of the catalytic subunit of PKA does not decrease in time in caveolar compartment, which results in a significant level of phosphorylation of β_2-ARs and leading to a significant fraction of constitutively active β_2-ARs. The PKA activity in other compartments is smaller. It increases upon inhibition of G_i as compared to control in the extracaveolar and cytosolic compartments (Fig. 4.4B and 4.4C), as well as in the

whole cell (Fig. 4.4D). Stimulation with 1 µM zinterol leads to a PKA activation which is similar to PTX in most compartments and at the cellular level, except for the extracaveolar compartment, where PKA activation with zinterol is about two-fold larger than that with PTX (Fig. 4.4B).

4.3.2 The effects on the L-type Ca^{2+} current

Experimental data consistently shows a decrease in the magnitude of the L-type Ca^{2+} current, $I_{CaL,}$ in TG mice overexpressing β_2-ARs as compared to WT mice[43,98,99], with an average value of decrease ~24%. In addition, I_{CaL} does not change significantly in TG mice upon stimulation with 1 µM zinterol and inhibition with PTX[59]. However, the magnitude of the L-type Ca^{2+} current significantly increases after the application of 1 µM zinterol in the presence of PTX[59].

Figure 4.5 shows simulations of these experimental findings in WT and TG mice. The magnitude of WT I_{CaL} is ~6.63 pA/pF with voltage pulse to +10 mV, which is about 30% larger than that from TG mice in control, ~5.10 pA/pF. Stimulation of β_2-ARs in TG mice with 1 µM zinterol increases the magnitude of I_{CaL} by ~15% only (long dashed line in Fig. 4.5A), which is within the accuracy of the experimental measurement[59]. Similarly, inhibition of G_i with PTX also slightly increases the L-type Ca^{2+} current magnitude by ~8% (medium dashed line in Fig. 4.5A). However, application of 1 µM zinterol plus PTX leads to a much larger increase in I_{CaL}, by ~40%, which is
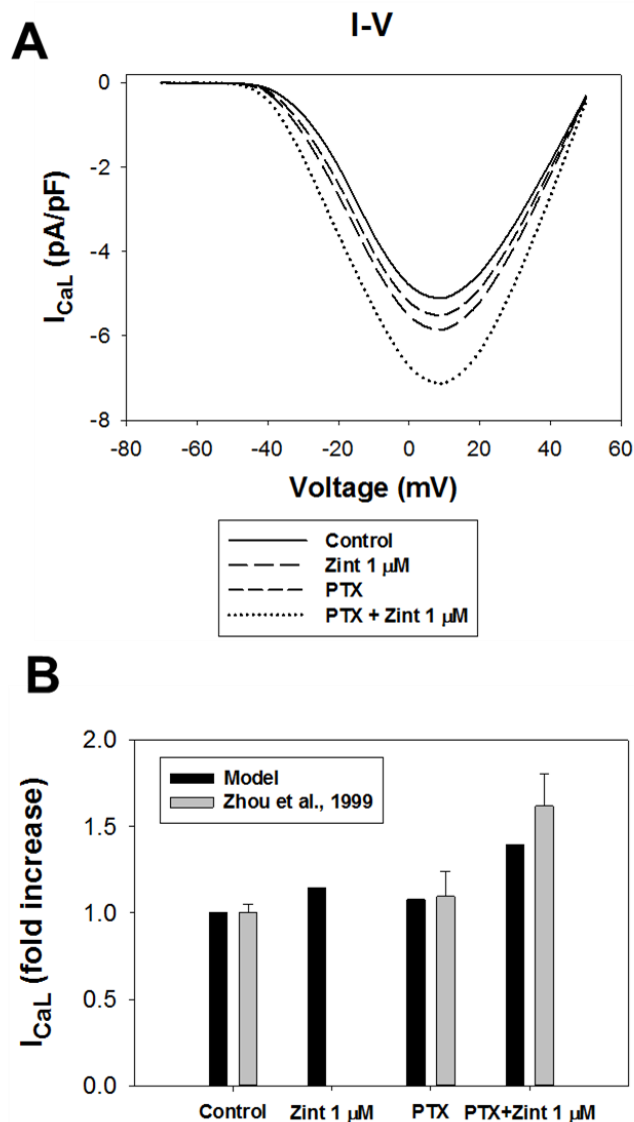
*Figure 4.5 The effects of stimulation of β_2-ARs on the L-type Ca^{2+} current. Currents are obtained by voltage pulses from −70 mV to +50 mV (in 10-mV increments) from a holding potential of −80 mV and without Ca^{2+}-induced Ca^{2+} release to account for heavy buffering conditions. **Panel A:** Simulated current-voltage relationships obtained for several physiological conditions: control (solid lines), after application of 1 μM zinterol (long dashed lines), after inhibition of G_i without isoproterenol (medium dashed lines), after application of 1 μM zinterol with inhibition of G_i (dotted lines). **Panel B:** Simulated (black bars) and experimental (gray bars) maximum magnitude of the L-type Ca^{2+} current under the same conditions as in **Panel A**. Experimental data are from Zhou et al.[59].*

consistent with the experiments by Zhou et al.[59] (~48% increase). Comparison of the experimental[59] and simulation data under different physiological conditions is shown in Fig. 4.5B.

Thus, our model describes well the effects of stimulation of β_2-ARs with 1 μM zinterol on the L-type Ca^{2+} current in TG mouse ventricular myocytes overexpressing β_2-ARs. Simulations show that the effects of β_2-ARs on the L-type Ca^{2+} current can be revealed by stimulation in the presence of PTX.

4.3.3   *The effects on $[Ca^{2+}]_i$ transients*

Experimental data demonstrates that intracellular $[Ca^{2+}]_i$ transients in TG mice overexpressing β_2-ARs is larger than in WT mice under control conditions[67]. Stimulation of β_2-ARs with zinterol in TG mice overexpressing β_2-ARs does not show remarkable effects on $[Ca^{2+}]_i$ without the inhibition of G_i. However, experimental data on the magnitude of myocyte contraction, which is dependent on the magnitude of $[Ca^{2+}]_i$ transients, demonstrates a trend towards an increase even without G_i inhibitor PTX[67]. The effect of zinterol is more pronounced in the presence of PTX, when significant difference between unstimulated and stimulated cells is observed.

Figure 4.6A shows simulated $[Ca^{2+}]_i$ transients obtained after 300 s stimulation for WT and TG mice under different physiological conditions. $[Ca^{2+}]_i$ transients are larger in TG mice (black solid line in Fig. 4.6A) than in WT mice (red solid line in Fig. 4.6A), which is consistent with experimental findings[67]. Application of PTX or 1 μM zinterol increases $[Ca^{2+}]_i$ transients in TG cells by ~24% and ~36%, respectively. Simultaneous application of PTX and 1 μM zinterol resulted in a much larger increase in $[Ca^{2+}]_i$ (by ~79%, dotted line in Fig. 4.6A).
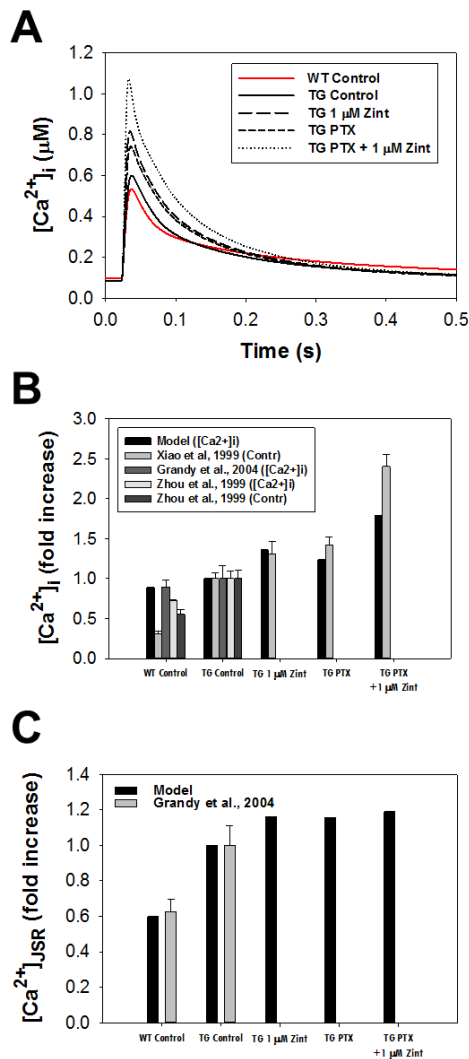
Figure 4.6 [Ca^{2+}]$_i$ transients in mouse ventricular myocytes under different physiological conditions. ***Panel A:*** *Simulated [Ca^{2+}]$_i$ transients obtained in WT mice for control (red solid line) and TG mice for control (black solid line), after application of 1 μM zinterol (black long dashed line), after inhibition of G$_i$ (PTX) (black short dashed line), after application of 1 μM zinterol with the inhibition of G$_i$ (black dotted line).* ***Panel B:*** *Simulated data on a relative increase in [Ca^{2+}]$_i$ transients and experimental data on a relative increase in [Ca^{2+}]$_i$ transients and myocyte contraction for WT and TG mice. Simulated data are obtained for the same physiological conditions as in* ***Panel A****. Experimental data by Grandy et al.[98] and Zhou et al.[63] are obtained for [Ca^{2+}]$_i$ transients; experimental data by Xiao et al.[67] and Zhou et al.[63] are obtained for myocyte contraction.* ***Panel C:*** *Simulated sarcoplasmic reticulum Ca^{2+} concentrations [Ca^{2+}]$_{JSR}$ (black bars) for the same physiological conditions as in* ***Panel A****. Experimental data (gray bars) for WT and TG mice are obtained by Grandy et al.[98]. [Ca^{2+}]$_i$ transients and [Ca^{2+}]$_{JSR}$ are shown after 300 s stimulation with 0.5 Hz.*

Detailed comparisons of the simulated and experimental data on the maximal [Ca^{2+}]$_i$ transients in WT and TG mouse ventricular myocytes under different physiological conditions is shown in

Fig. 4.6B. In addition to $[Ca^{2+}]_i$ transients, we also show data on myocyte contraction, which the behavior is quite similar to $[Ca^{2+}]_i$. The available experimental data for all simulated physiological conditions are from one source[67]. The data in Fig. 4.6B are normalized to the magnitude of $[Ca^{2+}]_i$ transients in TG mice in control. Simulation data on $[Ca^{2+}]_i$ transients for WT and TG mice upon stimulation of β_2-ARs under different physiological conditions. Control conditions compare well to the corresponding experimental data[67,98]. The experimental data on normalized myocyte contraction is somewhat smaller for WT mice under control than the data on $[Ca^{2+}]_i$[63,67]. Our simulation data are in line with the experimental data on myocyte contraction upon stimulation with 1 µM zinterol (without PTX), application of PTX, and combined application of 1 µM zinterol plus PTX (Fig. 4.6B). Unfortunately, consistent experimental data on those various physiological conditions for $[Ca^{2+}]_i$ is not available.

We also investigated the sarcoplasmic reticulum (SR) Ca^{2+} content ($[Ca^{2+}]_{JSR}$) under different physiological conditions (Fig. 4.6C). Experimental data shows significantly smaller (by ~37%) SR content in WT mice as compared to TG mice[98]. Our mathematical model for WT mice[92] and model for TG mice overexpressing β_2-ARs reproduced this difference. In addition, we simulated the SR Ca^{2+} content after application of 1 µM zinterol (without PTX), PTX, and 1 µM zinterol plus PTX (Fig. 4.6C). The simulations demonstrate consistent, but rather small increase in $[Ca^{2+}]_{JSR}$ under these different physiological conditions (~16%-19% increase).

Thus, model simulations of $[Ca^{2+}]_i$ transients in WT and TG mouse ventricular myocytes reproduces their differences under control conditions, and predict a moderate increase in $[Ca^{2+}]_i$

4.3.4   The effects on mouse action potential

There are virtually no experimental measurements of the action potential characteristics in TG mice overexpressing β_2-ARs, except for the only paper by Zhou et al.[63]. Zhou et al.[63] have found that there is no significant difference in APD_{50} between WT and TG mice. However, their data indicates a significant increase in APD_{90} in TG mice as compared to WT mice (by ~2 fold). Because there were no effects of ICI 118,551 found on APD_{90} in the TG mouse cell, it was concluded that such APD_{90} prolongation is not directly due to the overexpression of β_2-ARs. Figure 4.7 demonstrates the action potentials for WT and TG mice overexpressing β_2-ARs. Quite small difference between WT and TG mouse action potentials were found under control conditions (~10% decrease in APD_{50} and ~6% increase in APD_{90} in TG mice as compared to WT mice). Simulations with TG mice demonstrate virtually no change in APD_{50} upon stimulation with 1 µM zinterol (without PTX) or application of PTX (Fig. 4.7C). The combined application of 1 µM zinterol plus PTX resulted in ~14% increase in APD_{50} as compared to control. In contrast, APD_{90} in TG mice shows and increase by ~14%, ~10%, and ~21% upon application of 1 µM zinterol (without PTX), PTX, and combined application of 1 µM zinterol plus PTX, respectively (Fig. 4.7D).

The changes in ionic currents underlying the TG mouse action potential in control and after application of 1 µM zinterol + PTX are shown in Fig. 4.7E and 4.7F, respectively. The increase in APD_{50} after application of 1 µM zinterol + PTX is a result of changes in major repolarization currents: a decrease in $I_{Kto,f}$ and an increase in I_{CaL} tends to prolong the action potential, but an
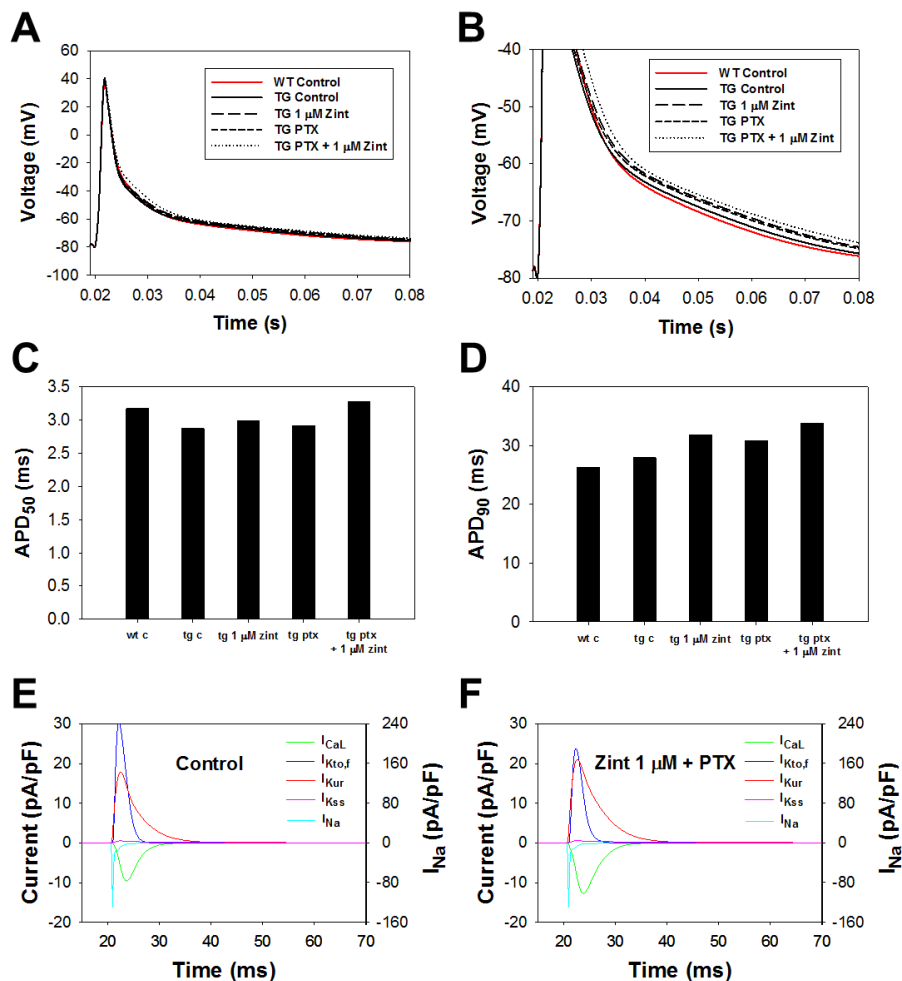
*Figure 4.7 Mouse action potentials in WT and TG mice, and APD$_{50}$ and APD$_{90}$ under different physiological conditions. **Panel A:** Simulated mouse action potentials for WT control (red solid line), for TG control (black solid line), after application of 1 µM zinterol (black long dashed line), upon inhibition of G$_i$ (black short dashed line), and after application of 1 µM zinterol and inhibition of G$_i$ (black dotted line). **Panel B** shows details of repolarization in the voltage range from −80 mV to −40 mV. **Panels C and D** show simulated APD$_{50}$ and APD$_{90}$, respectively, for the same physiological conditions as in **Panel A**. **Panel E:** Simulated major ionic currents underlying TG mouse action potential in control. **Panel F:** Simulated major ionic currents underlying TG mouse action potential after the application of 1 µM zinterol and the inhibition of G$_i$ with PTX. In **Panels A-D**, action potentials, APDs, and ionic currents are obtained after 300 s stimulation with 0.5 Hz.*

increase in I$_{Kur}$ tends to reduce the action potential. These tendencies continue towards later

repolarization stages resulting in prolongation of APD$_{90}$ as well.

Thus, our modeling data suggest that the most remarkable prolongation of the action potential

duration in TG mice overexpressing β$_2$-ARs can be observed with the application of zinterol in the

presence of PTX. The larger prolongation is observed for APD_{90} as compared to APD_{50}. The mechanism of this prolongation is discussed above. Further experiments are necessary to verify our model predictions.

4.3.5   *The effects of β₂-adrenoceptor inverse agonist ICI 118,551 in TG mouse ventricular myocytes*

Our mathematical model allows for evaluation of the effects of β_2-AR inverse agonist ICI 118,551 on the cellular activity of ventricular myocyte from TG mice. As we and others have shown[42,92] that β_1-ARs are primarily responsible for the changes in AP and $[Ca^{2+}]_i$ in WT mice. In TG mice overexpressing β_2-ARs, the application of ICI 118,551 revealed a major role of β_2-ARs in the changes in cardiac myocyte activities. Ventricular myocytes from TG mice demonstrate larger background AC activity as compared to WT cells[29]. Application of ICI 118,551 reduced AC activity in the TG cells by about two fold[100], and cAMP level in the TG cells can be comparable to that in WT cells[59]. Our model was able to reproduce these effects. Figure 4.8A shows simulations of AC activities in WT mice and TG mice before and after the application of ICI 118,551 normalized to AC activity in TG mice in control. Application of ICI 118,551 was simulated by a reduction of β_2-AR concentration by 10,000. Simulated TG cells in control demonstrate increased AC activity as compared to WT cells. Application of ICI 118,551 does not affect WT cells (data not shown), but it significantly reduced AC activity in TG cells. Such a reduction is comparable to the experimental data by Bond et al.[100].

We also simulated the effects of ICI 118,551 in PTX-pretreated TG ventricular myocytes to reproduce the effects in the experiments by Xiao et al.[67]. As Xiao et al.[67] measured myocyte contraction, which is closely related to the magnitude of $[Ca^{2+}]_i$ transient, we investigated the

behavior of $[Ca^{2+}]_i$ under three different physiological conditions: after application of PTX, after an application of 1 µM zinterol in PTX-pretreated cells, and upon inhibition of the effects of 1 µM zinterol in PTX-pretreated cells. The simulations show an increase in $[Ca^{2+}]_i$ transient after application of 1 µM zinterol in PTX-pretreated cells, which is suppressed by ICI 118,551 (Fig. 8B). Comparison of the simulations with the experiments by Xiao et al.[67] on TG myocyte contraction demonstrates qualitative agreement.

As TG ventricular myocytes overexpressing β_2-ARs show an increased AC activity in control that leads to increased activation of PKA, it is interesting to simulate the effects of ICI 118,551 on the action potential and $[Ca^{2+}]_i$ transient in TG myocytes under control conditions. These data are shown in Fig. 4.9. It is seen that the application of ICI 118,551 affects mostly the late stage of repolarization in the action potential (Fig. 4.9A), which is due to the larger reduction of the inward L-type Ca^{2+} current I_{CaL} comparing to that of the transient outward K^+ current $I_{Kto,f}$ (Figs. 4.9C and 4.9D). The application of ICI 118,551 also causes a decrease in $[Ca^{2+}]_i$ transients in TG myocytes (Fig. 4.9B).

Thus, our simulations suggest that an increased background $[Ca^{2+}]_i$ transient and myocyte contraction is primarily due to the activity of β_2-ARs in TG mice. $[Ca^{2+}]_i$ transient and myocyte contraction can be reduced to the values comparable to WT cells after application of β_2-AR inverse agonist ICI 118,551.
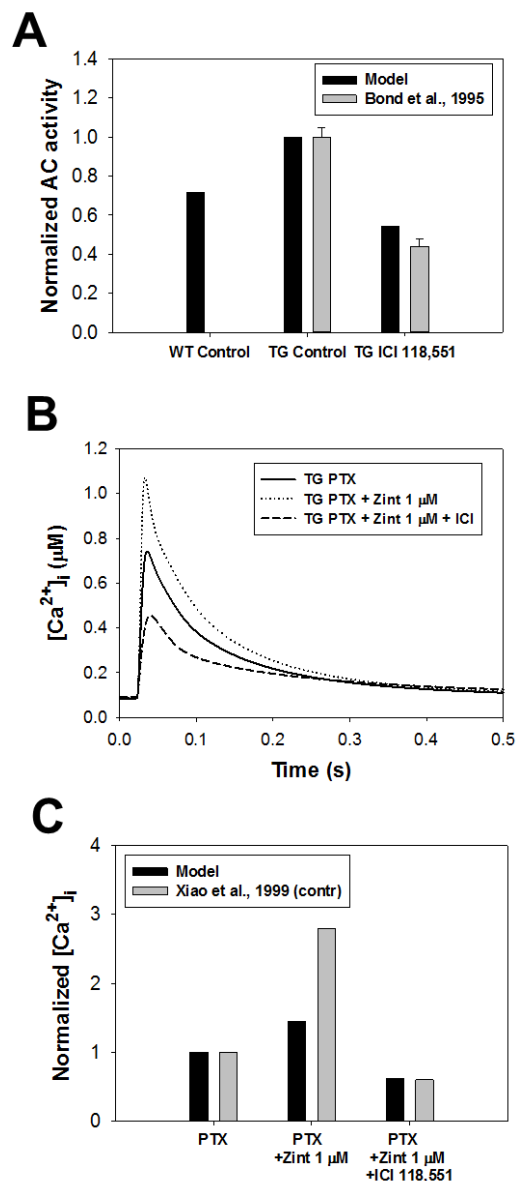
Figure 4.8 Simulation of the effects of selective inhibitor ICI 118,551 on the behavior of mouse ventricular myocytes overexpressing β₂-adrenoceptors. ***Panel A:*** *Simulated (black bars) and experimental (gray bars) by Bond et al.[100] normalized AC activities for WT mice (WT Control), TG mice (TG Control), and TG mice after application of ICI 118,551 (TG ICI 118,551). Data are normalized to TG (control).* ***Panel B:*** *Simulated $[Ca^{2+}]_i$ transients in TG mouse ventricular myocytes upon application of PTX, PTX + 1 µM zinterol, and PTX + 1 µM zinterol + ICI 118,551.* ***Panel C:*** *Comparison of simulated peak amplitudes of $[Ca^{2+}]_i$ transients (black bars) and experimental peak myocyte contractions (gray bars)[67] in TG mice upon application of PTX, PTX + 1 µM zinterol, and PTX + 1 µM zinterol + ICI 118,551.*
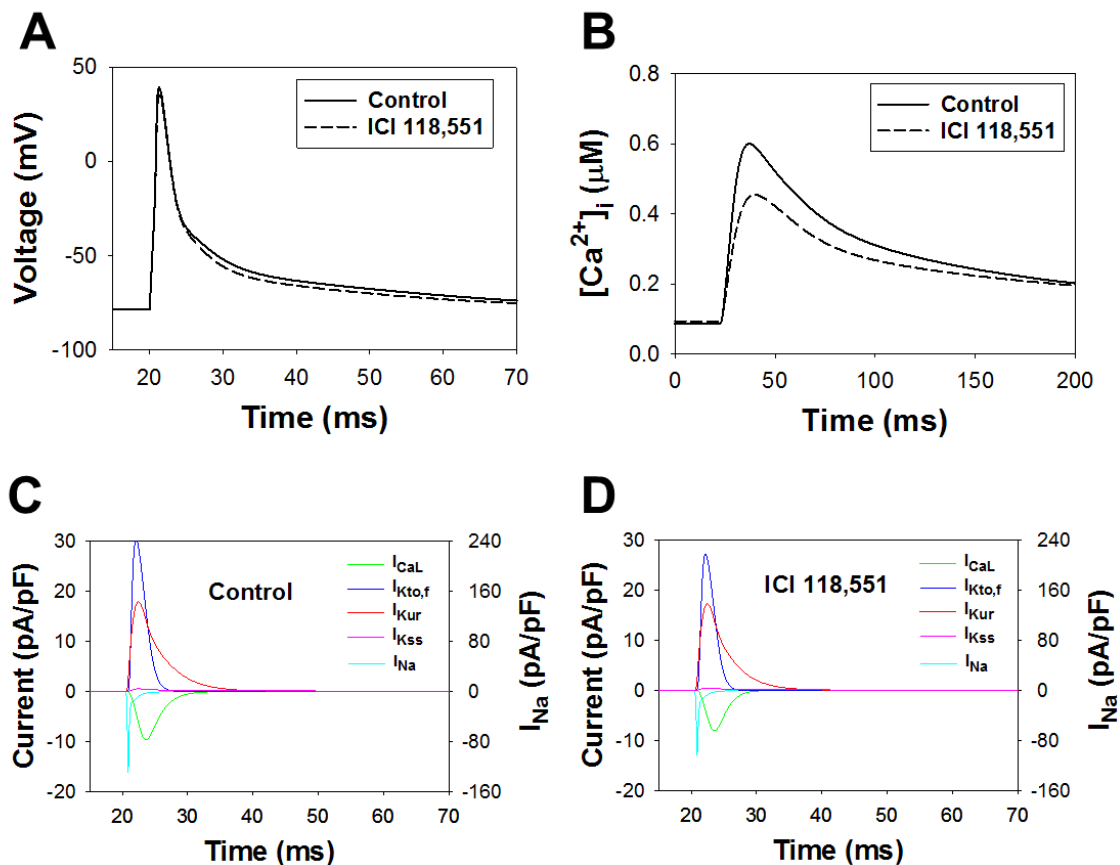
Figure 4.9 Mouse action potentials, [Ca^{2+}]$_i$ transients, and ionic currents in TG mice in control and after application of ICI 118,551. *Panel A: Simulated TG mouse action potentials for control (solid line) and after application of ICI 118,551 (dashed line). Panel B: Simulated TG mouse [Ca^{2+}]$_i$ transients for control (solid line) and after application of ICI 118,551 (dashed line). Panel C: Simulated major ionic currents underlying TG mouse action potential in control. Panel D: Simulated major ionic currents underlying TG mouse action potential after the application of ICI 118,551. In Panels A-D, action potentials, [Ca^{2+}]$_i$ transients, and ionic currents are obtained after 300 s stimulation with 0.5 Hz.*

4.4   Discussion

In this chapter, a new compartmentalized mathematical model for TG mouse ventricular myocytes overexpressing β$_2$-adrenergic receptors is developed. The model is based on the previously published model of the combined β$_1$- and β$_2$-adrenergic signaling systems[92], which includes compartmentalization and the effects on the action potential, ionic currents, and Ca^{2+} dynamics. The new model was explored to investigate the effects of the overexpression of β$_2$-ARs

on the regulation of cardiac cells upon stimulation with isoproterenol and zinterol under different physiological conditions. The model was able to simulate increased AC activities in TG cells and the effects of isoproterenol on AC activity. We found that zinterol causes significant effects on the L-type Ca^{2+} current only in the cells pretreated with G_i inhibitor PTX. The model allows for determination of the mechanisms of action potential prolongation and increase in $[Ca^{2+}]_i$ transients under stimulation of β_2-ARs with zinterol, inhibition of G_i with PTX, and stimulation of β_2-ARs with zinterol in the presence of PTX. In addition, we simulated the effects of β_2-AR inverse agonist ICI 118,551 on the adenylyl cyclase activity, action potential, and $[Ca^{2+}]_i$ transients in ventricular cells overexpressing β_2-adrenergic receptors.

4.4.1   *The effects of the overexpression of β_2-adrenergic receptors in mouse hearts*

β_1- and β_2-adrenergic receptors play different roles in the heart. Experimental data shows that cardiac-specific overexpression of β_1-ARs results in hypertrophy, which lead to heart failure[28]. On the other hand, moderate overexpression of β_2-ARs improved cardiac function[29]. To gain insights into the mechanisms of these different physiological effects, multiple experiments were performed on activation and inhibition of β_1-ARs and β_2-ARs in WT and TG mice and isolated myocytes.

β_1- and β_2-adrenergic receptors cause different physiological effects on the action potential, ionic currents, and Ca^{2+} dynamics in WT mouse ventricular myocytes. Stimulation of β_1-ARs with isoproterenol activates the G_s-mediated signaling pathway and leads to major inotropic effects in WT cells such as a large increase in $[Ca^{2+}]_i$ transient and myocyte contraction. Inhibition of β_1-ARs with antagonist CGP-20712A eliminates the effect of stimulation, while the effects of inverse agonist of β_2-ARs ICI-118,551 does not change the effect of stimulation. On the other hand, stimulation of β_2-ARs with isoproterenol in the presence of CGP-20712A in WT cells activates

both G_s- and G_i-mediated signaling systems, resulting in less pronounced effects or no effect at all[67]. The effects of β_2-ARs in WT myocytes can be revealed upon inhibition of G_i with PTX. TG mouse ventricular myocytes overexpressing β_2-ARs demonstrate different behaviors. Stimulation of TG mouse cells with isoproterenol in the presence of PTX shows a marked increase in the magnitude of myocyte contraction[59]. Application of β_1-AR antagonist CGP-20712A does not cause significant effects on contraction, while application of inverse agonist of β_2-ARs ICI-118,551 abolishes the effect of isoproterenol. Thus, experimental data shows that β_1-ARs produces pronounced effects in WT cells and are silent in TG mice overexpressing β_2-ARs, however, β_2-ARs produce pronounced effects in TG cells overexpressing β_2-ARs and are silent in WT mice in control conditions.

Our mathematical model for WT cells[92] and the model proposed in this paper for TG mice are able to simulate the different behaviors of these cell types. We found[92] that in WT ventricular myocytes, isoproterenol produced a significant increase in I_{CaL} and $[Ca^{2+}]_i$ transients when β_2-ARs were blocked, and cause virtually no effects when β_1-ARs are blocked. As most of the experimental data on TG mice are obtained with zinterol, we simulated the effects of this β_2-AR agonist within our new TG model. We found that the effect of 1 µM zinterol on the L-type Ca^{2+} current in TG mice is significant only in the presence of PTX (~40%). Application of PTX or 1 µM zinterol caused less pronounced effects on I_{CaL} (~8% and ~15%, respectively). While some noticeable effects of the application of PTX or 1 µM zinterol on $[Ca^{2+}]_i$ transients and myocyte contraction in TG cells are found, the effects are more significant in the presence of both pharmacological interventions. Finally, simulations of the effects of inverse agonist ICI-118,551 show that the increase in the background $[Ca^{2+}]_i$ transients and myocyte contraction in TG cell as compared to

WT cells is due to the overexpression of β_2-ARs. These simulations confirmed the corresponding experimental data[59,67].

There is virtually no data on the effects of the overexpression of β_2-ARs on the cardiac action potential. The action potential in TG mice overexpressing β_2-ARs was investigated only by Zhou et al.[63]. They found that APD$_{50}$ was identical for WT and TG mice, however, APD$_{90}$ was significantly increased in TG cells. Because there were no significant effects of ICI 118,551 on the action potential, Zhou et al.[63] suggested that APD$_{90}$ prolongation in TG mice is not directly due to β_2-AR overexpression. Our simulations show that APD$_{50}$ in TG cells is ~10% shorter than that in WT mice, but it does not change upon the application of PTX or 1 µM zinterol. APD$_{90}$ is slightly more prolonged in TG mice as compared to WT mice (~6%), however, application of PTX, 1 µM zinterol, or 1 µM zinterol plus PTX increases APD$_{90}$ in TG mice by ~10% - 21%.

4.4.2   *Model limitations*

Our mathematical model of the mouse ventricular myocyte overexpressing β_2-adrenergic receptors was derived from the previously published model of the combined β_1- and β_2-adrenergic signaling system[92], which was extensively verified by experimental data. In addition, this new model describes multiple experiments obtained in TG mice overexpressing β_2-ARs. However, it has the following limitations: 1) the model relies on the low accuracy of biochemical and physiological experiments, which can vary by multiple folds; 2) not all model parameters were measured directly in the experiments and were adjusted to fit the experimental data; 3) the model does not include the possible effects of the CaMKII-mediated signaling system. Nevertheless, the model replicates the published experimental data quite well and provides some insights into the mechanisms that lead to the differences between WT and TG mice overexpressing β_2-ARs.

4.5 Conclusions

We developed a comprehensive experimentally-based compartmentalized mathematical model of the mouse ventricular myocytes overexpressing β_2-adrenergic receptors. We found that most of the β_2-adrenergic receptors are active in control conditions in TG mice. The model describes the dynamics of major signaling molecules in different subcellular compartments; modifications of action potential shape and duration; and $[Ca^{2+}]_i$ dynamics upon stimulation of β_2-adrenergic receptors in control, after application of PTX, upon stimulation with zinterol, and upon stimulation with zinterol in the presence of PTX. The model also describes the effects of inverse agonist ICI-118,551 on cAMP production, action potential, and $[Ca^{2+}]_i$ transients. The simulation results are compared to the experimental data obtained in the ventricular myocytes from TG mice.

REFERENCES

1 Henriquez CS (2014) A Brief History of Tissue Models for Cardiac electrophysiology. *IEEE Transactions on Biomedical Engineering* **14**:1457

2 Aliev RR, Panfilov AV (1996) Modeling of Heart Excitation Patterns caused by a Local Inhomogeneity. *J. theor. Biol.* **181**:33-40

3 Noble D, (1962) A Modification of the Hodgkin-Huxley Equations Applicable to Purkinje Fibre Action and Pace-Maker Potentials. *J. Physiology* **160**: 317-352.

4 Hodgkin AL and Huxley AF, (1952) A quantitative description of membrane current and its application to conduction and excitation in nerve. *J. Physiology* **117:** 500-544

5 Hutter OF and NobleD, (1960) Rectifying Properties of Cardiac Muscle. *Nature* **188:** 495

6 Weidmann S, (1951) Effect of Current Flow of Membrane Potential of Cardiac Muscle. *J. Physiology* **115:** 227-236.

7 Beeler GW and Reuter H, (1977) Reconstruction of the Action Potential of Ventricular Myocardial Fibres. *J. Physiology* **268:** 177-210

8 McAllister RE, Noble D, and Tsien RW, (1975) Reconstruction of the Electrical Activity of Cardiac Purkinje Fibres. *J. Physiology* **251:** 1-59

9 Hass HG, Kern R, Einwachter HM, and Tarr M (1971) Kinetics of Na Inactivation in Frog Atria. *Plfugers Arch.* **323:** 141-157

10 Di Francesco D and Noble D (1985) A Model of Cardiac Electrical Activity Incorporating Ionic Pumps and Concentration Changes – Simulations of Ionic Currents and Concentration Changes. *Phil. Trans. Rl Soc. Lond.* **B307:** 353-398

11 Luo CH and Rudy Y (1994) A Dynamic Model of the Cardiac Ventricular Action Potential. Simulations of Ionic Currents and Concentration Changes. *Circ. Res.* **74:** 1071-1096.

12 Jafri S, Rice JJ, and Winslow RL (1998) Cardiac Ca^{2+} Dynamics: The Roles of Ryanodine Receptor Adaptation and Sarcoplasmic Reticulum Load. *Biophys J.* **74:**1149–1168

13 Winslow RL, Rice J, Jafri S, Marban E, and O'Rourke B (1999) Mechanisms of altered Excitation-Contraction coupling in Canine Tachycardia-Induced Heart failure, II Model Studies. *Circ. Res.* **84:** 571-586

14 Bondarenko VE, Szigeti GP, Bett GC, Kim SJ, and Rasmusson RL (2004) Computer Model of action Potential of Mouse Ventricular Myocytes. *Am J. Physiol. Heart Circ* Physiol. **287**: H1378-1403

15 Land S, Louch WE, Niederer, SA, Aronsen JM, Christensen G, Sjaastad I, Sejersted OM, Smith NP (2013) Beta-Adrenergic Stimulation Maintains Cardiac Function in Serca2 Knockout Mice *Biophysical Journal* **104**:1349-1356

16 Saucermann JJ, Brunton LL, Michailova AP, and McCulloch AD (2003) Modeling β-Adrenergic Control of Cardiac Myocyte Contractility in Silico. *J. Biol. Chem.* **278:** 47997-48003

17 Puglisi JL, Bers DM. LabHEART:an interactive computer model of rabbit ventricular myocyte ion channels and Ca transport. *Am J Physiology Cell Physiol* **281**:c2049 – c2060

18 Fedida D, Noble D, Rankin AC, Spindler AJ. (1987) The arrhythmogenic transient inward current iT0 and related contraction in isolated guinea-pig ventricular myocytes. *J Physiol (Lond).*;**392**:523-542.

19 Post SR, Hilal-Dandan R, Urasawa K, Brunton LL, and Insel PA (1995) Quantification of Signaling Components and Amplification in the Beta-adrenergic-receptor-adenylate cyclase Pathway in Isolated Adult Rat Ventricular Myocytes. *Biochem J.* **311:** 75-80

20 Rybin VO, Xu X, Lisanti MP, Steinberg SF (2000) Differential Targeting of Beta-adrenergic receptor subtypes and adenylyl cyclase to cardiomyocyte caveolae. A mechanism to functionally regulate the cAMP Signaling Pathway. *J. Biol Chem* **275:** 41447-41457

21 Pandit SV, Clark RB, Giles WR, Demir SS (2001) A mathematical model of action potential heterogeneity in adult rat left ventricular myocytes. *Biophys J.* 81:3029-51

22 Saucermann JJ, Healy SN, Belik ME, Puglisi, JL, and McCulloch AD (2004) Proarrhythmic Consequences of a KCNQ1 AKAP-Binding Domain Mutation. *Cir. Res.* **95:** 1216-1224

23 Kuzumoto M, Takeuchi A, Nakai H, Oka C, Noma A, Matsuoka S. (2008) Simulation analysis of intracellular Na^+ and Cl^- homeostasis during $\beta1$-adrenergic stimulation of cardiac myocytes. *Prog Biophys Mol Biol* 96: 171-186

24 Iancu RV, Jones SW, Harvey RD. (2007) Compartmentation of cAMP signaling in cardiac myocytes: a computational study. Biophys J 92: 3317-3331

25 Iancu RV, Ramamurthy G, Warrier S, Nikolaev VO, Lohse MJ, Jones SW, Harvey RD. (2008) Cytoplasmic cAMP concentrations in intact cardiac myocytes. Am J Physiol Cell Physiol 295: C414-C422]

26 Heijmann J, Volders PGA, Westra RL, and Rudy Y (2011) Local Control of β-adrenergic Stimulation: Effects on Ventricular Myocyte Electrophysiology and Ca^{2+}-transient. *J. Mol and Cell Cardio* **50:** 863-871

27 Bondarenko, VE (2014) A Compartmentalized Mathematical Model of the β_1-Adrenergic Signaling System in Mouse Ventricular Myocytes. *PLoS ONE* **9(2)**: e89913

28 Engelhardt S, Hein I, Wiesmann F, Lohse MJ (1999) Progressive hypertrophy and heart failure in β_1-adrenergic receptor transgenic mice. *Proc. Natl Academy of science USA* **96**: 7059-7064

29 Milano CA, Allen LF, Rockman HA, Dolber PC, McMinn TR, et al. (1994) Enhanced myocardial function in transgenic mice overexpressing the β_2-adrenergic receptor. *Science* **264:** 582-586

30 Grinshpon M, Bondarenko VE. Simulation of the effects of moderate stimulation/inhibition of the β_1-adrenergic signaling system and its components in mouse ventricular myocytes. *Am J Physiol Cell Physiol* **310**: C844-C856, 2016.

31 Balijepalli RC, Foell JD, Hall DD, Hell JW, Kamp TJ. Localization of cardiac L-type Ca^{2+} channels to a caveolar macromolecular signaling complex is required for β_2-adrenergic regulation. *Proc Natl Acad Sci USA* **103**: 7500-7505, 2006.

32 Hilal-Dandan R, Kanter JR, Brunton LL. Characterization of G-protein signaling in ventricular myocytes from the adult mouse heart: differences from the rat. *J Mol Cell Cardiol* **32**: 1211-1221, 2000

33 Rorabaugh BR, Gaivin RJ, Papay RS, Shi T, Simpson PC, Perez DM. Both α_{1A}- and α_{1B}-adrenergic receptors crosstalk to downregulate β_1-ARs in mouse heart: coupling to differential PTX-sensitive pathways. *J Mol Cell Cardiol* **3**9: 777-784, 2005.

34 Nikolaev VO, Moshkov A, Lyon AR, Miragoli M, Novak P, Paur H, Lohse MJ, Korchev YE, Harding SE, Gorelik J. β_2-adrenergic receptor redistribution in heart failure changes cAMP compartmentation. *Science* **327**: 1653-1657, 2010.

35 Lohse MJ, Hein P, Hoffmann C, Nikolaev VO, Vilardaga JP, Bünemann M. Kinetics of G-protein-coupled receptor signals in intact cells. *Br J Pharmacol* **153**: S125-S132, 2008.0

36 Zamah AM, Delahunty M, Luttrell LM, Lefkowitz. (2002) Protein kinase A-mediated phosphorylation of the β_2-adrenergic receptor regulates its coupling to G_s and G_i. *J Biol Chem* **277**: 31249-31256.

37 Shah AM, Mann Dl. (2011) In search of new therapeutic targets and strategies for heart failure: recent advances in basic science. *Lancet* **378**: 704-712

38 Steinberg SF (2004) β_2-adrenergic receptor signaling complexes in cardiomyocyte caveolae/lipid rafts. *J Mol Cell Cardiol* **37**: 404-415

39 Xiao RP, Zhu W, Zheng M, Chakir K, Bond R, Lakatta EG, Cheng H. (2004) Subtype-specific β-adrenergic signaling pathways in the heart and their potential clinical implications. *Trends Pharmacol Sci* **25**: 358-365

40 Kuschel M, Zhou YY, Spurgeon HA, Bartel S, Karczewski P, Zhang SJ, Krause EG, Lakatta EG, Xiao RP. (1999) β_2-adrenergic cAMP signaling is uncoupled from phosphorylation of cytoplasmic proteins in canine heart. *Circulation* **99**: 2458-2465

41 Timofeyev B, Myers RE, Kim HJ, Woltz RL, Sirish P, Heiserman JP, Li N, Singapuri A, Tang T, Yarov-Yarovoy V, Yamoah EN, Hammond HK, Chiamvimonvat N. (2013) Adenylyl cyclase subtype-specific compartmentalization. Differential regulation of L-type Ca $^{2+}$ current in Ventricular myocytes. *Circ Res* **112**: 1567-1576

42 Xiao RP, Cheng H, Zhou YY Kuschel M, Lakatta EG. (1999) Recent advances in cardiac β_2-adrenergic signal transduction. *Cir Res* **85**: 1092-1100

43 Heubach JF, Graf EM, Molenaar P, Jäger A, Schröder F, Herzig S, harding SE, Ravens U. (2001) Murine ventricular L-type Ca^{2+} current is enhanced by zinterol via β_1 -adrenoceptors, and is reduced in TG4 mice overexpressing the human β_2-adrenoceptor. *Br J Pharmacol* **133**: 73-82

44 Heubach JF, Rau T, Eschenhagen T, Ravens U, Kaumann AJ. (2002) Physiological antagonism between ventricular β_1-adrenoceptors and α_1-adrenoceptors but no evidence for β_2- and β_3-adrenocptor function in murine heart. *Br J Pharmacol* **136**: 217-229

45 Guerrero SW, Minneman KP. (1999) Coupling efficiencies of β_1- and β_2-adrenergic receptors expressed alone or together in transfected Gh3 pituitary cells *J Pharmacol Exp Ther* **290**: 980-988

46 Minneman KP, Hedberg A. Molinoff PB. (1979) Comparison of beta adrenergic receptor subtypes in mammalian tissues. *J Pharmacol Exp Ther* **211**: 502-508

47 Esprito Santo DPM, dos Santos RW, Leite SC, Novaes GM, Campos FO, Bondarenko VE. (2015) Simulations of spontaneous action potentials via the combination of β_1-adrenergic stimulation and NCX mutation in cardiac myocytes of mouse left ventricle. In: *IFMBE Proceedings,* edited by Braidot A and Hadad A. Cham, Heidelberg. New York, Dordrecht, London: Springer International Publishing 663-666

48 Chen-Goodspeed M. Lukan AN, Dessauer CW. (2005) Modeling of Gα_s and Gα_i regulation of human type V and VI adenylyl cyclase. *J Biol Chem* **280**: 1808-1516

49 Freedman NJ, Liggett SB, Drachman DE, Pei G, Caron MG, Lefkowitz RJ. (1995) Phosphorylation ad desensitization of the human β_1-adrenergic receptor: involvement of G protein-coupled receptor kinases and cAMP-dependent protein kinase. *J Biol Chem* **270**: 17953-17961

50 Tepe NM, Liggett SB. (1999) Transgenic replacement of type B adenylyl cyclase identifies a critical mechanism of β-adrenergic receptor dysfunction in the Gα_q overexpressing mouse. *FEBS Lett* **458**: 236-240

51 Lemire I, Allen BG, Rindt H, Hebert TE. (1998) Cardiac-specific overexpression of α_{1B}AR regulates βAR activity via molecular crosstalk *J Mol Cell Cardiol* **30**:1827-1839

52 Akhter SA, Milano CA, Shotwell KF, Cho MC, Rockman HA, Lefkowitz RJ, Koch WJ. (1997) Transgenic mice with cardiac overexpression of α_{1B} adrenergic receptors. In vivo α_1-

adrenergic receptor-mediated regulation of β-adrenergic signaling. *J Biol Chem* **272**: 21253-21259

53 Beavo JA, Bechtel PJ, Krebs EG. (1974) Activation of protein kinase by physiological concentrations of cyclic AMP. *Proc Natl Acad Sci USA* **71**: 3580-3583

54 Dao KK, Teigen K, Kopperud R, Hodneland E, Schwede F, Christensen AE, Marinez A, Deskeland SO. (2006) Epac1 and cAMP-dependent protein kinase holoenzyme have similar cAMP affinity, but their cAMP domains have distinct structural features and cyclic nucleotide recognition. *J Biol Chem* **281**: 21500-21511

55 Buxton ILO, Brunton LL. (1983) Compartments of cyclic AMP and protein kinase in mammalian cardiomyocytes. *J Biol Chem* **258**: 10233-10239

56 Kim SJ, Yatani A, Batner DE, Yamamoto S, Ishikawa Y, Wagner TE, Shannon RP, Kim YK, Takagi G, Asai K, Homey CJ, Vatner SF. (1999) Differential regulation of inotropy and lusitropy in overexpressed $G_{s\alpha}$ myocytes through cAMP and Ca^{2+} channel pathways *J Clin Invest* **103**: 1089-1097

57 Sako H, Green SA, Kranias EG, Yatani A. (1997) Modulation of cardia Ca^{2+} channels by isoproterenol studied in transgenic mice with altered SR Ca_{2+} content. *Am J Physiol Cell Physiol* **273**: C1666-C1672

58 Xu L, Lai D, Cheng J, Lim HJ, Keskanokwong T, Backs J, Olson EN, Wang Y. (2010) Alterations of L-type calcium current and cardiac function in CaMKIIδ knockout mice. *Circ Res* **107**: 398-407

59 Zhou YY, Cheng H, Song LS, Wang D, Lakatta EG, Xiao RP. (1999) Spontaneous $β_2$-adrenergic signaling fails to modulate L-type Ca^{2+} current in mouse ventricular myocytes. *Mol Pharmacol* **56**: 485-493

60 Soto D, De Arcangelis V, Zhang J, Xiang Y. (2009) Dynamic protein kinase A activities induced by β-adrenoceptors dictate signaling propagation for substrate phosphorylation and myocyte contraction. *Circ Res* **104**: 770-779

61 Liu R, Ramani B, Soto D, De Arcangelis, Xiang y. (2009) Agonist dose-dependent phosphorylation by protein kinase A and G protein-coupled receptor kinase regulates $β_2$ adrenoceptor coupling to G_i proteins in cardiomyocytes. *J Biol Chem* **284**: 32279-32287

62 Kuschel M, Zhou YY, Cheng H, Zhang SJ, Chen Y, Lakatta EG, Xiao RP. (1999) G_i protein-mediate functional compartmentalization of cardiac $β_2$-adrenergic signaling. *J Biol Chem* **274**: 22048-22052

63 Zhou YY, Song LS, Lakatta EG, Xiao RP, Cheng H. (1999) Constitutive $β_2$-adrenergic signaling enhances sarcoplasmic reticulum Ca^{2+} cycling to augment contraction in mouse heart. *J Physiol* **521**: 351-361

64 Despa S, Bers DM. (2013) Na^+ transport in the normal and failing heart – Remember the balance. *J Mol Cell Cardiol* **61**: 2-10

65 Wang H, Kohr MJ, Wheeler DG, Ziolo MT. (2008) Endothelial nitric oxide synthase decreases β-adrenergic responsiveness via inhibition of the L-type Ca^{2+} current. *Am J Physiol Heart Circ Physiol* **294**: H1473-H1480

66 Sabri A, Pak E, Alcott SA, Wilson BA, Steinberg SF. (2000) Coupling function of endogenous $α_1$- and β-adrenergic receptors in mouse cardiomyocytes. *Circ Res* **86**: 1047-1053

67 Xiao RP, Avdonin P, Zhou YY, Cheng H, Akhter SA, Eschenhagen T, Lefkowitz RJ, Koch WJ, Lakatta EG. (1999) Coupling of β_2-adrenoceptor to G_i proteins and its physiological relevance in murine cardiac myocytes. *Circ Res* **84**: 43-52

68 Despa S, Tucker AL, Bers DM. (2008) Phospholemman-mediated activation of Na/K-ATPase limits $[Na]_i$ and inotropic state during β-adrenergic stimulation in mouse ventricular myocytes. *Circulation* **117**: 1849-1855

69 Green SA, Holt BD, Liggett SB. (1992) β_1- and β_2-adrenergic receptors display subtype-selective coupling to G_s. *Mol Pharmacol* **41**: 889-893

70 Liu L, Askari A. (2006) β-Subunit of cardiac Na^+-K^+-ATPase dictates the concentration of the functional enzyme in caveolae. *Am J Physiol Cell Physiol* **291**: C569-C578

71 Chu G, Lester JW, Young KB, Luo W, Zhai J, Kranias EG. (2000) A single site (Ser^{16}) phosphorylation in phospholamban is sufficient in mediating its maximal cardiac responses to β-agonists. *J Biol Chem* **275**: 38938-38943

72 Bers DM. (2002) Cardiac excitation-contraction coupling. *Nature* **415**: 198-205

73 Bristow MR, Ginsburg R, Umans V, Fowler M, Minobe W, Rasmussen R, Zera P, Menlove R, Shah P, Jamieson S, Stinson EB. (1986) β_1- and β_2-adrenergic-receptor subpopulations in non-failing and failing human ventricular myocardium: coupling of both receptor subtypes to muscle contraction and selective β_1-receptor down-regulation in heart failure. *Circ Res* **59**:297-309

74 Xiao RP, Hohl C, Altschuld R, Jones L, Livingston B, Ziman B, Tantini B, Lakatta EG. (1994) β_2-adrenergic receptor-stimulated increase in cAMP in rat heart cells is not coupled to changes in Ca^{2+} dynamics, contractility, or phospholamban phosphorylation. *J Biol Chem* **269**:19151-19156

75 Pogwizd SM, Schlotthauer K, Li L, Yuan W, Bers DM. (2001) Arrhythmogenesis and contractile dysfunction in heart failure: roles of sodium-calcium exchange, inward rectifier potassium current, and residual β-adrenergic responsiveness. *Circ Res* **88**:1159-1167

76 Yamada KA, Corr PB. (1992) Effects of β-adrenergic receptor activation on intracellular calcium and membrane potential in adult cardiac myocytes. *J cardiovasc Electrophysiol* **3**:209-224

77 Calaghan S, Whte E. (2006) Caveolae modulate excitation-contraction coupling and β_2-adrenergic signaling in adult rat ventricular myocytes. *Cardiovasc Res* **69**:816-824

78 Chakir K, Depry C, Dimaano VL, Zhu WZ, Banderheyden M, Bartunek J, Apraham TP, Toaselli GF, Liu SB, Xiang YK, Zhang M, Takimoto E, Dulin N, Xiao RP, Zhang J, Kass DA. (2011) $G\alpha s$-biased $\beta2$-adremergic receptor signaling from restoring synchronous contraction in the failing heart. *Sci Transl Med* **3**: 100ra88

79 DeSantiago J, Ai X, Islam M, Aeuna G, Ziolo MT, Bers DM, Pogwizd SM. (2008) Arrhythmogenic effects of $\beta2$-adrenergic stimulation in the failing heart are attributable to enhanced sarcoplasmic reticulum Ca load. *Circ Res* **102**:1389-1397

80 Kobayashi T, Solaro RJ. (2005) Calcium, thin filaments, and the interative biology of cardiac contractility. *Annu Rev Physiol* **67**:39-67

81 Roden DM, Balser JR, George AL, Jr, Anderson ME. (2002) Cardiac ion channels. *Annu Rev Physiol* **64**: 431-475

82 Bristow MR, Feldman AM. (1992) Changes in the receptor-G protein-adenylyl cyclase system in heart failure from various types of heart muscle disease. *Basic Res Cardiol* **87**(suppl 1): 15-35

83 Nattel S, Maguy A, Le Bouter S, Yeh YH. (2007) Arrhythmogenic ion-channel remodeling in the heart: heart failure, myocardial infarction, and atrial fibrillation. *Physiol Rev* **87**: 425-456

84 Schröder F, Handrock R, Beuckelmann DJ, Hirt S, Hullin R, Priebe L, Schwinger RHG, Weil J, Herzig S. (1998) Increased availability and open probability of single L-type calcium channels from failing compared with nonfailing human ventricle. *Circulation* **98**:969-976

85 El-Armouche A, Eschenhagen T. (2009) β-adrenergic stimulation and myocardial function in the failing heart. *Heart Fail Rev* **14**: 225-241

86 London B, Baker LC, Lee JS, Shusterman B, Choi BR, Kubota T, McTiernan CF, Feldman AM, Salama G. (2003) Calcium-dependent arrhythmias in transgenic mice with heart failure. *Am J Physiol Heart Circ Physiol* **284**:H431-H441

87 Harding VB, Jones LR, Lefkowitz RJ, Koch WJ. Rockman HA. (2001) Cardiac βark1 inhibition prolongs survival and augments β blocker therapy in a mouse model of severe heart failure. *Proc Natl Acad Sci USA* **98**: 5809-5814

88 Englehardt S, Hein L, Dyachenkow V, Kranias EG, Isenberg G, Lohse MJ. (2004) Altered calcium handling is critically involved in the cardiotoxic effects of chronic β-adrenergic stimulation. *Circulation* **109**: 1154-1160

89 Lehnart SE, Wehrens XHT, Reiken S, Warrier S, Belebych AE, Harvey RD, Richter W, Jin SLC, Conti M, Marks AR. (2005) Phosphodiesterase 4D deficiency in the ryanodine receptor complex promotes heart failure and arrhythmias. *Cell* **123**: 25-35

90 Nerbonne JM. (2014) Mouse models of arrhythmogenic cardiovascular disease: challenges and opportunities. *Curr Opin Pharmacol* **15**: 107-114

91 Liggett SB, Tepe NM, Lorenz JN, Canning AM, Jantz TD, Mitarai S, Yatani A, Dorn GW, II. (2000) Early and delayed consequences of β_2-adrenergic receptor overexpression in mouse hearts. Critical role for expression level. *Circulation* **101**: 1707-1714

92 Rozier K, Bondarenko VE. (2017) Distinct physiological effects of β_1- and β_2-adrenoceptors in mouse ventricular myocytes: insights from a compartmentalized mathematical model. *Am J Physiol Cell Physiol* 2017 (in press). Published online: http://ajpcell.physiology.org/content/early/2017/01/25/ajpcell.00273.2016.

93 Zhang SJ, Cheng H, Zhou YY, Wang DJ, Zhu W, Ziman B, Spurgoen H, Lefkowitz RJ, Lakatta EG, Koch WJ, Xiao RP. (2000) Inhibition of spontaneous β_2-adrenergic activation rescues β_1-adrenergic contractile response in cardiomyocytes overexpressing β_2-adrenoceptors. *J Biol Chem* **275**: 21773-21779

94 Gong H, Adamson DL, Ranu HK, Koch WJ, Heubach JF, Ravens U, Zolk O, Harding SE. (2000) The effect of G_i-protein inactivation on basal, and β_1- and β_2-AR stimulated contraction of myocytes from transgenic mice overexpressing the β_2-adrenoceptors. *Br J Pharmacol* **131**: 594-600

95 Rockman HA, Hamilton RA, Jones LR, Milano CA, Mao L, Lefkowitz RJ. (1996) Enhanced myocardial relaxation in vivo in transgenic mice overexpressing the β_2-adrenergic receptor is associated with reduced phospholamban protein. *J Clin Invest* **97**: 1618-1623

96 Luo W, Grupp IL, Harrer J, Ponniah S, Grupp G, Duffy JJ, Doetschman T, Kranias EG. (1994) Targeted ablation of the phospholamban gene is associated with markedly enhanced myocardial contractility and loss of β-agonist stimulation. *Circ Res* **75**: 401-409

97 Kadambi VJ, Ponniah S, Harrer JM, Hoit BD, Dom GW, II, Walsh RA, Kranias EG. (1996) Cardiac-specific overexpression of phospholamban alters calcium kinetics and resultant cardiomyocyte mechanics in transgenic mice. *J Clin Invest* **97**: 533-539

98 Grandy SA, Denovan-Wright EM, Ferrier GR, Howlett SE. (2004) Overexpression of human β_2-adrenergic receptors increases gain of excitation-contraction coupling in mouse ventricular myocytes. *Am J Pysiol Heart Circ Physiol* **287**: H1029-H1038

99 Heubach JF, Trebess I, Wettwer E, Himmel HM, Michel MC, Kaumann AJ, Koch WJ, Harding SE, Ravens U. (1999) L-type calcium current and contractility in ventricular myocytes from mice overexpressing the cardiac β_2-adrenoceptor. *Cardiovasc Res* **42**: 173-182

100 Bond RA, Leff P, Johnson TD, Milano CA, Rockman HA, Meminn TR, Apparsundaram S, Hyek MF, Kenakin TP, Allen LF, Lefkowitz RJ. (1995) Physiological effects of inverse agonists in transgenic mice with myocardial overexpression of the β_2-adrenoceptor. *Nature* **374**: 272-276

101 Bondarenko BE, Bett GCL, Rasmusson RL. (2004) A model of graded calcium release and L-type Ca^{2+} channel inactivation in cardiac muscle. *Am J Physiol Heart Circ Physiol* **286**: H1154-H1169

102 Wenzel-Seifort K, Seifert R. (2000) Molecular analysis of β_2-adrenoceptor coupling to G_s-, G_i- and G_q-proteins. **58**: 954-956

103 Gao X, Sadana R, Dessauer CW, Patel TB. (2007) Conditional stimulation of type V and VI adenylyl cyclases by G protein $\beta\gamma$ subunits. *J Biol Chem* **282**: 294-302

104 Zimmermann G, Taussig R. (1996) Protein kinase C alters responsiveness of adenylyl cyclases to G protein α and $\beta\gamma$ subunits. *J Biol Chem* **271**: 27161-27166

APPENDIX

MODEL EQUATIONS AND PARAMETERS.

Mathematical model of the combined β_1- and β_2-adrenergic signaling system consists of the model equations (A.1)-(A.125) and model parameters presented in this Appendix plus 238 model equations (A.64)-(A.301) and model parameters from Ref. 27.

BIOCHEMICAL PART

Cell compartments

Parameter	Definition	Value	Reference
A_{cap}	Capacitive membrane area	1.534×10^{-4} cm^2	Bondarenko et al. (101)
V^{cell}	Cell volume	38.00×10^{-6} µl	Bondarenko et al. (101)
V^{cyt}	Cytosolic volume	25.84×10^{-6} µl	Bondarenko et al. (101)
V_{JSR}	Junctional SR volume	0.12×10^{-6} µl	Bondarenko et al. (101)
V_{NSR}	Network SR volume	2.098×10^{-6} µl	Bondarenko et al. (101)
V_{ss}	Subspace volume	1.485×10^{-9} µl	Bondarenko et al. (101)
V^{cav}	Caveolar volume	$0.02\times V_{cell}$	Heijman et al. (26)
V^{ecav}	Extracaveolar volume	$0.04\times V_{cell}$	Heijman et al. (26)

The protein P concentrations in the cell ([P]^{cell}), caveolar, extracaveolar, and cytosol

$$[P]^{cav} = f_P^{cav}\cdot[P]^{cell}\cdot\frac{V^{cell}}{V^{cav}} \tag{A.1}$$

$$[P]^{ecav} = f_P^{ecav}\cdot[P]^{cell}\cdot\frac{V^{cell}}{V^{ecav}} \tag{A.2}$$

$$[P]^{cyt} = (1 - f_P^{cav} - f_P^{ecav}) \cdot [P]^{cell} \cdot \frac{V^{cell}}{V^{cyt}} \qquad (A.3)$$

β₁- and β₂-adrenergic receptor module

Parameter	Definition	Value	Reference
$[L]$	Ligand concentration	0.100 μM	
$[R_{\beta 1}]_{tot}$	Total β₁-adrenoceptor concentration	0.0103 μM	Hilal-Dandan et al. (32)
$[R_{\beta 2}]_{tot}$	Total β₂-adrenoceptor concentration	0.0053 μM	Hilal-Dandan et al. (32)
$f_{\beta 1}^{cav}$	Fraction of β₁-adrenoceptors located in caveolar	0.01	Rybin et al. (20) Balijepali et al. (31)
$f_{\beta 1}^{ecav}$	Fraction of β₁-adrenoceptors located in extracaveolar	0.5	Rybin et al. (20) Balijepali et al. (31)
$f_{\beta 1}^{cyt}$	Fraction of β₁-adrenoceptors located in cytosol	$f_{\beta 1}^{cyt} = 1 - f_{\beta 1}^{cav} - f_{\beta 1}^{ecav}$	
$f_{\beta 2}^{cav}$	Fraction of β₂-adrenoceptors located in caveolar	0.99	Nikolaev et al. (34)
$f_{\beta 2}^{ecav}$	Fraction of β₂-adrenoceptors located in extracaveolar	$f_{\beta 2}^{ecav} = 1 - f_{\beta 2}^{cav}$	
$[G_s]_{tot}$	Total concentration of G_s protein	2.054 μM	Post et al. (19)
$[G_i]_{tot}$	Total concentration of G_i protein	10.086 μM	Rorabaugh et al. (33)
f_{Gs}^{cav}	Fraction of G_s protein located in caveolar	0.4	Rybin et al. (20)
f_{Gs}^{ecav}	Fraction of G_s protein located in extracaveolar	0.4	Rybin et al. (20)

f_{Gs}^{cyt}	Fraction of G_s protein located in cytosol	$f_{Gs}^{cyt} = 1 - f_{Gs}^{cav} - f_{Gs}^{ecav}$	
f_{Gi}^{cav}	Fraction of G_i protein located in caveolar	0.99	Nikolaev et al. (34)
f_{Gi}^{ecav}	Fraction of G_i protein located in extracaveolar	$f_{Gi}^{ecav} = 1 - f_{Gi}^{cav}$	
$K_{\beta1,L}$	Low affinity constant of β_1-adrenoceptor for isoproterenol	0.567 μM	Heijman et al. (26)
$K_{\beta1,H}$	High affinity constant of β_1-adrenoceptor for isoproterenol	0.0617 μM	Heijman et al. (26)
$K_{\beta1,C}$	Affinity constant of β_1-adrenoceptor for G_s protein	2.86 μM	Bondarenko (27)
$K_{\beta2,L}$	Low affinity constant of β_2-adrenoceptor for isoproterenol	1.053 μM	Green et al. (69)
$K_{\beta2,H}$	High affinity constant of β_2-adrenoceptor for isoproterenol	0.0118 μM	Green et al. (69)
$K_{\beta2,C}$	Affinity constant of β_2-adrenoceptor for G_s protein	5.86 μM	Rozier-Bondarenko (92)
$K_{\beta2,F}$	High affinity constant of phosphorylated β_2 receptor/ligand	0.0189 μM	Wenzel-Seifert and Seifert (102)
$K_{\beta2,A}$	Affinity constant of phosphorylated β_2 receptor/G_i protein	28.79 μM	Rozier-Bondarenko (92)
k_{PKA+}	Rate of PKA phosphorylation of β_1- and β_2- adrenoceptor	0.00081 μM^{-1} s^{-1}	Freedman et al. (49)
k_{PKA-}	Rate of PKA dephosphorylation of β_1- and β_2- adrenoceptor	0.0002025 s^{-1}	Bondarenko (27)

k_{GRK2+}	Rate of GRK2 phosphorylation of β_1- and β_2- adrenoceptor	0.000243 s^{-1}	Bondarenko (27)
k_{GRK2-}	Rate of GRK2 dephosphorylation of β_1- and β_2- adrenoceptor	k_{PKA-}	Bondarenko (27)
$k_{act1,Gs\beta1}$	Activation rate for G$_s$ by β_1-ARs high affinity complex	4.9 s^{-1}	Heijman et al. (26)
$k_{act2,Gs\beta1}$	Activation rate for G$_s$ by β_1-ARs low affinity complex	0.26 s^{-1}	Heijman et al. (26)
$k_{act1,Gs\beta2}$	Activation rate for G$_s$ by β_2-ARs high affinity complex	0.196 s^{-1}	Rozier-Bondarenko (92)
$k_{act2,Gs\beta2}$	Activation rate for G$_s$ by β_2-ARs low affinity complex	0.0104 s^{-1}	Rozier-Bondarenko (92)
$k_{hyd,Gs}$	Hydrolysis rate of G$_{s\alpha\text{-GTP}}$	0.8 s^{-1}	Saucerman et al. (16)
$k_{reas,Gs}$	Re-association rate for G$_s$	1200 μM^{-1} s^{-1}	Saucerman et al. (16)
$k_{act1,Gi}$	Activation rate for G$_i$ by high affinity complex	2.0 s^{-1}	Rozier-Bondarenko (92)
$k_{act2,Gi}$	Activation rate for G$_i$ by low affinity complex	0.050 s^{-1}	Saucerman et al. (16)
$k_{hyd,Gi}$	Hydrolysis rate of G$_{i\alpha\text{-GTP}}$	$k_{hyd,Gs}$	Saucerman et al. (16)
$k_{reas,Gi}$	Re-association rate for G$_i$	$k_{reas,Gs}$	Saucerman et al. (16)

Caveolar

$$[R_{\beta1}]_{tot}^{cav} = f_{\beta1}^{cav} \cdot [R_{\beta1}]_{tot} \cdot \frac{V_{cell}}{V_{cav}} \tag{A.4}$$

$$[R_{\beta2}]_{tot}^{cav} = f_{\beta2}^{cav} \cdot [R_{\beta2}]_{tot} \cdot \frac{V_{cell}}{V_{cav}} \tag{A.5}$$

$$[G_s]_{\alpha\beta\gamma}^{cav} = f_{Gs}^{cav} \cdot [G_s]_{tot} \cdot \frac{V_{cell}}{V_{cav}} - [G_s]_{\alpha,GTP}^{cav} - [G_s]_{\alpha,GDP}^{cav} \tag{A.6}$$

$$[G_i]^{cav}_{\alpha\beta\gamma} = f^{cav}_{Gi} \cdot [G_i]_{tot} \cdot \frac{V_{cell}}{V_{cav}} - [G_i]^{cav}_{\alpha,GTP} - [G_i]^{cav}_{\alpha,GDP} \tag{A.7}$$

$$[R_{\beta 1}]^{cav}_{np,tot} = [R_{\beta 1}]^{cav}_{tot} - [R_{\beta 1}]^{cav}_{PKA,tot} - [R_{\beta 1}]^{cav}_{GRK2,tot} \tag{A.8}$$

$$[R_{\beta 2}]^{cav}_{np,tot} = [R_{\beta 2}]^{cav}_{tot} - [R_{\beta 2}]^{cav}_{PKA,tot} - [R_{\beta 2}]^{cav}_{GRK2,tot} \tag{A.9}$$

$$a^{cav}_{\beta 2,i} = \frac{1}{K_{\beta 2,L}} \left(K_{\beta 2,L} + [L] \right) \left(K_{\beta 2,F} + [L] \right) \tag{A.10}$$

$$b^{cav}_{\beta 2,i} = [G_i]^{cav}_{\alpha\beta\gamma} \left(K_{\beta 2,F} + [L] \right) - \left(K_{\beta 2,F} + [L] \right) [R_{\beta 2}]^{cav}_{PKA,tot} + K_{\beta 2,A} K_{\beta 2,F} + K_{\beta 2,A} K_{\beta 2,F} \frac{[L]}{K_{\beta 2,L}} \tag{A.11}$$

$$c^{cav}_{\beta 2,i} = -[R_{\beta 2}]^{cav}_{PKA,tot} K_{\beta 2,A} K_{\beta 2,F} \tag{A.12}$$

$$[R_{\beta 2}]^{cav}_{PKA,f} = \frac{-b^{cav}_{\beta 2,i} + \sqrt{\left(b^{cav}_{\beta 2,i}\right)^2 - 4a^{cav}_{\beta 2,i} c^{cav}_{\beta 2,i}}}{2a^{cav}_{\beta 2,i}} \tag{A.13}$$

$$[G_i]^{cav}_f = \frac{[G_i]^{cav}_{\alpha\beta\gamma}}{1 + [R_{\beta 2}]^{cav}_{PKA,f} \left[\dfrac{1}{K_{\beta 2,A}} + \dfrac{[L]}{K_{\beta 2,A} K_{\beta 2,F}} \right]} \tag{A.14}$$

$$[LR_{\beta 2}]^{cav}_{PKA} = \frac{[L][R_{\beta 2}]^{cav}_{PKA,f}}{K_{\beta 2,L}} \tag{A.15}$$

$$[LR_{\beta 2} G_i]^{cav}_{PKA} = \frac{[L][R_{\beta 2}]^{cav}_{PKA,f} [G_i]^{cav}_f}{K_{\beta 2,A} K_{\beta 2,F}} \tag{A.16}$$

$$[R_{\beta 2} G_i]^{cav}_{PKA} = \frac{[R_{\beta 2}]^{cav}_{PKA,f} [G_i]^{cav}_f}{K_{\beta 2,A}} \tag{A.17}$$

$$a^{cav}_{\beta 2,s} = \left([L] + K_{\beta 1,H} \right) \left([L] + K_{\beta 2,H} \right) \tag{A.18}$$

$$b_{\beta2,s}^{cav} = \left([L]+K_{\beta1,H}\right)\left([L]+K_{\beta2,H}\right)\left([R_{\beta1}]_{np,tot}^{cav}+[R_{\beta2}]_{np,tot}^{cav}\right)+$$

$$\left(K_{\beta1,C}K_{\beta1,H}+\frac{[L]K_{\beta1,C}K_{\beta1,H}}{K_{\beta1,L}}\right)\left([L]+K_{\beta2,H}\right)+\left(K_{\beta2,C}K_{\beta2,H}+\frac{[L]K_{\beta2,C}K_{\beta2,H}}{K_{\beta2,L}}\right)\left([L]+K_{\beta1,H}\right)-$$

$$[G_s]_{\alpha\beta\gamma}^{cav}\left([L]+K_{\beta1,H}\right)\left([L]+K_{\beta2,H}\right) \tag{A.19}$$

$$c_{\beta2,s}^{cav} = \left([L]+K_{\beta1,H}\right)\left(K_{\beta2,C}K_{\beta2,H}+\frac{[L]K_{\beta2,C}K_{\beta2,H}}{K_{\beta2,L}}\right)\left([R_{\beta1}]_{np,tot}^{cav}-[G_s]_{\alpha\beta\gamma}^{cav}\right)+$$

$$\left([L]+K_{\beta2,H}\right)\left(K_{\beta1,C}K_{\beta1,H}+\frac{[L]K_{\beta1,C}K_{\beta1,H}}{K_{\beta1,L}}\right)\left([R_{\beta2}]_{np,tot}^{cav}-[G_s]_{\alpha\beta\gamma}^{cav}\right)+$$

$$\left(K_{\beta1,C}K_{\beta1,H}+\frac{[L]K_{\beta1,C}K_{\beta1,H}}{K_{\beta1,L}}\right)\left(K_{\beta2,C}K_{\beta2,H}+\frac{[L]K_{\beta2,C}K_{\beta2,H}}{K_{\beta2,L}}\right) \tag{A.20}$$

$$d_{\beta2,s}^{cav} = -[G_s]_{\alpha\beta\gamma}^{cav}\left(K_{\beta1,C}K_{\beta1,H}+\frac{[L]K_{\beta1,C}K_{\beta1,H}}{K_{\beta1,L}}\right)\left(K_{\beta2,C}K_{\beta2,H}+\frac{[L]K_{\beta2,C}K_{\beta2,H}}{K_{\beta2,L}}\right) \tag{A.21}$$

$$p^{cav} = \frac{b_{\beta2,s}^{cav}}{a_{\beta2,s}^{cav}}; \qquad q^{cav} = \frac{c_{\beta2,s}^{cav}}{a_{\beta2,s}^{cav}}; \qquad r^{cav} = \frac{d_{\beta2,s}^{cav}}{a_{\beta2,s}^{cav}} \tag{A.22}$$

$$A^{cav} = \frac{1}{3}\left(3q^{cav}-(p^{cav})^2\right) \tag{A.23}$$

$$B^{cav} = \frac{1}{27}\left(2(p^{cav})^3-9p^{cav}q^{cav}+27r^{cav}\right) \tag{A.24}$$

$$D^{cav} = \frac{(A^{cav})^3}{27}+\frac{(B^{cav})^2}{4} \tag{A.25}$$

$$M^{cav} = \left(-\frac{B^{cav}}{2}+\sqrt{D^{cav}}\right)^{1/3} \tag{A.26}$$

$$N^{cav} = \left(-\frac{B^{cav}}{2}-\sqrt{D^{cav}}\right)^{1/3} \tag{A.27}$$

If $D^{cav} > 0$ then $y_1^{cav} = M^{cav} + N^{cav}$; $y_2^{cav} = y_3^{cav} = 0$;

If $D^{cav} = 0$ then $y_1^{cav} = M^{cav} + N^{cav}$; $y_2^{cav} = y_3^{cav} = -(M^{cav} + N^{cav})/2$;

If $D^{cav} < 0$ and $B^{cav} > 0$ then

$$\phi^{cav} = \arccos\left(-\sqrt{\frac{(B^{cav})^2/4}{(-A^{cav})^3/27}}\right) \tag{A.28}$$

$$y_1^{cav} = 2\sqrt{-\frac{A^{cav}}{3}}\cos(\phi^{cav}); \; y_2^{cav} = 2\sqrt{-\frac{A^{cav}}{3}}\cos(\phi^{cav} + 2\pi/3); \; y_3^{cav} = 2\sqrt{-\frac{A^{cav}}{3}}\cos(\phi^{cav} + 4\pi/3) \tag{A.29}$$

If $D^{cav} < 0$ and $B^{cav} \leq 0$ then

$$\phi^{cav} = \arccos\left(\sqrt{\frac{(B^{cav})^2/4}{(-A^{cav})^3/27}}\right) \tag{A.30}$$

$$y_1^{cav} = 2\sqrt{-\frac{A^{cav}}{3}}\cos(\phi^{cav}); \; y_2^{cav} = 2\sqrt{-\frac{A^{cav}}{3}}\cos(\phi^{cav} + 2\pi/3); \; y_3^{cav} = 2\sqrt{-\frac{A^{cav}}{3}}\cos(\phi^{cav} + 4\pi/3) \tag{A.31}$$

$$z_i^{cav} = y_i^{cav} - \frac{p^{cav}}{3}, \quad i = 1, 2, 3. \tag{A.32}$$

$$[G_s]_f^{cav} = \max\{z_1^{cav}, z_3^{cav}, z_3^{cav}\} \tag{A.33}$$

$$[R_{\beta 1}]_{np,f}^{cav} = \frac{[R_{\beta 1}]_{np,tot}^{cav}}{\left[1 + \dfrac{[L]}{K_{\beta 1,L}} + [G_s]_f^{cav}\left(\dfrac{[L]}{K_{\beta 1,C}K_{\beta 1,H}} + \dfrac{1}{K_{\beta 1,C}}\right)\right]} \tag{A.34}$$

$$[R_{\beta 2}]_{np,f}^{cav} = \frac{[R_{\beta 2}]_{np,tot}^{cav}}{\left[1 + \dfrac{[L]}{K_{\beta 2,L}} + [G_s]_f^{cav}\left(\dfrac{[L]}{K_{\beta 2,C}K_{\beta 2,H}} + \dfrac{1}{K_{\beta 2,C}}\right)\right]} \tag{A.35}$$

$$[LR_{\beta 1}]_{np}^{cav} = \frac{[L] \cdot [R_{\beta 1}]_{np,f}^{cav}}{K_{\beta 1,L}} \tag{A.36}$$

$$[R_{\beta 1} G_s]_{np}^{cav} = \frac{[R_{\beta 1}]_{np,f}^{cav} \cdot [G_s]_f^{cav}}{K_{\beta 1,C}} \tag{A.37}$$

$$[LR_{\beta 1} G_s]_{np}^{cav} = \frac{[L] \cdot [R_{\beta 1}]_{np,f}^{cav} \cdot [G_s]_f^{cav}}{K_{\beta 1,C} \cdot K_{\beta 1,H}} \tag{A.38}$$

$$[LR_{\beta 2}]_{np}^{cav} = \frac{[L] \cdot [R_{\beta 2}]_{np,f}^{cav}}{K_{\beta 2,L}} \tag{A.39}$$

$$[R_{\beta 2} G_s]_{np}^{cav} = \frac{[R_{\beta 2}]_{np,f}^{cav} \cdot [G_s]_f^{cav}}{K_{\beta 2,C}} \tag{A.40}$$

$$[LR_{\beta 2} G_s]_{np}^{cav} = \frac{[L] \cdot [R_{\beta 2}]_{np,f}^{cav} \cdot [G_s]_f^{cav}}{K_{\beta 2,C} K_{\beta 2,H}} \tag{A.41}$$

$$\frac{d[R_{\beta 1}]_{PKA,tot}^{cav}}{dt} = k_{PKA+} \cdot [C]^{cav} \cdot [R_{\beta 1}]_{np,tot}^{cav} - k_{PKA-} \cdot [R_{\beta 1}]_{PKA,tot}^{cav} \tag{A.42}$$

$$\frac{d[R_{\beta 1}]_{GRK2,tot}^{cav}}{dt} = k_{GRK2+} \cdot \left[[LR_{\beta 1}]_{np}^{cav} + [LR_{\beta 1} G_s]_{np}^{cav} \right] - k_{GRK2-} \cdot [R_{\beta 1}]_{GRK2,tot}^{cav} \tag{A.43}$$

$$\frac{d[R_{\beta 2}]_{PKA,tot}^{cav}}{dt} = k_{PKA+} \cdot [C]^{cav} \cdot [R_{\beta 2}]_{np,tot}^{cav} - k_{PKA-} \cdot [R_{\beta 2}]_{PKA,tot}^{cav} \tag{A.44}$$

$$\frac{d[R_{\beta 2}]_{GRK2,tot}^{cav}}{dt} = k_{GRK2+} \cdot \left[[LR_{\beta 2}]_{np}^{cav} + [LR_{\beta 2} G_s]_{np}^{cav} \right] - k_{GRK2-} \cdot [R_{\beta 2}]_{GRK2,tot}^{cav} \tag{A.45}$$

$$\frac{d[G_s]_{\alpha,GTP}^{cav}}{dt} = k_{act2,Gs\beta 1}[R_{\beta 1} G_s]_{np}^{cav} + k_{act2,Gs\beta 2}[R_{\beta 2} G_s]_{np}^{cav} + k_{act1,Gs\beta 1}[LR_{\beta 1} G_s]_{np}^{cav} + k_{act1,Gs\beta 2}[LR_{\beta 2} G_s] \tag{A.46}$$
$$- k_{hyd,Gs} \cdot [G_s]_{\alpha,GTP}^{cav}$$

$$\frac{d[G_s]_{\alpha,GDP}^{cav}}{dt} = k_{hyd,Gs} \cdot [G_s]_{\alpha,GTP}^{cav} - k_{reas,Gs} \cdot [G]_{\beta\gamma}^{cav} \cdot [G_s]_{\alpha,GDP}^{cav} \tag{A.47}$$

$$\frac{d[G_i]_{\alpha,GTP}^{cav}}{dt} = k_{act2,Gi} \cdot [R_{\beta 2} G_i]_{PKA}^{cav} + k_{act1,Gi} \cdot [LR_{\beta 2} G_i]_{PKA}^{cav} - k_{hyd,Gi} \cdot [G_i]_{\alpha,GTP}^{cav} \tag{A.48}$$

$$\frac{d[G_i]_{\alpha,GDP}^{cav}}{dt} = k_{hyd,Gi} \cdot [G_i]_{\alpha,GTP}^{cav} - k_{reas,Gi} \cdot [G]_{\beta\gamma}^{cav} \cdot [G_i]_{\alpha,GDP}^{cav} \tag{A.49}$$

$$\frac{d[G]_{\beta\gamma}^{cav}}{dt} = k_{act2,Gs\beta1}[R_{\beta1}G_s]_{np}^{cav} + k_{act2,Gs\beta2}[R_{\beta2}G_s]_{np}^{cav} + k_{act1,Gs\beta1}[LR_{\beta1}G_s]_{np}^{cav} + k_{act1,Gs\beta2}[LR_{\beta2}G_s]_{np}^{cav}$$
$$+ k_{act2,Gi} \cdot [R_{\beta2}G_i]_{PKA}^{cav} + k_{act1,Gi} \cdot [LR_{\beta2}G_i]_{PKA}^{cav} - k_{reas,Gs} \cdot [G]_{\beta\gamma}^{cav} \cdot [G_s]_{\alpha,GDP}^{cav} \tag{A.50}$$
$$- k_{reas,Gi} \cdot [G]_{\beta\gamma}^{cav} \cdot [G_i]_{\alpha,GDP}^{cav}$$

Extracaveolar

$$[R_{\beta1}]_{tot}^{ecav} = f_{\beta1}^{ecav} \cdot [R_{\beta1}]_{tot} \cdot \frac{V_{cell}}{V_{ecav}} \tag{A.51}$$

$$[R_{\beta2}]_{tot}^{ecav} = f_{\beta2}^{ecav} \cdot [R_{\beta2}]_{tot} \cdot \frac{V_{cell}}{V_{ecav}} \tag{A.52}$$

$$[G_s]_{\alpha\beta\gamma}^{ecav} = f_{Gs}^{ecav} \cdot [G_s]_{tot} \cdot \frac{V_{cell}}{V_{ecav}} - [G_s]_{\alpha,GTP}^{ecav} - [G_s]_{\alpha,GDP}^{ecav} \tag{A.53}$$

$$[G_i]_{\alpha\beta\gamma}^{ecav} = f_{Gi}^{ecav} \cdot [G_i]_{tot} \cdot \frac{V_{cell}}{V_{ecav}} - [G_i]_{\alpha,GTP}^{ecav} - [G_i]_{\alpha,GDP}^{ecav} \tag{A.54}$$

$$[R_{\beta1}]_{np,tot}^{ecav} = [R_{\beta1}]_{tot}^{ecav} - [R_{\beta1}]_{PKA,tot}^{ecav} - [R_{\beta1}]_{GRK2,tot}^{ecav} \tag{A.55}$$

$$[R_{\beta2}]_{np,tot}^{ecav} = [R_{\beta2}]_{tot}^{ecav} - [R_{\beta2}]_{PKA,tot}^{ecav} - [R_{\beta2}]_{GRK2,tot}^{ecav} \tag{A.56}$$

$$a_{\beta2,i}^{ecav} = \frac{1}{K_{\beta2,L}} \left(K_{\beta2,L} + [L] \right) \left(K_{\beta2,F} + [L] \right) \tag{A.57}$$

$$b_{\beta2,i}^{ecav} = [G_i]_{\alpha\beta\gamma}^{ecav} \left(K_{\beta2,F} + [L] \right) - \left(K_{\beta2,F} + [L] \right) [R_{\beta2}]_{PKA,tot}^{ecav} + K_{\beta2,A} K_{\beta2,F} + K_{\beta2,A} K_{\beta2,F} \frac{[L]}{K_{\beta2,L}} \tag{A.58}$$

$$c_{\beta2,i}^{ecav} = -[R_{\beta2}]_{PKA,tot}^{ecav} K_{\beta2,A} K_{\beta2,F} \tag{A.59}$$

$$[R_{\beta2}]_{PKA,f}^{ecav} = \frac{-b_{\beta2,i}^{ecav} + \sqrt{\left(b_{\beta2,i}^{ecav} \right)^2 - 4a_{\beta2,i}^{ecav} c_{\beta2,i}^{ecav}}}{2a_{\beta2,i}^{ecav}} \tag{A.60}$$

$$[G_i]_f^{ecav} = \frac{[G_i]_{\alpha\beta\gamma}^{ecav}}{1 + [R_{\beta2}]_{PKA,f}^{ecav}\left[\dfrac{1}{K_{\beta2,A}} + \dfrac{[L]}{K_{\beta2,A}K_{\beta2,F}}\right]} \tag{A.61}$$

$$[LR_{\beta2}]_{PKA}^{ecav} = \frac{[L][R_{\beta2}]_{PKA,f}^{ecav}}{K_{\beta2,L}} \tag{A.62}$$

$$[R_{\beta2}G_i]_{PKA}^{ecav} = \frac{[R_{\beta2}]_{PKA,f}^{ecav}[G_i]_f^{ecav}}{K_{\beta2,A}} \tag{A.63}$$

$$[LR_{\beta2}G_i]_{PKA}^{ecav} = \frac{[L][R_{\beta2}]_{PKA,f}^{ecav}[G_i]_f^{ecav}}{K_{\beta2,A}K_{\beta2,F}} \tag{A.64}$$

$$a_{\beta2,s}^{ecav} = \left([L] + K_{\beta1,H}\right)\left([L] + K_{\beta2,H}\right) \tag{A.65}$$

$$
\begin{aligned}
b_{\beta2,s}^{ecav} = & \left([L] + K_{\beta1,H}\right)\left([L] + K_{\beta2,H}\right)\left([R_{\beta1}]_{np,tot}^{ecav} + [R_{\beta2}]_{np,tot}^{ecav}\right) + \\
& \left(K_{\beta1,C}K_{\beta1,H} + \frac{[L]K_{\beta1,C}K_{\beta1,H}}{K_{\beta1,L}}\right)\left([L] + K_{\beta2,H}\right) + \left(K_{\beta2,C}K_{\beta2,H} + \frac{[L]K_{\beta2,C}K_{\beta2,H}}{K_{\beta2,L}}\right)\left([L] + K_{\beta1,H}\right) - \\
& [G_s]_{\alpha\beta\gamma}^{ecav}\left([L] + K_{\beta1,H}\right)\left([L] + K_{\beta2,H}\right)
\end{aligned}
\tag{A.66}
$$

$$
\begin{aligned}
c_{\beta2,s}^{ecav} = & \left([L] + K_{\beta1,H}\right)\left(K_{\beta2,C}K_{\beta2,H} + \frac{[L]K_{\beta2,C}K_{\beta2,H}}{K_{\beta2,L}}\right)\left([R_{\beta1}]_{np,tot}^{ecav} - [G_s]_{\alpha\beta\gamma}^{ecav}\right) + \\
& \left([L] + K_{\beta2,H}\right)\left(K_{\beta1,C}K_{\beta1,H} + \frac{[L]K_{\beta1,C}K_{\beta1,H}}{K_{\beta1,L}}\right)\left([R_{\beta2}]_{np,tot}^{ecav} - [G_s]_{\alpha\beta\gamma}^{ecav}\right) + \\
& \left(K_{\beta1,C}K_{\beta1,H} + \frac{[L]K_{\beta1,C}K_{\beta1,H}}{K_{\beta1,L}}\right)\left(K_{\beta2,C}K_{\beta2,H} + \frac{[L]K_{\beta2,C}K_{\beta2,H}}{K_{\beta2,L}}\right)
\end{aligned}
\tag{A.67}
$$

$$d_{\beta2,s}^{ecav} = -[G_s]_{\alpha\beta\gamma}^{ecav}\left(K_{\beta1,C}K_{\beta1,H} + \frac{[L]K_{\beta1,C}K_{\beta1,H}}{K_{\beta1,L}}\right)\left(K_{\beta2,C}K_{\beta2,H} + \frac{[L]K_{\beta2,C}K_{\beta2,H}}{K_{\beta2,L}}\right) \tag{A.68}$$

$$p^{ecav} = \frac{b_{\beta2,s}^{ecav}}{a_{\beta2,s}^{ecav}}; \qquad q^{ecav} = \frac{c_{\beta2,s}^{ecav}}{a_{\beta2,s}^{ecav}}; \qquad r^{ecav} = \frac{d_{\beta2,s}^{ecav}}{a_{\beta2,s}^{ecav}}$$

(A.69)

$$A^{ecav} = \frac{1}{3}\left(3q^{ecav} - (p^{ecav})^2\right)$$

(A.70)

$$B^{ecav} = \frac{1}{27}\left(2(p^{ecav})^3 - 9p^{ecav}q^{ecav} + 27r^{ecav}\right)$$

(A.71)

$$D^{ecav} = \frac{(A^{ecav})^3}{27} + \frac{(B^{ecav})^2}{4}$$

(A.72)

$$M^{ecav} = \left(-\frac{B^{ecav}}{2} + \sqrt{D^{ecav}}\right)^{1/3}$$

(A.73)

$$N^{ecav} = \left(-\frac{B^{ecav}}{2} - \sqrt{D^{ecav}}\right)^{1/3}$$

(A.74)

If $D^{ecav} > 0$ then $y_1^{ecav} = M^{ecav} + N^{ecav}$; $y_2^{ecav} = y_3^{ecav} = 0$;

If $D^{ecav} = 0$ then $y_1^{ecav} = M^{ecav} + N^{ecav}$; $y_2^{ecav} = y_3^{ecav} = -(M^{ecav} + N^{ecav})/2$;

If $D^{ecav} < 0$ and $B^{ecav} > 0$ then

$$\phi^{ecav} = \arccos\left(-\sqrt{\frac{(B^{ecav})^2/4}{(-A^{ecav})^3/27}}\right)$$

(A.75)

$$y_1^{ecav} = 2\sqrt{-\frac{A^{ecav}}{3}}\cos(\phi^{ecav}); \; y_2^{ecav} = 2\sqrt{-\frac{A^{ecav}}{3}}\cos(\phi^{ecav} + 2\pi/3); \; y_3^{ecav} = 2\sqrt{-\frac{A^{ecav}}{3}}\cos(\phi^{ecav} + 4\pi/3)$$

(A.76)

If $D^{ecav} < 0$ and $B^{ecav} \leq 0$ then

$$\phi^{ecav} = \arccos\left(\sqrt{\frac{(B^{ecav})^2/4}{(-A^{ecav})^3/27}}\right) \tag{A.77}$$

$$y_1^{ecav} = 2\sqrt{-\frac{A^{ecav}}{3}}\cos(\phi^{ecav}); \; y_2^{ecav} = 2\sqrt{-\frac{A^{ecav}}{3}}\cos(\phi^{ecav}+2\pi/3); \; y_3^{ecav} = 2\sqrt{-\frac{A^{ecav}}{3}}\cos(\phi^{ecav}+4\pi/3)$$
$$\tag{A.78}$$

$$z_i^{ecav} = y_i^{ecav} - \frac{p^{ecav}}{3}, \quad i=1,2,3. \tag{A.79}$$

$$[G_s]_f^{ecav} = \max\{z_1^{ecav}, z_2^{ecav}, z_3^{ecav}\} \tag{A.80}$$

$$[R_{\beta1}]_{np,f}^{ecav} = \frac{[R_{\beta1}]_{np,tot}^{ecav}}{\left[1+\frac{[L]}{K_{\beta1,L}}+[G_s]_f^{ecav}\left(\frac{[L]}{K_{\beta1,C}K_{\beta1,H}}+\frac{1}{K_{\beta1,C}}\right)\right]} \tag{A.81}$$

$$[R_{\beta2}]_{np,f}^{ecav} = \frac{[R_{\beta2}]_{np,tot}^{ecav}}{\left[1+\frac{[L]}{K_{\beta2,L}}+[G_s]_f^{ecav}\left(\frac{[L]}{K_{\beta2,C}K_{\beta2,H}}+\frac{1}{K_{\beta2,C}}\right)\right]} \tag{A.82}$$

$$[LR_{\beta1}]_{np}^{ecav} = \frac{[L]\cdot[R_{\beta1}]_{np,f}^{ecav}}{K_{\beta1,L}} \tag{A.83}$$

$$[R_{\beta1}G_s]_{np}^{ecav} = \frac{[R_{\beta1}]_{np,f}^{ecav}\cdot[G_s]_f^{ecav}}{K_{\beta1,C}} \tag{A.84}$$

$$[LR_{\beta1}G_s]_{np}^{ecav} = \frac{[L]\cdot[R_{\beta1}]_{np,f}^{ecav}\cdot[G_s]_f^{ecav}}{K_{\beta1,C}\cdot K_{\beta1,H}} \tag{A.85}$$

$$[LR_{\beta2}]_{np}^{ecav} = \frac{[L]\cdot[R_{\beta2}]_{np,f}^{ecav}}{K_{\beta2,L}} \tag{A.86}$$

$$[R_{\beta 2} G_s]_{np}^{ecav} = \frac{[R_{\beta 2}]_{np,f}^{ecav} \cdot [G_s]_f^{ecav}}{K_{\beta 2,C}} \qquad (A.87)$$

$$[LR_{\beta 2} G_s]_{np}^{ecav} = \frac{[L] \cdot [R_{\beta 2}]_{np,f}^{ecav} \cdot [G_s]_f^{ecav}}{K_{\beta 2,C} \cdot K_{\beta 2,H}} \qquad (A.88)$$

$$\frac{d[R_{\beta 1}]_{PKA,tot}^{ecav}}{dt} = k_{PKA+} \cdot [C]^{ecav} \cdot [R_{\beta 1}]_{np,tot}^{ecav} - k_{PKA-} \cdot [R_{\beta 1}]_{PKA,tot}^{ecav} \qquad (A.89)$$

$$\frac{d[R_{\beta 1}]_{GRK2,tot}^{ecav}}{dt} = k_{GRK2+} \cdot \left([LR_{\beta 1}]_{np}^{ecav} + [LR_{\beta 1} G_s]_{np}^{ecav} \right) - k_{GRK2-} \cdot [R_{\beta 1}]_{GRK2,tot}^{ecav} \qquad (A.90)$$

$$\frac{d[R_{\beta 2}]_{PKA,tot}^{ecav}}{dt} = k_{PKA+} \cdot [C]^{ecav} \cdot [R_{\beta 2}]_{np,tot}^{ecav} - k_{PKA-} \cdot [R_{\beta 2}]_{PKA,tot}^{ecav} \qquad (A.91)$$

$$\frac{d[R_{\beta 2}]_{GRK2,tot}^{ecav}}{dt} = k_{GRK2+} \cdot \left([LR_{\beta 2}]_{np}^{ecav} + [LR_{\beta 2} G_s]_{np}^{ecav} \right) - k_{GRK2-} \cdot [R_{\beta 2}]_{GRK2,tot}^{ecav} \qquad (A.92)$$

$$\frac{d[G_s]_{\alpha,GTP}^{ecav}}{dt} = k_{act2,Gs\beta1}[R_{\beta 1} G_s]_{np}^{ecav} + k_{act2,Gs\beta2}[R_{\beta 2} G_s]_{np}^{ecav} + k_{act1,Gs\beta1}[LR_{\beta 1} G_s]_{np}^{ecav} + k_{act1,Gs\beta2}[LR_{\beta 2} G_s]_{np}^{ecav}$$
$$- k_{hyd,Gs} \cdot [G_s]_{\alpha,GTP}^{ecav} \qquad (A.93)$$

$$\frac{d[G_s]_{\alpha,GDP}^{ecav}}{dt} = k_{hyd,Gs} \cdot [G_s]_{\alpha,GTP}^{ecav} - k_{reas,Gs} \cdot [G]_{\beta\gamma}^{ecav} \cdot [G_s]_{\alpha,GDP}^{ecav} \qquad (A.94)$$

$$\frac{d[G_i]_{\alpha,GTP}^{ecav}}{dt} = k_{act2,Gi} \cdot [R_{\beta 2} G_i]_{PKA}^{ecav} + k_{act1,Gi} \cdot [LR_{\beta 2} G_i]_{PKA}^{ecav} - k_{hyd,Gi} \cdot [G_i]_{\alpha,GTP}^{ecav} \qquad (A.95)$$

$$\frac{d[G_i]_{\alpha,GDP}^{ecav}}{dt} = k_{hyd,Gi} \cdot [G_i]_{\alpha,GTP}^{ecav} - k_{reas,Gi} \cdot [G]_{\beta\gamma}^{ecav} \cdot [G_i]_{\alpha,GDP}^{ecav} \qquad (A.96)$$

$$\frac{d[G]_{\beta\gamma}^{ecav}}{dt} = k_{act2,Gs\beta1}[R_{\beta 1} G_s]_{np}^{ecav} + k_{act2,Gs\beta2}[R_{\beta 2} G_s]_{np}^{ecav} + k_{act1,Gs\beta1}[LR_{\beta 1} G_s]_{np}^{ecav} + k_{act1,Gs\beta2}[LR_{\beta 2} G_s]_{np}^{ecav}$$
$$+ k_{act2,Gi} \cdot [R_{\beta 2} G_i]_{PKA}^{ecav} + k_{act1,Gi} \cdot [LR_{\beta 2} G_i]_{PKA}^{ecav} - k_{reas,Gs} \cdot [G]_{\beta\gamma}^{ecav} \cdot [G_s]_{\alpha,GDP}^{ecav}$$
$$- k_{reas,Gi} \cdot [G]_{\beta\gamma}^{ecav} \cdot [G_i]_{\alpha,GDP}^{ecav} \qquad (A.97)$$

Cytosol

$$[R_{\beta 1}]_{tot}^{cyt} = f_{\beta 1}^{cyt} \cdot [R_{\beta 1}]_{tot} \cdot \frac{V_{cell}}{V_{cyt}} \tag{A.98}$$

$$[G_s]_{\alpha\beta\gamma}^{cyt} = f_{Gs}^{cyt} \cdot [G_s]_{tot} \cdot \frac{V_{cell}}{V_{cyt}} - [G_s]_{\alpha,GTP}^{cyt} - [G_s]_{\alpha,GDP}^{cyt} \tag{A.99}$$

$$[R_{\beta 1}]_{np,tot}^{cyt} = [R_{\beta 1}]_{tot}^{cyt} - [R_{\beta 1}]_{PKA,tot}^{cyt} - [R_{\beta 1}]_{GRK2,tot}^{cyt} \tag{A.100}$$

$$a_{\beta 1}^{cyt} = \frac{1}{K_{\beta 1,L}} \cdot \left K_{\beta 1,L} + [L] \right \cdot \left K_{\beta 1,H} + [L] \right \tag{A.101}$$

$$b_{\beta 1}^{cyt} = [G_s]_{\alpha\beta\gamma}^{cyt} \cdot \left K_{\beta 1,H} + [L] \right - [R_{\beta 1}]_{np,tot}^{cyt} \cdot \left K_{\beta 1,H} + [L] \right + K_{\beta 1,C} \cdot K_{\beta 1,H} \left(1 + \frac{[L]}{K_{\beta 1,L}} \right) \tag{A.102}$$

$$c_{\beta 1}^{cyt} = -[R_{\beta 1}]_{np,tot}^{cyt} \cdot K_{\beta 1,C} \cdot K_{\beta 1,H} \tag{A.103}$$

$$[R_{\beta 1}]_{np,f}^{cyt} = \frac{-b_{\beta 1}^{cyt} + \sqrt{(b_{\beta 1}^{cyt})^2 - 4 \cdot a_{\beta 1}^{cyt} \cdot c_{\beta 1}^{cyt}}}{2 \cdot a_{\beta 1}^{cyt}} \tag{A.104}$$

$$[G_s]_f^{cyt} = \frac{[G_s]_{\alpha\beta\gamma}^{cyt}}{1 + [R_{\beta 1}]_{np,f}^{cyt} \left(\dfrac{1}{K_{\beta 1,C}} + \dfrac{[L]}{K_{\beta 1,C} \cdot K_{\beta 1,H}} \right)} \tag{A.105}$$

$$[LR_{\beta 1}]_{np}^{cyt} = \frac{[L] \cdot [R_{\beta 1}]_{np,f}^{cyt}}{K_{\beta 1,L}} \tag{A.106}$$

$$[R_{\beta 1}G_s]_{np}^{cyt} = \frac{[R_{\beta 1}]_{np,f}^{cyt} \cdot [G_s]_f^{cyt}}{K_{\beta 1,C}} \tag{A.107}$$

$$[LR_{\beta 1}G_s]_{np}^{cyt} = \frac{[L] \cdot [R_{\beta 1}]_{np,f}^{cyt} \cdot [G_s]_f^{cyt}}{K_{\beta 1,C} \cdot K_{\beta 1,H}} \tag{A.108}$$

$$\frac{d[R_{\beta 1}]^{cyt}_{PKA,tot}}{dt} = k_{PKA+} \cdot [C]^{cyt} \cdot [R_{\beta 1}]^{cyt}_{np,tot} - k_{PKA-} \cdot [R_{\beta 1}]^{cyt}_{PKA,tot} \tag{A.109}$$

$$\frac{d[R_{\beta 1}]^{cyt}_{GRK2,tot}}{dt} = k_{GRK2+} \cdot \left[[LR_{\beta 1}]^{cyt}_{np} + [LR_{\beta 1}G_s]^{cyt}_{np} \right] - k_{GRK2-} \cdot [R_{\beta 1}]^{cyt}_{GRK2,tot} \tag{A.110}$$

$$\frac{d[G_s]^{cyt}_{\alpha,GTP}}{dt} = k_{act2,Gs\beta 1} \cdot [R_{\beta 1}G_s]^{cyt}_{np} + k_{act1,Gs\beta 1} \cdot [LR_{\beta 1}G_s]^{cyt}_{np} - k_{hyd,Gs} \cdot [G_s]^{cyt}_{\alpha,GTP} \tag{A.111}$$

$$\frac{d[G]^{cyt}_{\beta\gamma}}{dt} = k_{act2,Gs\beta 1} \cdot [R_{\beta 1}G_s]^{cyt}_{np} + k_{act1,Gs\beta 1} \cdot [LR_{\beta 1}G_s]^{cyt}_{np} - k_{reas,Gs} \cdot [G]^{cyt}_{\beta\gamma} \cdot [G_s]^{cyt}_{\alpha,GDP} \tag{A.112}$$

$$\frac{d[G_s]^{cyt}_{\alpha,GDP}}{dt} = k_{hyd,Gs} \cdot [G_s]^{cyt}_{\alpha,GTP} - k_{reas,Gs} \cdot [G]^{cyt}_{\beta\gamma} \cdot [G_s]^{cyt}_{\alpha,GDP} \tag{A.113}$$

Adenylyl cyclase module

Parameter	Definition	Value	Reference
$K_{m,ATP}$	Adenylyl cyclase affinity for ATP	340 μM	Bondarenko (27)
$[ATP]$	ATP concentration	5000 μM	Heijman et al. (26)
$[AC]_{tot}$	Total cellular AC concentration	0.02622 μM	Post et al. (19)
$f_{AC56,AC47}$	Fraction of AC that is of type 5 or 6	0.74	Heijman et al. (26)
f^{cav}_{AC56}	Fraction of AC5/6 located in caveolar	0.0875	Heijman et al. (26)
f^{ecav}_{AC47}	Fraction of AC4/7 located in extracaveolar	0.1648	Heijman et al. (26)
$K^{AC56}_{m,Gs\alpha}$	AC5/6 affinity for $G_{s\alpha}$	0.0852 μM	Heijman et al. (26)

$h_{AC56,Gs\alpha}$	Hill coefficient for AC5/6 activation by $G_{s\alpha}$	1.357	Heijman et al. (26)
$V_{G\beta\gamma}^{AC56}$	Maximum amplification of AC5/6 by $G_{\beta\gamma}$	1.430	Gao et al. (103)
$K_{m,G\beta\gamma}^{AC56}$	Affinity constant for $G_{\beta\gamma}$ modulation of AC5/6	0.003793 μM	Gao et al. (103)
$h_{AC56,G\beta\gamma}$	Hill coefficient for $G_{\beta\gamma}$ modulation of AC5/6	1.0842	Gao et al. (103)
$AC56_{basal}$	Basal AC5/6 activity	0.0377	Heijman et al. (26)
AF_{56}	Amplification factor for AC5/6	51.1335 s^{-1}	Bondarenko (27)
$K_{m,Gs\alpha}^{AC47}$	AC4/7 affinity for $G_{s\alpha}$	0.05008 μM	Zimmermann and Taussig (104)
$h_{AC47,Gs\alpha}$	Hill coefficient for AC4/7 activation by $G_{s\alpha}$	1.1657	Zimmermann and Taussig (104)
$V_{G\beta\gamma}^{AC47}$	Maximum amplification of AC4/7 by $G_{\beta\gamma}$	1.3500	Zimmermann and Taussig (104)
$K_{m,G\beta\gamma}^{AC47}$	Affinity constant for $G_{\beta\gamma}$ modulation of AC4/7	0.004466 μM	Zimmermann and Taussig (104)
$h_{AC47,G\beta\gamma}$	Hill coefficient for $G_{\beta\gamma}$ modulation of AC4/7	0.8700	Zimmermann and Taussig (104)
$AC47_{basal}$	Basal AC4/7 activity	0.04725	Bondarenko (27)
AF_{47}	Amplification factor for AC4/7	9.283 s^{-1}	Bondarenko (27)
$K_{m,GsGi}^{AC56}$	G_s-dependence of inactivation by G_i for AC56	0.482 μM	Heijman et al. (26)
$h_{AC56,GsGi}$	Hill coefficient for G_s/G_i interaction of AC56	0.662	Heijman et al. (26)

V_{GsGi}^{AC56}	Maximum reduction in G_i inhibition by G_s	0.857	Heijman et al. (26)
$K_{m,Gi}^{AC56}$	AC56 affinity for inhibition by G_i	0.0465 µM	Heijman et al. (26)

Caveolar

$$[AC56]^{cav} = f_{AC56}^{cav} \cdot f_{AC56,AC47} \cdot [AC]_{tot} \cdot \frac{V_{cell}}{V_{cav}} \tag{A.114}$$

$$k_{AC56}^{cav} = AF_{56} \cdot \left(AC56_{basal} + \frac{[G_s]_{\alpha,GTP}^{cav}{}^{h_{AC56,Gs\alpha}}}{K_{m,Gs\alpha}^{AC56} + [G_s]_{\alpha,GTP}^{cav}{}^{h_{AC56,Gs\alpha}}} \right) \cdot \left(1 + \frac{V_{G\beta\gamma}^{AC56} \cdot [G_s]_{\beta\gamma}^{cav}{}^{h_{AC56,Gs\beta\gamma}}}{K_{m,Gs\beta\gamma}^{AC56} + [G_s]_{\beta\gamma}^{cav}{}^{h_{AC56,Gs\beta\gamma}}} \right)$$
$$\cdot \left[1 - \left(1 - \frac{V_{GsGi}^{AC56} \cdot [G_s]_{\alpha,GTP}^{cav}{}^{h_{AC56,GsGi}}}{K_{m,GsGi}^{AC56} + [G_s]_{\alpha,GTP}^{cav}{}^{h_{AC56,GsGi}}} \right) \cdot \frac{[G_i]_{\alpha,GTP}^{cav}}{K_{m,Gi}^{AC56} + [G_i]_{\alpha,GTP}^{cav}} \right] \tag{A.115}$$

$$\frac{d[cAMP]_{AC56}^{cav}}{dt} = k_{AC56}^{cav} \cdot \frac{[AC56]^{cav} \cdot [ATP]}{K_{m,ATP} + [ATP]} \tag{A.116}$$

Extracaveolar

$$[AC47]^{ecav} = f_{AC47}^{ecav} \cdot (1 - f_{AC56,AC47}) \cdot [AC]_{tot} \cdot \frac{V_{cell}}{V_{ecav}} \tag{A.117}$$

$$k_{AC47}^{ecav} = AF_{47} \cdot \left(AC47_{basal} + \frac{[G_s]_{\alpha,GTP}^{ecav}{}^{h_{AC47,Gs\alpha}}}{K_{m,Gs\alpha}^{AC47} + [G_s]_{\alpha,GTP}^{ecav}{}^{h_{AC47,Gs\alpha}}} \right) \cdot \left(1 + \frac{V_{G\beta\gamma}^{AC47} \cdot [G_s]_{\beta\gamma}^{ecav}{}^{h_{AC47,Gs\beta\gamma}}}{K_{m,Gs\beta\gamma}^{AC47} + [G_s]_{\beta\gamma}^{ecav}{}^{h_{AC47,Gs\beta\gamma}}} \right) \tag{A.118}$$

$$\frac{d[cAMP]_{AC47}^{ecav}}{dt} = k_{AC47}^{ecav} \cdot \frac{[AC47]^{ecav} \cdot [ATP]}{K_{m,ATP} + [ATP]} \tag{A.119}$$

Cytosol

$$[AC56]^{cyt} = (1 - \mathrm{f}_{AC56}^{cav}) \cdot \mathrm{f}_{AC56,AC47} \cdot [AC]_{tot} \cdot \frac{V_{cell}}{V_{cyt}} \tag{A.120}$$

$$[AC47]^{cyt} = (1 - \mathrm{f}_{AC47}^{ecav}) \cdot (1 - \mathrm{f}_{AC56,AC47}) \cdot [AC]_{tot} \cdot \frac{V_{cell}}{V_{cyt}} \tag{A.121}$$

$$k_{AC56}^{cyt} = AF_{56} \cdot \left(AC56_{basal} + \frac{[G_s]_{\alpha,GTP}^{cyt}{}^{h_{AC56,Gs\alpha}}}{K_{m,Gs\alpha}^{AC56} + [G_s]_{\alpha,GTP}^{cyt}{}^{h_{AC56,Gs\alpha}}} \right) \cdot \left(1 + \frac{V_{G\beta\gamma}^{AC56} \cdot [G_s]_{\beta\gamma}^{cyt}{}^{h_{AC56,Gs\beta\gamma}}}{K_{m,Gs\beta\gamma}^{AC56} + [G_s]_{\beta\gamma}^{cyt}{}^{h_{AC56,Gs\beta\gamma}}} \right) \tag{A.122}$$

$$\frac{d[cAMP]_{AC56}^{cyt}}{dt} = k_{AC56}^{cyt} \cdot \frac{[AC56]^{cyt} \cdot [ATP]}{K_{m,ATP} + [ATP]} \tag{A.123}$$

$$k_{AC47}^{cyt} = AF_{47} \cdot \left(AC47_{basal} + \frac{[G_s]_{\alpha,GTP}^{cyt}{}^{h_{AC47,Gs\alpha}}}{K_{m,Gs\alpha}^{AC47} + [G_s]_{\alpha,GTP}^{cyt}{}^{h_{AC47,Gs\alpha}}} \right) \cdot \left(1 + \frac{V_{G\beta\gamma}^{AC47} \cdot [G_s]_{\beta\gamma}^{cyt}{}^{h_{AC47,Gs\beta\gamma}}}{K_{m,Gs\beta\gamma}^{AC47} + [G_s]_{\beta\gamma}^{cyt}{}^{h_{AC47,Gs\beta\gamma}}} \right) \tag{A.124}$$

$$\frac{d[cAMP]_{AC47}^{cyt}}{dt} = k_{AC47}^{cyt} \cdot \frac{[AC47]^{cyt} \cdot [ATP]}{K_{m,ATP} + [ATP]} \tag{A.125}$$